STRUCTURAL DESIGN AND FINITE ELEMENT ANALYSIS OF DESCENT CUBESATS

JUDE JOSEPH FURTAL

A THESIS SUBMITTED TO
THE FACULTY OF GRADUATE STUDIES
IN PARTIAL FULFILLMENT OF THE REQUIREMENTS
FOR THE DEGREE OF
MASTER OF APPLIED SCIENCE

GRADUATE PROGRAM IN MECHANICAL ENGINEERING
YORK UNIVERSITY
TORONTO, ONTARIO

August 2019

Abstract

This thesis outlines the development of a two custom CubeSat structures used for the DESCENT mission. DESCENT is a two 1U CubeSat mission that aims to test the feasibility of an Electrodynamic Tether (EDT) to deorbit spacecrafts. The payloads and other bus components require DESCENT to have its own custom structural design. The design is initially completed using a Computer Aided Design (CAD) software to create a solid model that fulfills the requirements stated by the launch provider. Next, a Computer Aided Engineering (CAE) tool is then used to create a Finite Element Model (FEM) of the satellites. The FEM is then used to run a Finite Element Analysis (FEA) to validate the structural integrity of the satellites in the launch and thermal environments. After the structure had been validated, technical drawings of structural components were completed and sent to be manufactured. Finally, the manufactured parts were assembled together in a dry assembly and a fit check was completed to confirm outer dimensions of the satellites.

Acknowledgements

To begin, I would like to thank my supervisor Dr. George Zhu for supporting me throughout all phases of my research. Dr. Zhu has been very patient and provided me with all the resources I needed to complete my work successfully. Moreover, I would like to thank him for the guidance he has shown me during the difficult moments of my research. Dr. Zhu had taught me a wide variety of soft and technical skills, to not only help me succeed during my masters but to also further my professional growth. I would also like to thank both Dr. Dan Zhang and Dr. Franz Newland for their encouragement and support. I am very grateful for having them share their ideas and providing me with the knowledge to conduct my research. I would also like to thank all my fellow graduate students for assisting me throughout my experiments and simulations. Next, I would like to thank God, my family and friends for giving me the strength and motivation during my masters. Finally, I would like to thank the Canadian Space Agency (CSA) for financial support of the DESCENT mission. Thanks to the CSA, I had an opportunity to take part in a space mission and become part of an amazing team of researchers.

Table of Contents

List of Tables

List of Figures

Symbols and Conventions

All units stated in this thesis are in SI units, unless otherwise specified.

List of Symbols

q	Charge of particle
c	Damping constant
$\boldsymbol{E}$	Electric field
ε	Emissivity
$\dot{q}$	Energy radiated per unit surface area, per unit time
ω	Frequency
$\boldsymbol{F}$	Lorentz force
$\boldsymbol{B}$	Magnetic field
m	Mass
ω_n	Natural Frequency
$\dot{Q}$	Heat transfer rate
k	Spring constant
σ	Stress or Stefan–Boltzmann constant
A	Surface area
T	Temperature
v	Velocity
F	View factor

List of Abbreviations

ADCS	Attitude Determination and Control System
CAD	Computer Aided Design
CG	Center of Gravity
CINEMA	CubeSat for Ion, Neutral, Electron, MAgneticfields
COTS	Commercial of The Shelf
CSA	Canadian Space Agency
DESCENT	DEorbiting SpaceCrafts using ElectrodyNamic Tether
DoD	Department of Defence
ECOSat	Enhanced Communications Satellite
EDT	Electro Dynamic Tether
ENAs	Energetic Neutral Atoms
FEA	Finite Element Analysis
FEM	Finite Element Model
LEO	Low Earth Orbit
NRCSD	NanoRacks CubeSat Deployer
OBC	On-Board Computer
PPOD	Poly Picosat Orbital Deployer
RBF	Remove Before Fight
SSN	Space Surveillance Network
TRIO	TRiplet Ionospheric Observatory
UHF	Ultra High Frequency

Chapter 1 INTRODUCTION TO RESEARCH

1.1 Introduction

This chapter of the thesis aims to introduce the research to be undertaken. The chapter will begin by providing a background on the orbital debris crisis, then the concept of the Electrodynamic Tether (EDT) and the DESCENT mission will be outlined. Then, the motivation, justification, objectives and method of approach for the research will be stated. Finally, the thesis document layout will be described.

1.2 Background on the Orbital Debris Crisis

There are a number of environmental crises on Earth ranging from climate change to pollution. However, there also exists an environmental crisis beyond the Earth and this is the environmental crisis caused by orbital debris. Orbital debris is defined by NASA as, "Any man-made object in orbit about the Earth which no longer serves a useful function" [1]. The most common contents of orbital debris often include, retired satellites, mission related debris, fragmentation debris caused from collisions, and rocket stages. Before the launch of the first artificial satellite named Sputnik 1, the space surrounding the Earth orbit was only composed of natural debris (ex. meteoroids). However, after the launch of Sputnik 1 there has been an increase in the number of artificial orbital debris. The increase in orbital debris has been a concern to many space organizations around the world. Orbital debris can travel at speeds as high as 52,000 km/h

[2] relative to the ground. Due to these extremely high speeds a piece of debris the size of a paint chip can be very harmful to a spacecraft. Being aware of potential threats caused by orbital debris, the United States Department of Defence (DoD) has been using the Space Surveillance Network (SSN) to track debris greater than 10 cm in diameter in Low Earth Orbit (LEO) and objects greater than 1 m in Geostationary Orbit (GEO) [3].

Figure 1. 1: Orbital debris in LEO and GEO orbits [4]

The SSN uses a wide variety of ground-based radar and electro-optical sensor systems to find and track debris. Currently, from LEO and beyond the SSN has tracked over 24,500 objects orbiting the Earth [3]. In addition to the SSN, NASA also tracks orbital debris using statistical assessment methods. NASA tracks debris less than 10 cm in LEO and greater than 1 m in GEO [5]. Figure 1.2 shows the number of catalogued orbital debris from the launch of Sputnik 1 in 1957 to 2013 and it can be noticed that the amount of orbital debris is being increased drastically.

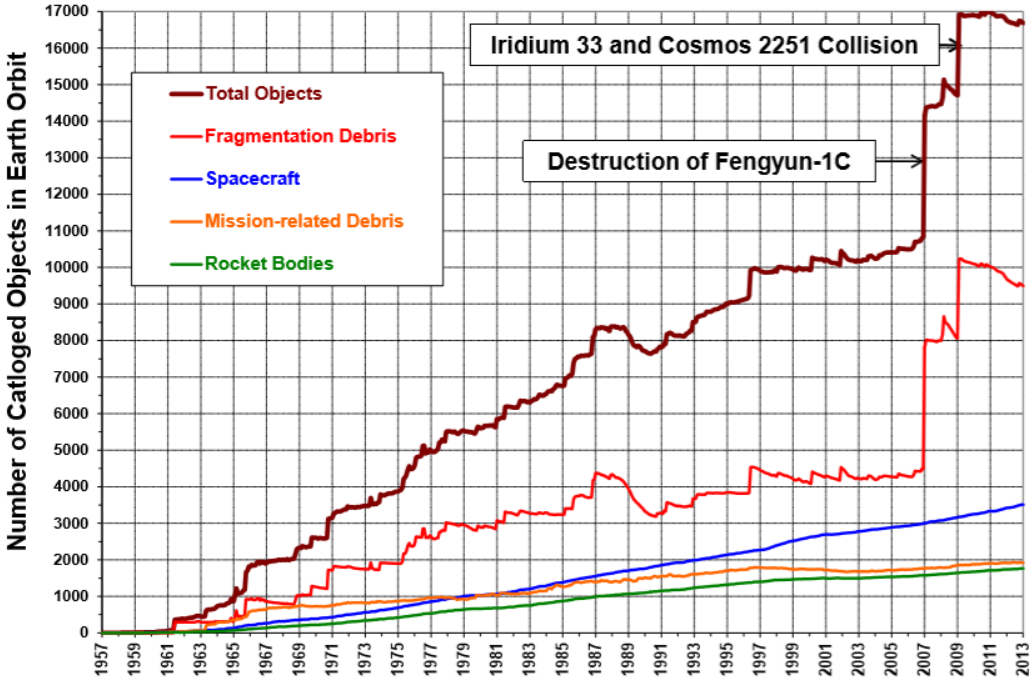

Figure 1. 2: Number of catalogued orbital debris from 1957 to 2013 [5]

According to NASA it is estimated that the total number of orbital debris in LEO greater than 10 cm will be greater than 11,000 by 2190 [5]. As the amount of orbital debris increases so does the probability of collisions. Therefore, the increased probability of collisions and the fast traveling speeds of orbital debris can be very harmful to future human and robotic space missions.

1.3 Electrodynamic Tethers and the DESCENT Mission

There have been various methods and concepts developed over the years to mitigate and reduce the amount of orbital debris around Earth's orbit. One of the most recent and appealing concepts is known as the Electrodynamic Tether (EDT). The EDT is a metal tether similar to a metal tape or wire that is suspended from a spacecraft or can be held between two spacecrafts. As the EDT moves across the Earth's magnetic field, electric charges are then collected from the ambient plasma that surrounds the Earth's orbit by the positively biased EDT. These charges move along the length of the tether to form an electric current if an electron emitter is installed at the

cathodic end of the EDT. The electric current then reacts with the Earth's magnetic field to produce a Lorentz force.

The Lorentz force (**F**) is a force experienced by a charged particle with charge q and velocity v, when it travels through an electric field (**E**) and magnetic field (**B**). This force is described using the following equation:

$$\boldsymbol{F} = q\boldsymbol{E} + qv \times \boldsymbol{B}$$

As it can be seen from the equation above, the Lorentz force is a combination of both electric and magnetic forces experienced by a charged particle. In an EDT system the Lorentz force then acts as an electrical 'drag' force to reduce the orbital speed of the spacecraft and thus deorbit the spacecraft much sooner than if the orbit of the spacecraft were to decay naturally. The EDT technology has great potential for deorbiting spacecrafts after their use and therefore, preventing the spacecraft from adding to the orbital debris field [6]. Additional advantages of the EDT technology include its compact size, low weight, no consumption of propellant, no need of an operational spacecraft and ease of operation [7].

The concept of the EDT shows that it has great potential for reducing orbital debris. As a result, there have been 12 missions launched in the past few decades to prove the effectiveness of the EDT [8]. Likewise, the Lassonde School of Engineering in partnership with Ryerson University and Honeywell Aerospace has been sponsored by the Canadian Space Agency (CSA) to launch its own mission to further analyze the feasibility of the EDT. This mission is known as DESCENT, which stands for DEorbiting SpaceCraft using ElectrodyNamic Tether. The mission consists of two 1U CubeSats (a satellite with dimensions 10 x 10 x 10 cm) placed in a Low Earth Orbit (LEO) at an altitude of roughly 400 km. The satellites will be connected together by a 100 m long aluminum tape tether. One of the 1U CubeSat's is referred to as the Mother Satellite and the other

1U CubeSat is referred to as the Daughter Satellite. The DESCENT mission makes use of the EDT technology to prove that the satellites can be deorbited within a specific time frame. The concept of operation of the EDT used in the DESCENT mission is shown in Figure 1.5.

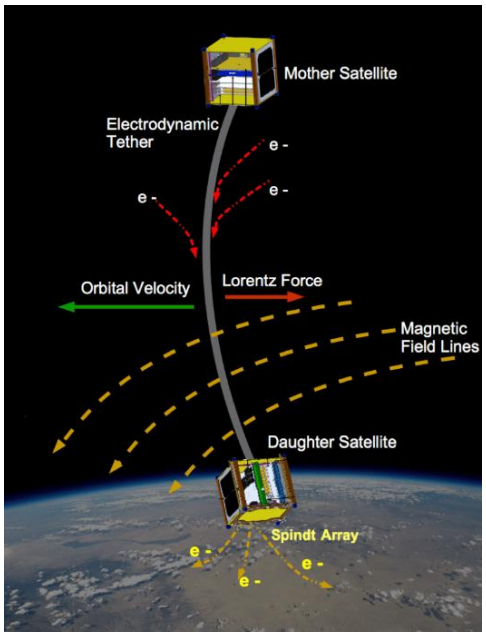

Figure 1. 3: Concept of operation for the DESCENT mission [9]

Without the use of the EDT, the natural orbital decay of the DESCENT satellites will take around 10 months. However, with the use of the EDT system, the expected deorbit time for the satellites is reduced to one week [9].

1.4 CubeSat Class Spacecraft

Spacecrafts come in a wide variety of classifications. The satellites used in the DESCENT mission are CubeSats which fall under the Nano Satellite classification. Nano Satellites are spacecrafts that weigh 1 to 10kg [10]. CubeSats in particular typically weight 1 to 1.33kg for 1-unit with dimensions of roughly 10 x 10 x 10 cm [10]. A 1-unit CubeSat is referred to as a 1U CubeSat and Figure 1.6 shows a typical model of a 1U CubeSat in orbit.

Figure 1. 4: 1U CubeSat in orbit [11]

However, CubeSats are not limited to being 1U in size. They can be stacked to form larger units. Larger units range from 2U to 12U (see figure 1.7).

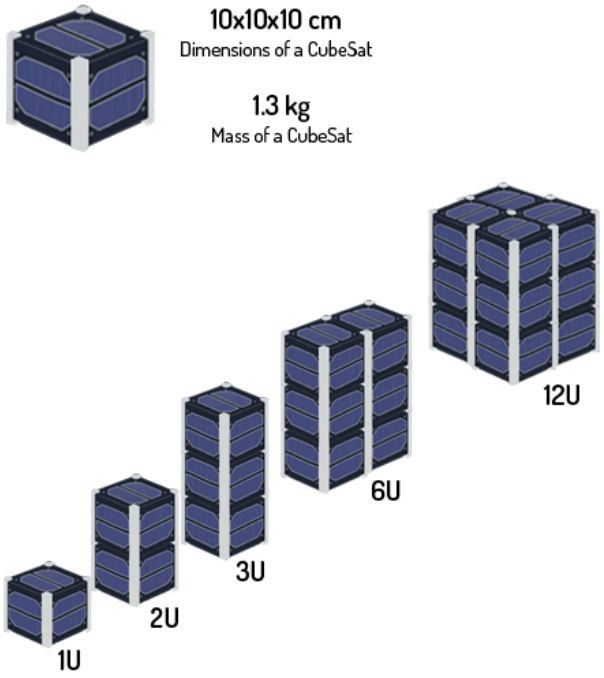

Figure 1. 5: Various CubeSat stack configurations [12]

The CubeSat standard was developed by California Polytechnic State University and Stanford University in the late 1990's to create a platform for university students to gain access to

space at a relatively affordable price [13]. Furthermore, the standard was created so that the satellites would be able to interface with the CubeSat deployer developed by California Polytechnic State University. This deployer is called the Poly Picosatellite Orbital Deployer (PPOD) [19]. Therefore, due to their simple design, affordable cost, and short development time, CubeSats were ideal to test the feasibility of the EDT.

1.5 Research Motivation

When developing the DESCENT spacecrafts there are multiple critical subsystems needed in order for the mission to fulfill its requirements. One of these major subsystems is the CubeSat structure. During the development of CubeSats, designers have two options to get access to the CubeSat structure. The first option is to buy Commercial of The Shelf (COTS) CubeSat structures from a third-party manufacturer (see figure 1.8).

Figure 1. 6: An example of a COTS CubeSat Structure [14]

The second option is to create a structure in-house. Both options have their own advantages and disadvantages, which are highlighted in table1.1.

Table 1. 1: COTS vs. In-House CubeSat Structure Development

	Advantages	Disadvantages
COTS	• No development time • Reliable structure • Basic structural tests required	• High cost • No learning opportunity
In-House Development	• Low cost • Allows learning opportunity • Can custom make structure	• Long development time • Advanced structural testing and simulations

As it can be seen from table 1.1 one of the main advantage of developing in-house CubeSat structures is the learning opportunity. In the previous section, it was mentioned that the CubeSat standard was first created to provide a platform for university students to develop satellites. Initially, the main target of CubeSats were to provide a learning experience for students. So, the motivation is to have the opportunity to design, validate and build an in-house structure that will ultimately provide a learning opportunity. Furthermore, by developing the satellite structures in-house, various lessons will be learned during different phases of the structure's development. These lessons learned can be shared with the CubeSat developer community to aid other developers in the construction of their CubeSat structures.

1.6 Research Justification

In addition to the reasons stated in the previous section, the DESCENT team decided to develop the CubeSat structures in-house because the DESCENT mission has multiple custom payloads that will be integrated into the CubeSats. By creating custom CubeSat structures will allow the flexibility for payload integration into the spacecraft structures. Since these are new

CubeSat structures a structural design must be created, and simulations must be done to validate the structural designs. Once this is completed, the structures can be used for future CubeSat missions that require the use of tethers. Additionally, the design methodology, validation techniques and lessons learned will provide meaningful data for future CubeSat developers.

1.7 Research Objectives

In order to successfully conduct the research in developing new CubeSat structures a series of objectives must be met. These objectives are listed below:

- Create a solid model of both DESCENT spacecrafts using a Computer Aided Design (CAD) software
- The structure must meet all the design requirements placed by the payloads and other bus components
- The structure must meet all the structural requirements outlined by the launch provider
- A Finite Element Model (FEM) of both spacecrafts must be created
- Structural and thermal simulations must be run to validate the structural integrity of the CubeSats
- Detailed technical drawings of structural parts must be completed for fabrication
- After fabrication is complete, a dry assembly and fit check of the structure must be completed

1.8 Research Method Approach

To meet the objectives outlined in the previous section, a series of steps are to be taken. These steps are outlined in figure 1.9.

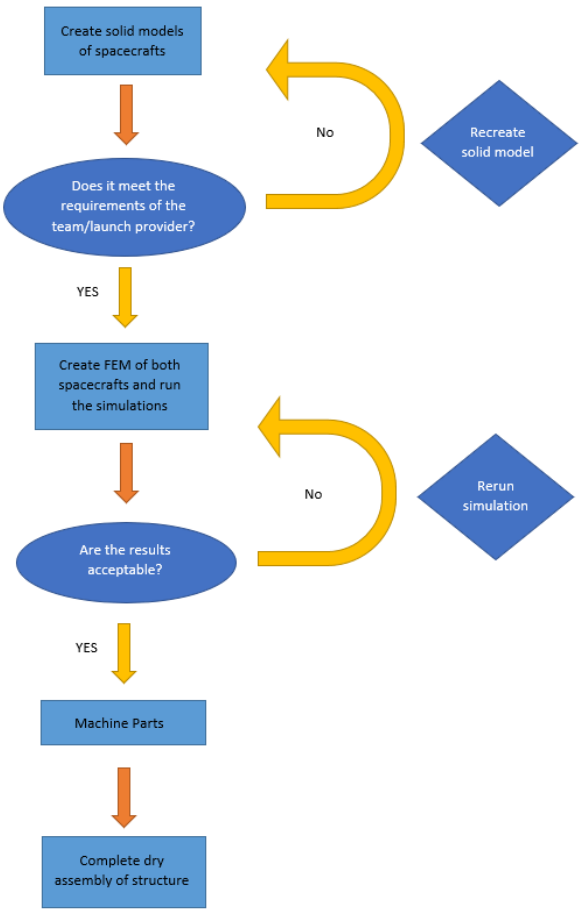

Figure 1. 7: Method of approach diagram

As it can be seen from Figure 1.9, the process to meet the objectives are recursive. Once the solid models are created, they must be checked with the payload team and the launch provider to confirm that the structure meets all their requirements. If the solid model does not meet the requirements, then the solid model must be remodeled until all the requirements are met. Likewise, the FEM must provide an acceptable output (accepted 1st natural frequency and temperature range). If the output is not acceptable then the FEM must be remodeled and, in some cases, the solid model would also have to be remodeled until the desired output has been reached. Finally, after the FEM provides the desired output, the structural components can be machined, and a dry assembly can be completed.

1.9 Thesis Document Layout

This section outlines the layout of the thesis document. In Chapter 1, an introduction was given regarding the motivation of the research and the procedure needed to complete the research. In chapter 2, a literature review will be conducted, showing the different types of CubeSat structures currently developed by other researchers. Chapter 3 will show an overview of the NanoRacks CubeSat Deployer (NRCSD) and its interface requirements. It will also give an overview of the requirements needed by the payloads and other bus components. Then in chapter 4 the solid model of the CubeSats will be displayed and a summary will be made on how the structure meets all the requirements. In chapters 5 and 6 the FEM of both satellites will be discussed, and the results of the simulations will be shown. Chapter 7 will show how the detailed drawings of the structural components were created and the dry assembly of the CubeSat structures has been completed. Finally, in chapter 8 a summary of the results of this paper will be conducted as well as the future work plan will be outlined.

Chapter 2 LITERATURE REVIEW

2.1 Introduction

In this chapter of the thesis, the literature review will be completed. There are numerous CubeSat missions that have been developed worldwide. This literature review will describe a variety of CubeSat missions and their structural designs.

2.2 TRIO CINEMA CubeSat Structure

TRIO (TRiplet Ionospheric Observatory) CINEMA (CubeSat for Ion, Neutral, Electron, MAgneticfields) is a 3U mission developed by the School of Space Research at Kyung Hee University, Space Science Lab at University of California, Berkeley and Imperial College in London, England [15]. The primary objective of the mission is to provide measurements of space weather, and high sensitivity mapping of ENAs (Energetic Neutral Atoms), in low Earth orbit. Figure 2.1 shows a model of the TRIO CINEMA CubeSat.

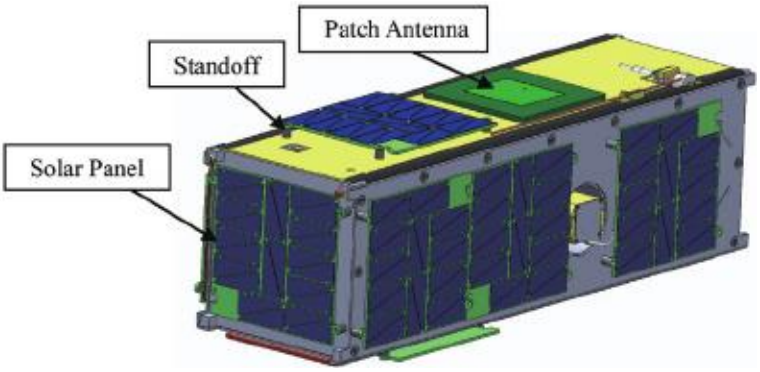

Figure 2. 1: Solid model of TRIO CINEMA Spacecraft [15]

The spacecraft chassis is built completely from aluminum 6061-T6 except for the top and bottom plates, which are made from aluminum 5052-H32. The TRIO CINEMA spacecraft has dimensions of 10 x 10 x 30 cm and has a mass of 2.726 kg. The spacecraft interfaces with the Poly Picosat Orbital Deployer (PPOD) launcher and the TRIO CINEMA team modeled the spacecraft to meet all the interface requirements.

Next, the team created a FEM of the spacecraft and ran a mechanical analysis, which includes a normal modes analysis and a vibrational analysis. After completing the normal modes analysis, the first order natural frequency was found to be at 339.1 Hz. Figure 2.2 shows the CubeSat's excitation at this frequency.

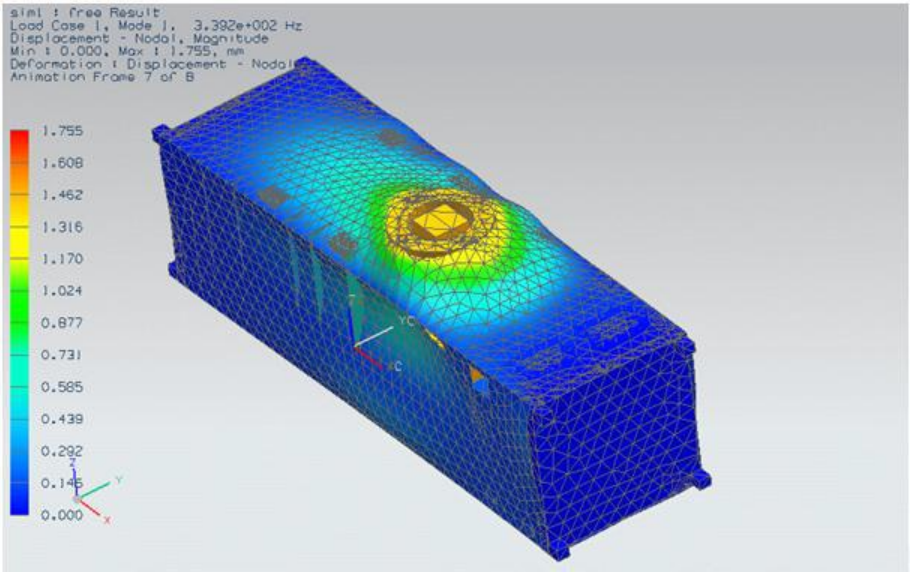

Figure 2. 2: First natural frequency excitation of TRIO CINEMA [15]

Next, a random vibrational analysis was conducted using a random vibrational profile obtained from PPOD. The vibrational simulation was run in all 3 axes (X, Y and Z). The results of the vibrational simulation are shown in table 2.1.

Table 2. 1: Result for the Vibrational Simulation

Direction	**Maximum Displacement**	**Direction**	**Maximum Stress**
X	0.272 [mm]	XY	2459 [MPa]
Y	0.494 [mm]	YZ	2521 [MPa]
Z	0.421 [mm]	ZX	1721 [MPa]

Finally, a thermal analysis was conducted to determine the temperature range of the spacecraft and its vital components. A separate and more simplified FEM was generated for the thermal analysis. Figure 2.3 shows the FEM used for the thermal analysis.

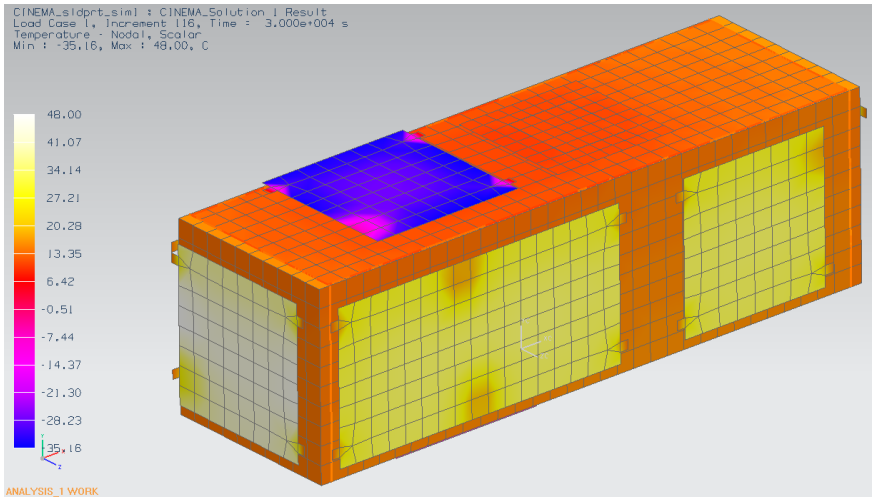

Figure 2. 3: FEM used for the thermal analysis [15]

The simulation was run for 5 orbits and the results of the simulation are summarized in table 2.2.

Table 2. 2: Results from the thermal analysis

Components	**Analysis Temperature (℃)**
Chassis	avg:+10℃ , +4to +13
Solar Panels (Top & bottom)	avg:-23℃ , -46 to 0
Solar panels(side)	avg:+5℃ , -49 to +42
AvionicsPCB	avg:-7℃ , -14 to 0
Magnetometer	avg:+93℃ , +87to +98
STEINDetector	avg:-5℃

2.3 ECOSat-III CubeSat Structure

ECOSat stands for Enhanced Communications Satellite and is a 3U CubeSat developed by the University of Victoria. Aboobakar gives a detailed overview of the structural and thermal analysis of the ECOSat CubeSat in her paper *Dynamic and Thermal Models for ECOSat-III* [16]. The CubeSat has dimensions of 10 x 10 x 34 cm and has a mass of 4.0 kg. Figure 2.4 shows the model of the satellite.

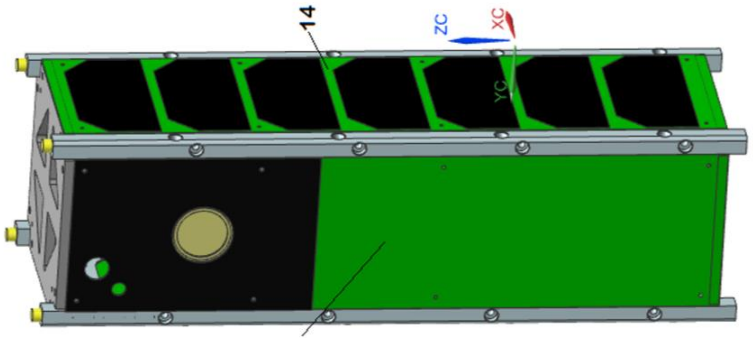

Figure 2. 4: Solid model of the ECOSat-III CubeSat [16]

After the completion of a solid model, the team created a FEM to run a normal modes analysis of the spacecraft. The FEM of ECOSat is shown in Figure 2.5.

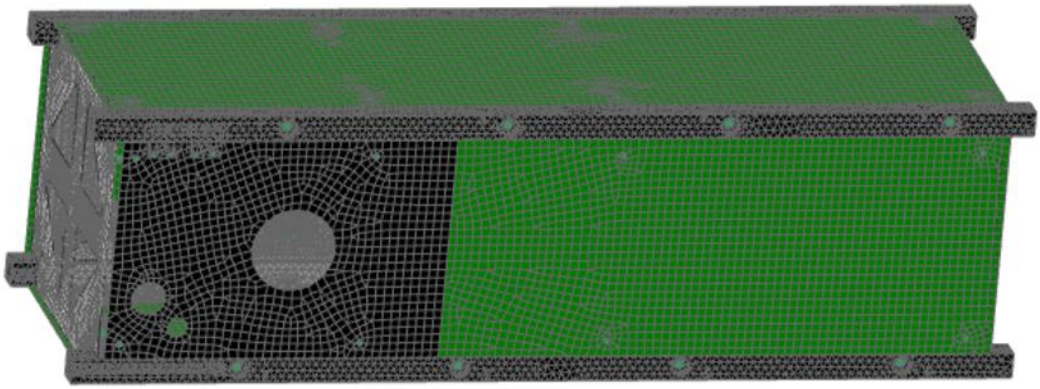

Figure 2. 5: FEM of the ECOSat-III CubeSat [16]

After conducting the normal modes analysis, the first order natural frequency was found to be 248.7 Hz, thus proving that the CubeSat structure is rigid. Next, the thermal analysis was conducted for the spacecraft. A second and more simplified FEM was created for the thermal analysis and is shown in Figure 2.6.

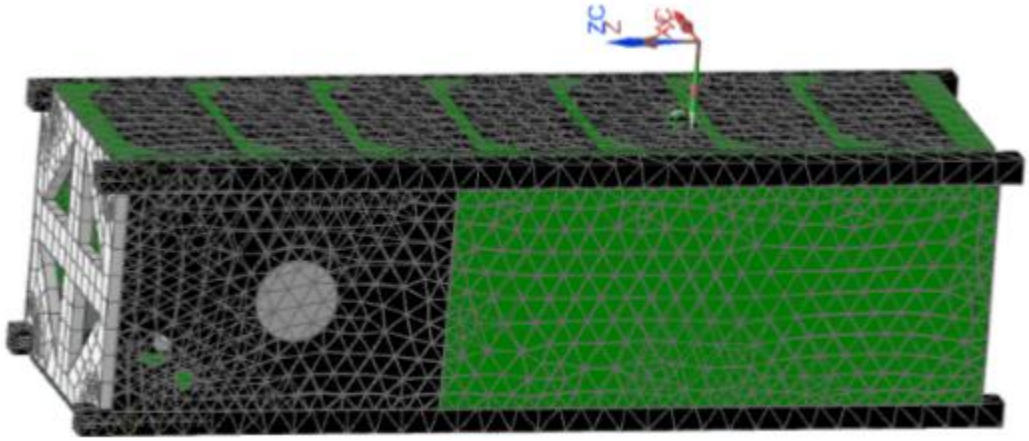

Figure 2. 6: FEM of ECOSat-III used for the thermal analysis [16]

Two different orbits at two different launch times were used for the simulation. The maximum and minimum temperatures are shown in table 2.3.

Table 2. 3: Temperatures Ranges for Two Different Orbits and Launch Times

Altitude	Launch	Position	$T_{\max}$	$T_{\min}$
600 km	9 am	Aphelion	12.7	-17.41
		Perihelion	45.8	-9.1
	12 pm	Aphelion	29.3	-12.5
		Perihelion	62.8	-4.2
800 km	9 am	Aphelion	11.8	-17.4
		Perihelion	50.2	-7.6
	12 pm	Aphelion	28.3	-13.7
		Perihelion	62.5	-4.5

2.4 ITU-pSAT II CubeSat Structure

ITU-pSAT II is a 3U student satellite project that seeks to demonstrate an advanced three axis Attitude Determination and Control System (ADCS) experiment. In their paper *Design and Analysis of an Innovative Modular CubeSat Structure for ITU-pSAT II*, Melahat Cıhan et.al described the details of the ITU-pSATs structural design [17]. The CubeSat must interface with the PPOD launcher, so its maximum dimensions are 10 x 10 x 30 cm and has a mass no greater than 4 kg. Aluminum 7075 was chosen as the material for the CubeSat structure due to its light weight, manufacturability, thermal expansion, strength and cost. Figure 2.7 shows the solid model of the ITU-pSAT CubeSat.

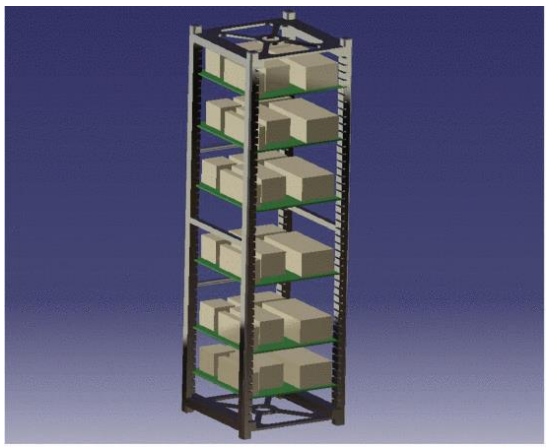

Figure 2. 7: ITU-pSAT CubeSat solid model [17]

After the creation of a solid model, a FEM was created to conduct a normal modes analysis for the CubeSat structure. Table 2.4 shows the first 31 modes of the ITU-pSAT CubeSat.

Table 2. 4: Normal Modes of the ITU-pSAT CubeSat

Modes	Natural Frequencies (Hz)	Modes	Natural Frequencies (Hz)
1	216,25	17	1317,7
2	730,57	18	1331,9
3	769,53	19	1338,1
4	775,01	20	1338,8
5	788,06	21	1359,1
6	802,12	22	1379,8
7	843,02	23	1386,9
8	1086,6	24	1439,4
9	1193,2	25	1538,9
10	1221	26	1596,3
11	1226,3	27	1610,7
12	1239,2	28	1630,7
13	1244,1	29	1807,9
14	1272,7	30	1820,6
15	1276	31	1917,6
16	1293,1		

Finally, Figure 2.8 shows the deformation of the structure at its first natural frequency.

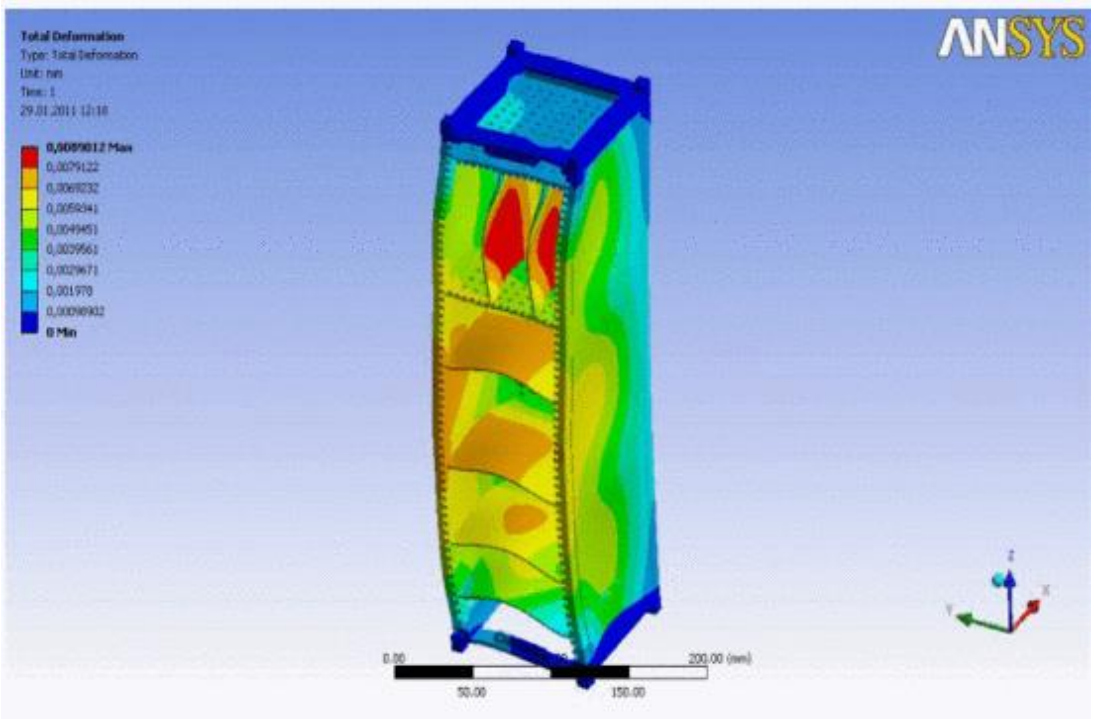

Figure 2. 8: Deformation of ITU-pSAT CubeSat at the first normal mode

2.5 KUFASAT CubeSat Structure

KUFASAT is a 1U CubeSat mission developed by the students at Kufa University in Iraq. Firas T et.al has written the paper *Structural Analysis of KUFASAT using ANSYS Program* and includes details on the development of the KUFASAT structure [18]. In this paper the normal modes analysis is completed for three different CubeSat structures. The geometry of the structures are identical; however, their materials vary. The three different materials considered for the spacecraft chassis are Aluminum 5052-H32, Aluminum 6061-T6, and Aluminum 7075-T6. The properties of the three materials are shown in Table 2.5

Table 2. 5: Material properties of Al 5052-H32, Al 6061-T6, and Al 7075-T6

Material	Aluminum 5052-H32	Aluminum 6061-T6	Aluminum 7075-T6
Physical Properties			
Density	2680 kg/m^3	2700 kg/m^3	2810 kg/m^3
Mechanical Properties			
Ultimate Tensile Strength	228 MPa	310 MPa	572 MPa
Tensile Yield Strength	193 MPa	276 MPa	503 MPa
Modulus of Elasticity	70.3 GPa	68.9 GPa	71.7 Gpa
Poisson's Ratio	0.33	0.33	0.33

Using the above values, the FEM was created for the KUFASAT and the normal modes simulation was run for all three structures. The results are shown in Table 2.6.

Table 2. 6: Results of the Normal Modes Analysis for all Three Structures

Modes	Aluminum 5052		Aluminum 6061		Aluminum 7075	
	Freq. [Hz]	Def. [m]	Freq. [Hz]	Def. [m]	Freq. [Hz]	Def. [m]
1	643.819	0.146	654.738	0.146	654.705	0.143
2	646.573	0.152	657.454	0.151	657.422	0.148
3	726.275	1.101	736.065	0.997	736.029	0.978
4	736.421	0.111	746.073	0.110	746.036	0.108
5	805.090	0.123	813.803	0.122	813.763	0.120

Figure 2.9 shows the deformation at the first normal mode of the KUFASAT structure for aluminum 6061 and aluminum 7075.

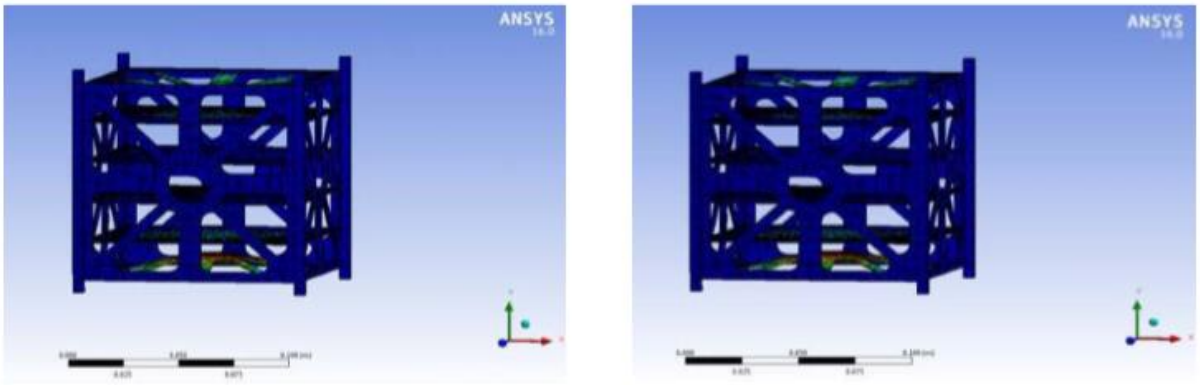

a. Mode 1: Al-6061: Def=0.146 m

b. Mode 1: Al-7075: Def=0.143 m

Figure 2. 9: a) First mode for Al 6061 b) First mode for Al 7075 [18]

It can be noticed from table 2.6 that aluminum 6061 and 7075 have the similar frequencies for the normal modes. Therefore, either material is capable of serving as the CubeSats structure. However, it can be seen from figure 2.9 that during its first normal mode, aluminum 7075 has a lower maximum deformation then aluminum 6061. Thus, Aluminum 7075 was chosen for the KUFASAT structure.

Chapter 3 REQUIREMENTS FOR STRUCTURAL DESIGN

3.1 Introduction

One of the major advantages of the standardized size of CubeSats are its ability to interface with CubeSat deployers. There are two popular CubeSat deployers used by most developers. Mentioned in section 1.4, the first deployer is called the Poly Picosatellite Orbital Deployer (PPOD) and is a deployer developed by California Polytechnic State University [19]. Figure 3.1 shows an image of the PPOD CubeSat deployer.

Figure 3. 1: PPOD CubeSat deployer [20]

The second popular CubeSat deployer is the known as the NanoRacks CubeSat Deployer (NRCSD) and is developed by a private organization called NanoRacks [21]. Figure 3.2 shows an image of the NanoRacks deployer

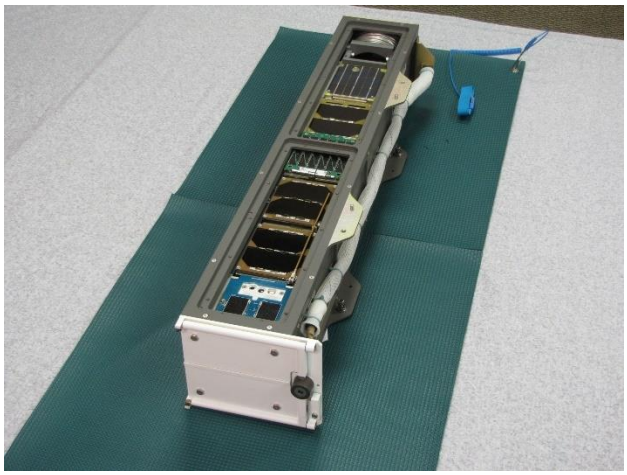

Figure 3. 2: NanoRacks CubeSat deployer [22]

Regardless of the choice of CubeSat deployers, CubeSat developers must design the CubeSat structure to meet the requirements of the CubeSat launch provider. In addition to the requirements placed by the launch providers, the CubeSat structure must also follow the requirements placed by the payloads, other bus components and the mission itself. The following chapter will highlight the mission requirements, design requirements and the structural requirements. Then the procedure to create a structural design and Finite Element Analysis (FEA) will be outlined.

3.2 Description of the NRCSD

For the DESCENT mission the NRCSD will be used as the CubeSat deployer. Therefore, before developing the CubeSat structure it is worth understanding the NRCSD itself. The details for the NRCSD are obtained from the *NanoRacks CubeSat Interface Control Document* [21]. The NRCSD is a rectangular tube/rack that can fit up to six 1U CubeSats. One end of the rack contains the deployer doors, this is where the CubeSats will exit the rack. The opposite end of the rack contains the base plate with a compressed spring. This end of the rack will use the spring to push the CubeSats out of the rack. Finally, on the top face of the rack are access panels. These are

windows that give access to CubeSat faces that contain Remove Before Fight (RBF) pins and charging systems. Figure 3.3 shows the outer dimensions of the NRCSD, Figure 3.4 shows the top view of the NRCSD along with the access panel dimensions and Figure 3.5 shows the coordinates used to describe the NRCSD.

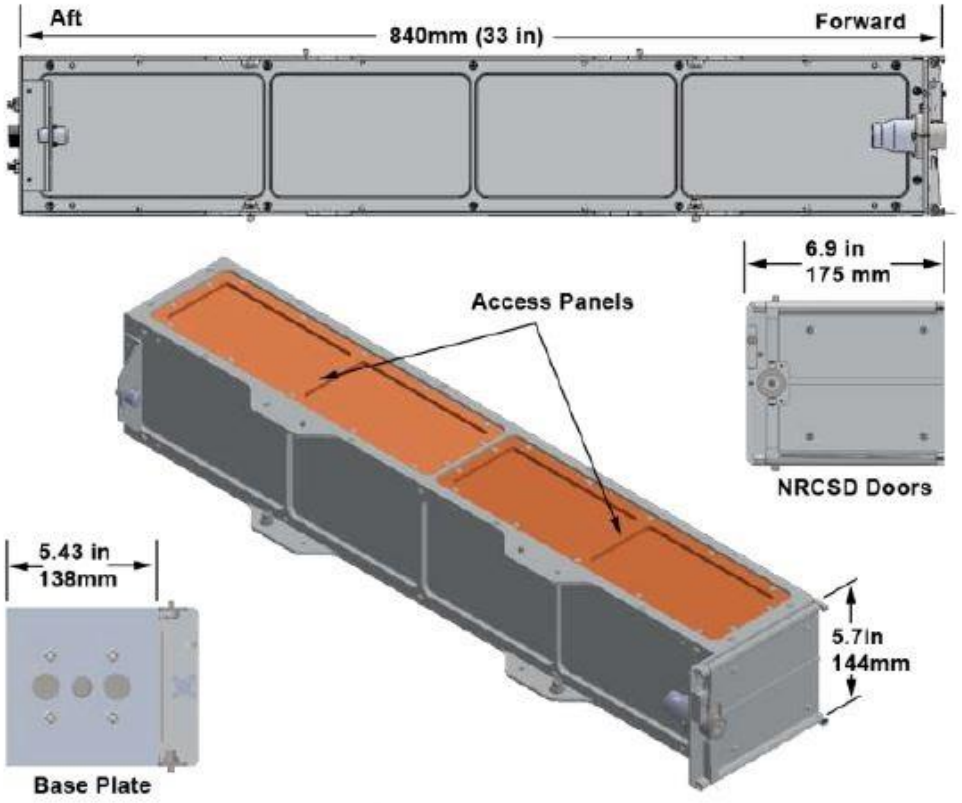

Figure 3. 3: Outer Dimensions of the NRCSD [21]

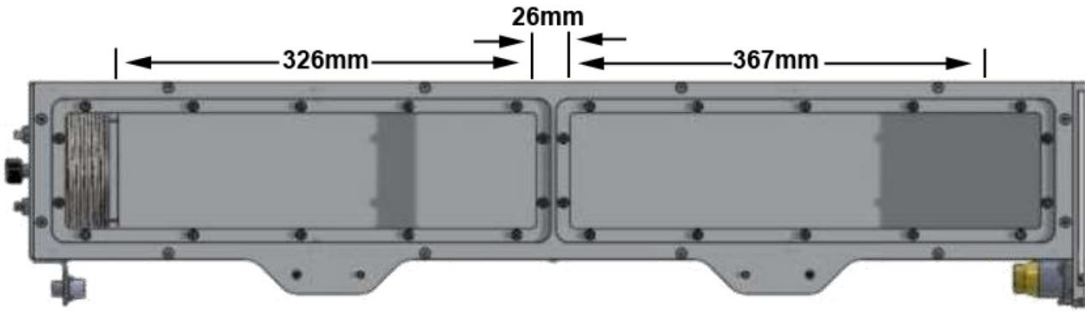

Figure 3. 4: Top view of the NRCSD and access panel dimensions [21]

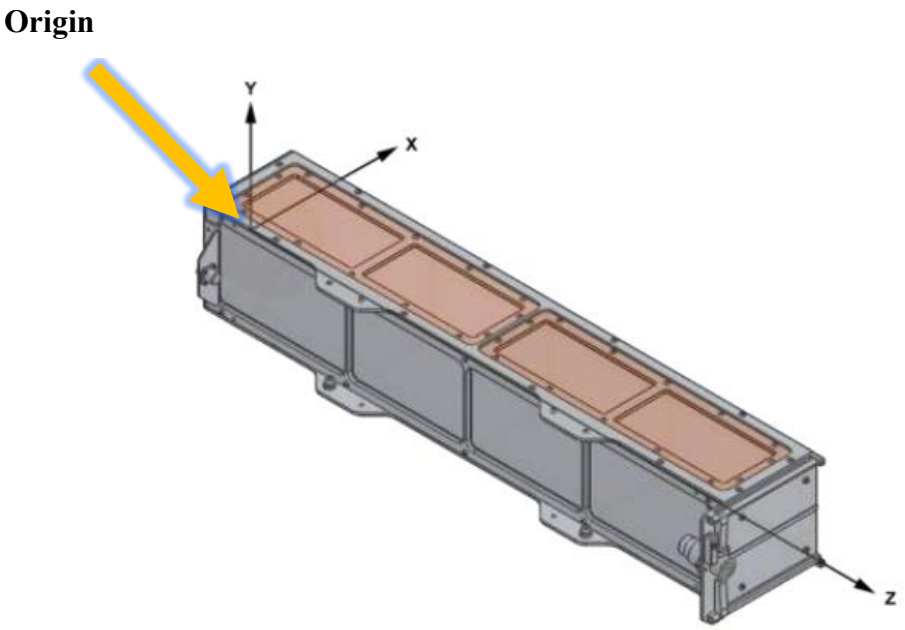

Figure 3. 5: Coordinates for the NRCSD [21]

3.3 Mission Requirements

The DESCENT mission has a number of requirements for the design of the CubeSat structure. These requirements need to be fulfilled to ensure that the mission is successful. The requirements for the mission are as follows:

- The structure shall be able to house the EDT before deployment
- The EDT shall be attached to both spacecraft structures once deployed
- The structure shall survive launch
- The structure shall withstand all thermal loads in orbit
- All components shall be able to mount to the spacecraft chassis

3.4 Design Requirements

The NRCSD has placed a number of requirements for the design of the CubeSats. These requirements are not specific to the structure but are applied to the CubeSat as a whole. The main

purpose of these requirements are to provide general requirements for CubeSat developers. They also place a minimum standard for the interface with the NRCSD. The following is a list of all the design requirements obtained from the *NanoRacks CubeSat Interface Control Document*:

- CubeSats shall be passive and self-contained from the time they are loaded into the NRCSD for transport to the ISS and until after deployment from the NRCSD. No charging of batteries, support services, and or support from ISS crew is provided after final integration.
- CubeSats shall not contain pyrotechnics unless the design approach is pre-approved by NanoRacks. Electrically operated melt-wire systems for deployables that are necessary controls for hazard potentials are permitted.
- CubeSats must have a timer (set to a minimum of 30 minutes) before satellite operation or deployment of appendages. If deploy switches should be released causing the timer to run, the timer must automatically re-set whenever the Remove Before Flight (RBF) feature is replaced and/or the deploy switches are returned to the open state.
- CubeSats should not have detachable parts or create any space debris during launch or normal mission operations.
- CubeSats shall use a secondary locking feature for fasteners external to the CubeSat chassis. An acceptable secondary locking compound is LocTite. Contact NanoRacks for the proper locking compound application procedure. Other secondary locking methods must be approved by NanoRacks.

3.5 Structural Requirements

In addition to the requirements shown in the previous section further structural requirements are specified so that the CubeSats can interface correctly with the NRCSD. These set of design requirements are placed specifically on the CubeSat structure. The first major

requirement is the outer dimensions of the CubeSat. Depending on the number of units of the CubeSat (example 1U, 2U, etc.) there are specific end to end lengths the CubeSat can be. These lengths are shown in figure 3.6.

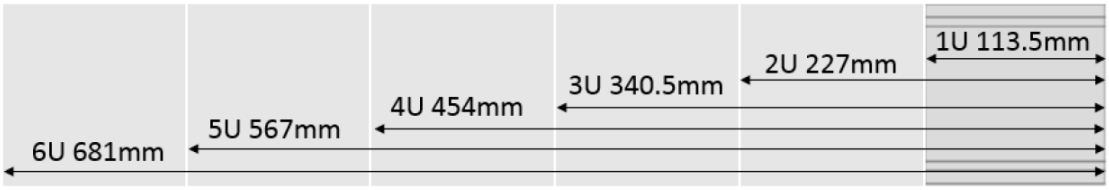

Figure 3. 6: CubeSat end to end lengths for different CubeSat configurations [21]

The envelope dimensions for the CubeSats are shown in figure 3.7 and is independent of the CubeSat configuration.

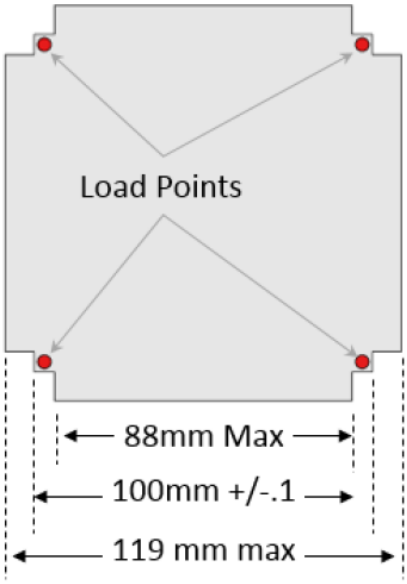

Figure 3. 7: Dimensions of CubeSat envelope [21]

The next requirement is not specific to the structure of the CubeSat but applies to the CubeSat as a whole and this is the mass requirement. Depending on the configuration of the CubeSats, different mass requirements are placed. The mass requirements are shown in table 3.1.

Table 3. 1: CubeSat Mass Requirements

Form Factor	Maximum Mass (Kg)
1U	2.82
2U	5.657
3U	8.485
4U	11.314
5U	14.142
6U	16.971

Furthermore, the center of gravity of the satellite must be within 2cm of its geometric center.

Next, NanoRacks requires that each CubeSat contains 3 mechanical deployment switches on 3 separate CubeSat rails/posts. The purpose of these switches are to inhibit the main electrical power system from operating before deployment of the CubeSat. The *NanoRacks CubeSat Interface Control Document* states the following requirements for the deployment switches:

- Deployment switches can be of the pusher variety, located on the –Z face on one or more of the rail end faces, or roller/lever switches embedded in a CubeSat rail and riding along the NRCSD guide rail
- A roller or slider shall be centered on the deployer guide rail, allowing for placement accuracy, the roller or slider shall maintain a minimum of 75% (ratio of roller/slider width-to-guide rail width) contact along the entire Z-axis
- Deployment switches force exerted shall not exceed 3N

Furthermore, CubeSats that are not 6U CubeSats must contain two separation springs on diagonal rails of the CubeSats. This is shown in figure 3.8.

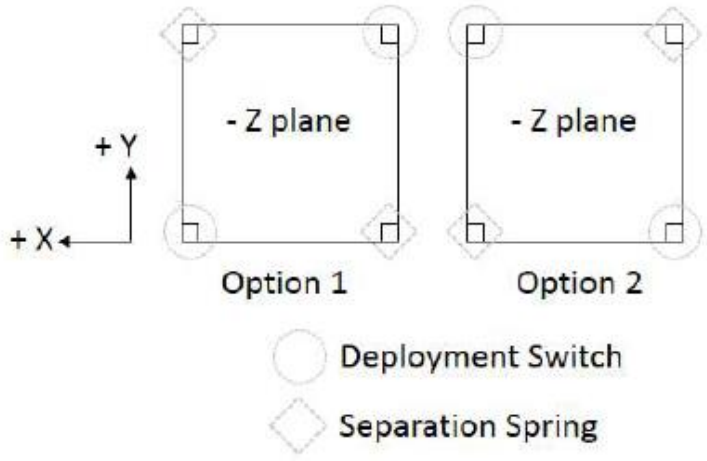

Figure 3. 8: Placement of separation springs [21]

The purpose of the separation springs is to ease the deployment process of the CubeSats relative to other CubeSats contained within the rack. The *NanoRacks CubeSat Interface Control Document* states the following additional requirements for the separation springs:

- Each spring shall be captive. When compressed the spring shall be contained within the maximum rail length
- Individual separation spring force shall not exceed 3.34 N (0.75 lbs) with the total force for both springs not to exceed 6.67 N (1.5 lbs)

Next, NanoRacks places requirements on the CubeSat rails. These requirements are stated in the *NanoRacks CubeSat Interface Control Document* and are as follows:

- A CubeSat shall have four (4) rails, one per corner, along the Z axis.
- Each rail shall have a minimum width of 6mm +0.1mm/ -0.0mm tolerance.
- The edges of the rails shall be rounded to a radius of at least 0.5mm +/-.1mm.
- Each rail end face shall have a minimum surface area of 4mm x 4mm for contact with the adjacent CubeSats.
- The minimum extension of the CubeSat rail standoffs beyond the CubeSat +/-Z face shall be

6.5mm

- Rail length variance in the Z axis between rails shall not exceed ± 0.1 mm
- CubeSat rail surfaces that contact the NRCSD guide rails shall have a hardness equal to or greater than hard anodized aluminum (Rockwell C 65-70).

This concludes the requirements the launch provider requires for the CubeSats. When developing the CubeSat structures, it is vital to incorporate these requirements into the design.

3.6 Payloads and Bus Components Requirements

Similar to requirements placed by the CubeSat deployer, the payloads and other CubeSat bus components also place requirements onto the CubeSat structure. In this subsection of the paper, each payload and its requirements will be outlined. Then, the other CubeSat bus components and their requirements will also be covered.

One of the primary objectives of the DESCENT mission is to test the feasibility of an EDT. Therefore, an EDT must be stored within one of the two 1U CubeSats. A 100 m aluminum tape tether of 5 mm width and 60µm thickness will act as the EDT. The EDT will be stored inside a Tether Storage Box. Figure 3.9 shows the exterior and interior of the tether storage box.

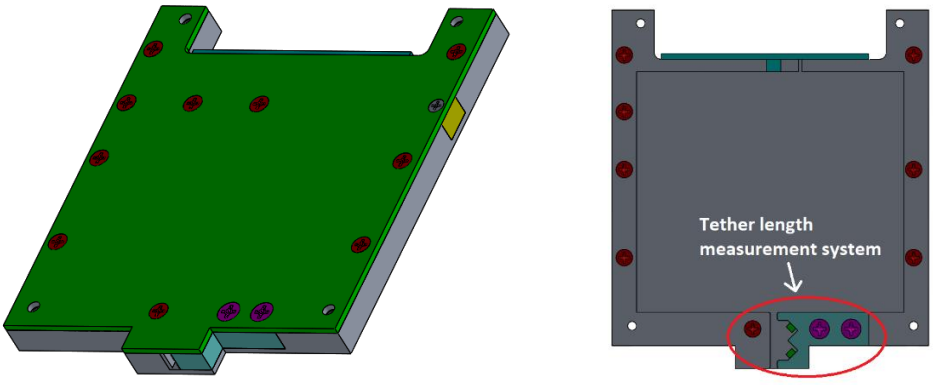

(a) **(b)**

Figure 3. 9: a) Exterior of tether storage box b) Interior of tether storage box

In figure 3.9 b) there is a secondary payload within the tether storage box called the Tether Length Measurement System. This device uses a LED and photodiode combination to measure the post deployment length of the EDT. Due to the addition of the length measurement system inside the storage box a portion of the bottom face of the storage box was extruded outwards. The CubeSat structure must consider the placement of the tether storage box and the extrusion due to the length measurement system.

The next payload is known as the Spindt Array. The spindt array is a series of miniature needles spread out on a 2-dimensional rectangular plane that emit electrons into the surrounding environment. In DESCENT the spindt array will be used to draw the electrons from the EDT and then will emit these electrons back into the plasma surrounding the spacecrafts. By doing so a closed current loop is formed within the EDT and the Lorentz force can be formed to decelerate the spacecrafts. Figure 3.10 shows the model of the spindt array.

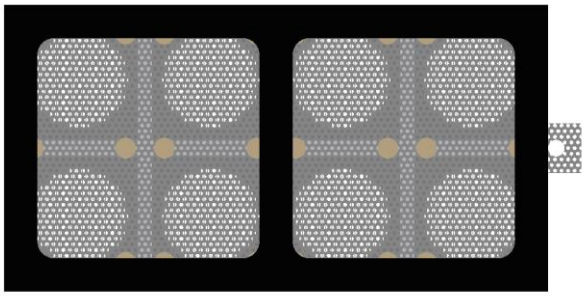

Figure 3. 10: Spindt array used for DESCENT

The spindt array must be mounted onto an exterior face of one of the CubeSats. So, the spacecraft structure must provide a suitable mounting point for the spindt array. Furthermore, it is also important to keep the spindt array mesh electrically insulated from the CubeSat chassis.

The next payload is the SCIENCE payload. This payload is an external auxiliary payload developed by a reach team from the Suborbital Payload Research Centre/ Nanosatellite Research Laboratory in York University. The payload aims to test a new solar panel coating that will increase

the efficiency of solar panels. Figure 3.11 shows the Science Payload PCB.

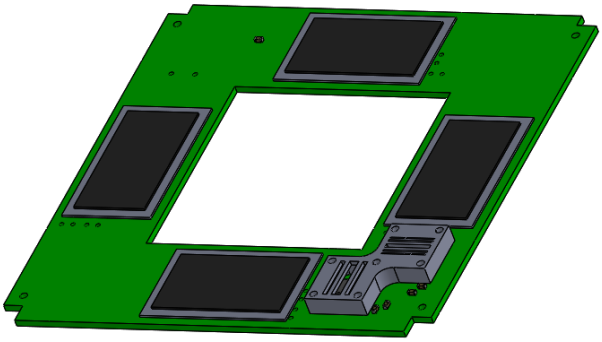

Figure 3. 11: Model of the SCIENCE Payload PCB

The SCIENCE payload contains four solar cells attached to a single PCB. The payload must be mounted to an exterior face of one of the CubeSats.

The final payload onboard the DESCENT spacecraft is the SUGAR Payload. This device is also an auxiliary payload developed by an external research team. The payload is a solar proton detector developed by a research team in the University of Sydney. The SUGAR payload is a PCB that contains a dosimeter to detect the energy levels and density of solar protons found in LEO. Figure 3.12 shows the image of the SUGAR dosimeter.

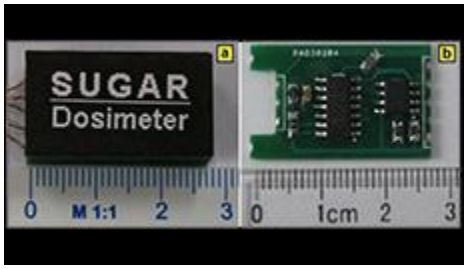

Figure 3. 12: SUGAR dosimeter [23]

The sugar dosimeter will be placed on a PC104 PCB board; therefore, the payload must be mounted within one of the DESCENT CubeSats.

The first bus component that needs to be placed onto the CubeSat structure is an Ultra High Frequency (UHF) antenna. The antenna used on the DESCENT mission is the GOMspace

NanoCom ANT430. It is a deployable, omnidirectional, canted turnstile antenna system with rigid antenna elements [24]. The UHF antenna is needed for the daughter spacecraft to communicate with the ground station. When the spacecraft establishes communicates with the ground station it can send and receive telemetry and control data. Figure 3.13 shows the model of the ANT430 antenna.

Figure 3. 13: UHF antenna used for DECSENT [25]

The antenna must be mounted on the nadir face of the spacecraft in lower altitude so that the antenna lobe can be pointed towards the ground station on the Earth. The CubeSat structure must be designed so that when the antenna is in its stowed configuration, the antenna rods will not interfere with the walls of the CubeSat deployer.

The second spacecraft bus components are the solar panels. The solar panels used for DESCENT are purchased from ClydeSpace. The solar panels are needed to power the spacecraft during the daylight. They are also used to recharge the onboard batteries. Figure 3.14 shows the model of the ClydeSpace solar panels.

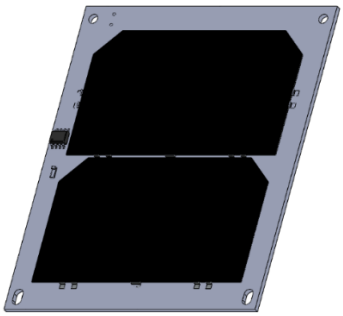

Figure 3. 14: Solar panels used for DESCENT

The solar panels are for a 1U CubeSat and each panel contains two Spectrolab UTJ solar cells. There shall be a minimum of 4 solar panels on each DESCENT CubeSat. This will allow for the maximum usage of the solar cell area.

The third spacecraft bus components are two cameras. Its decided by the DESCENT team that one of the CubeSats will use two Raspberry PI Zeros in cold redundancy as an On-Board Computer (OBC). Therefore, it is convenient to use Raspberry PI cameras. Figure 3.15 shows the PI cameras that will be used for the mission.

Figure 3. 15: Camera used for DESCENT mission [26]

The PI cameras provide many advantages for the mission. The cameras are light weight, small in size and are compatible with the Raspberry PI Zero. The main purpose of the cameras is to record the separation of the two CubeSats and the deployment of the tether. Secondary usage of the cameras is to take pictures of the Earth. The CubeSat structure must allow for a mount so that the cameras are able to get a clear view of the separation of the spacecraft and the deployment of the tether.

Chapter 4 STRUCTURAL DESIGN OF DESCENT CUBESATS

4.1 Introduction

In this chapter the complete structural design of the DESCENT CubeSats will be covered. To begin, the design objectives of the satellite structures will be outlined. Next, details of individual components of the structure will be covered. Then, the structural parts will be put together into a complete assembly for each satellite. The payloads and bus components will then be mounted to the CubeSat structures. Finally, both CubeSats will be connected together into a single 2U CubeSat assembly. This is the configuration of the DESCENT CubeSats before deployment and separation.

4.2 Design Objectives

In order to design suitable CubeSat structures a series of objectives must be met. This section of the paper will state these objectives and how they will be met during the design phase of the structures. To begin, the first objective is to create solid models of individual CubeSat structural components. These models must meet all the requirements placed by the NanoRacks deployer, payloads and bus components as stated in chapter 3. Once the models have been created the second objective is to create a complete solid model assembly of the spacecraft structures. The third objective is to verify that the completed assemblies have the correct outer dimensions and the tolerances are within the NanoRacks requirements for the NRCSD. Finally, the fourth objective is to create a solid model assembly of the 2U satellite, as this is the configuration in the NRCSD.

4.3 Detailed Structural Component Designs for Daughter Satellite

The details pertaining to the daughter satellite's structural design will be covered in this chapter. This includes the individual structural components and the solid model of the satellite's complete assembly.

4.3.1 Daughter Satellite's Rails

When designing the rails, the first step is to select the material. According to section 3.5 for the rail requirements placed by NanoRacks, the CubeSat rails must have a Rockwell hardness greater than Rockwell C 65-70. Stainless Steel 316 was chosen as the rail material. Appendix A1 shows the material properties of stainless steel 316. The Rockwell hardness of stainless steel 316 is Rockwell C 95. Therefore, the material selected meets NanoRacks' hardness requirement. An added benefit of stainless steel 316 is that it is not magnetic. This is a major advantage as the material will not interfere with the CubeSat's electronics, communication systems and magnetic torquers used for attitude control. Figure 4.1 shows the CAD model of the daughter CubeSats post. It can be seen from the figure that all the NanoRacks requirements for the posts are met.

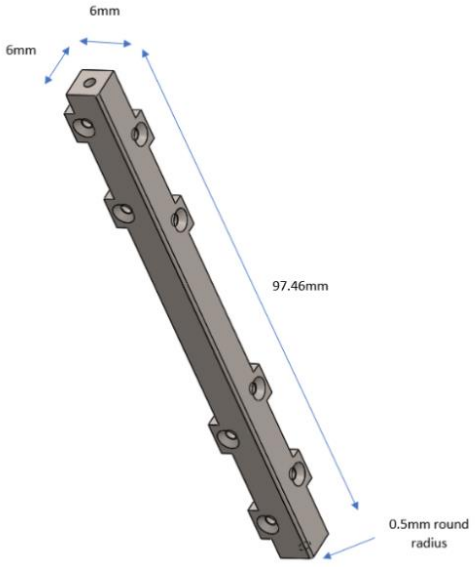

Figure 4. 1: CAD model of daughter satellite post

It was stated in section 3.5 that each CubeSat is required to have three deployment switches to inhibit the electrical system from activating the CubeSat before deployment from the NRCSD. For the DESCENT CubeSats, it was decided to place the three deployment switches along the three CubeSat rails. Therefore, three of the daughter satellite's rails were modified to house the deployment switches. This is shown in Figure 4.2.

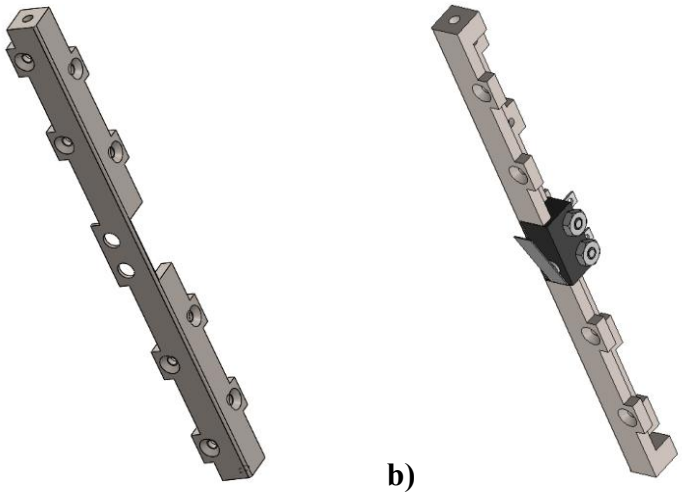

a) **b)**

Figure 4. 2: a) Daughter post with switch housing b) Daughter post with switch

In Figure 4.2 b), it can be seen that the housing perfectly fits the deployment switch. The Honeywell ZX Series deployment switch, which is a lever type switch is used for the deployment switches on both the daughter and mother CubeSats.

4.3.2 Daughter Satellite's Walls

The next major CubeSat structural components are the CubeSat walls. The walls are used to encapsulate the satellite and provide fixtures for the CubeSat posts/rails. Using stainless steel 316 for the walls would be acceptable, however the high density of stainless steel 316 would lead to a higher weight. So, a strong but light weight material is needed. Aluminum 6061-T6 meets this requirement and the specifications for this material is shown in appendix A1. It is desired to maximize the interior volume of the CubeSat so that there is sufficient room for interior

components and cables. On the other hand, it is necessary that the thickness of the walls are sufficient enough to hold enough threads to mount the CubeSat solar panels. Taking these two factors into consideration, a wall thickness of 1.6 mm was chosen. Figure 4.3 shows the daughter CubeSat's wall.

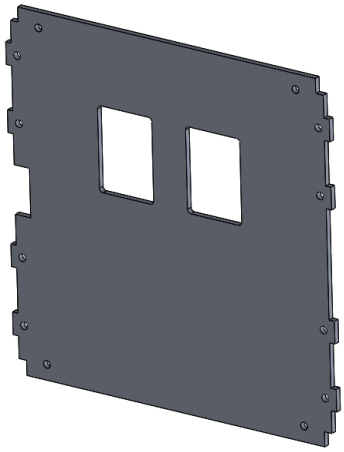

Figure 4. 3: Daughter CubeSat's wall

The large cut-out seen on the left side of the wall in figure 4.3 is for the deployment switch and the two identical cut-outs near the center of the wall are a passthrough for the connectors found on the back face of the solar panels. The sides of the walls have staggered 'teeth' to help interlock with adjacent walls. The posts will then be fitted onto the outside faces of the walls.

4.3.3 Daughter Satellite's Plates

Along with the posts and walls, the next major structural components are the top and bottom plates. The top and bottom plates shelter the interior of the CubeSat from above and below. The plates also hold together the posts and help keep the full satellite structure square. For the same reasons as the walls, the top and bottom plates were chosen to be manufactured using aluminum 6061-T6. Figure 4.4 shows the top and bottom plates.

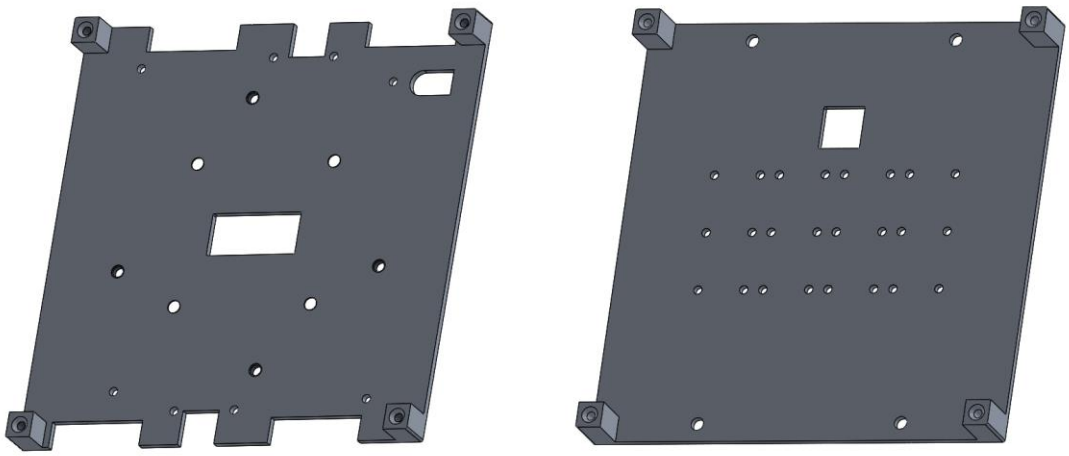

Figure 4. 4: Top (left) and bottom (right) plates of the daughter satellite

The major difference between the top and bottom plates are the external components that will be mounted to them.

The components that mount to the top plate are:

- Separation base
- Separation guiders
- External PCBs

The center cut-out for the top plate is for the passthrough of the extrusion found on the tether storage box. The other cut-outs are for wire harnesses and for the CubeSat tensioners. The components that mount to the bottom plate are:

- UHF antenna
- Spindt array

The single cut-out on the bottom plate is to allow an RF cable to run from the interior of the CubeSat to the UHF antenna.

4.3.4 Daughter Satellite's Miscellaneous Components

The final set of structural components for the daughter satellite are the separation base and

the separation guiders. The purpose of the separation base is to lock the intersatellite faces of the daughter and mother satellite interface. The mother satellite will contain a coil spring used for the CubeSats separation. Prior to separation, this spring will be compressed and housed inside the separation base. The separation base is designed to be manufactured using aluminum 6061-T6 and an image of it is shown in figure 4.5.

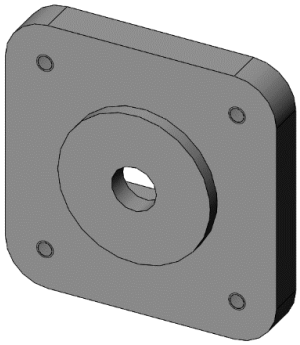

Figure 4. 5: Daughter CubeSat separation base

The separation guiders are a series of male and female metal connectors located on the intersatellite faces of both CubeSats. The guiders help to keep the satellites in-line when the two CubeSats separate from each other. Each CubeSat has two male and two female guiders. The male guiders on one satellite interlock with the female guiders on the other satellite. Since the guiders are subject to possible shear stress during separation, stainless steel 316 was chosen for the material for the guiders. Figure 4.6 shows an image of the guiders.

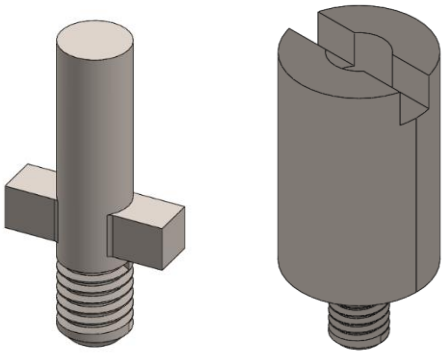

Figure 4. 6: Male guider (left) and female guider (right)

All the structural components for the daughter satellite chassis have been described. The next step is to assemble the individual parts to form the full structural assembly. When creating the assembly, the walls were assembled first. Then the posts were attached to the walls from the outside. Next, the top and bottom plates were attached to the posts from above and underneath. Finally, the separation base and guiders were mounted to the top plate.

4.3.5 Daughter Satellite's Complete Solid Model

Now that all the structural components have been designed, the next step is to create the complete solid model of the daughter spacecraft. Figure 4.7 shows the complete CAD assembly of the daughter CubeSat structure.

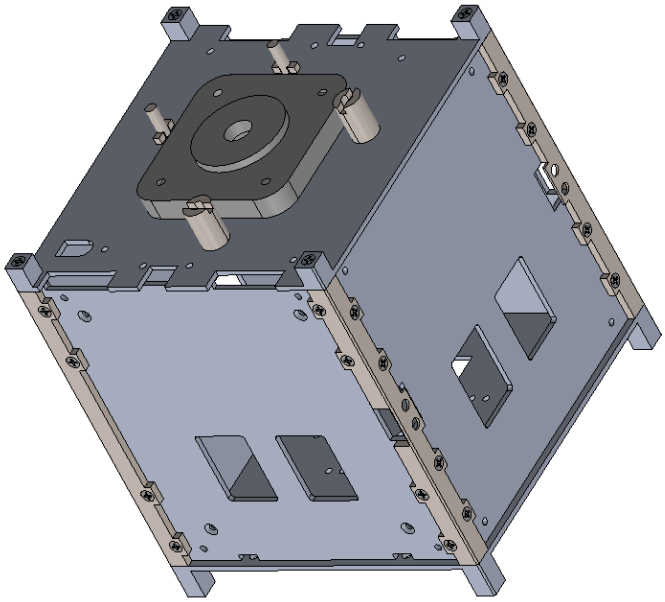

Figure 4. 7: Daughter CubeSat structure assembly

The structure in its current form allows for external payloads and bus components to be mounted to the chassis. However, the tether storage box and the PCB boards containing the spacecrafts electrical systems do not currently have a way to be mounted to the chassis. Therefore, standoffs will be needed to mount these components. In order to reduce weight, aluminum hex

standoffs were selected for the satellite. The standoffs will have to be selected so that the PCB boards are separated correctly, and the ends of the standoffs must connect to the spacecraft chassis. When trying to fit the standoffs to the spacecraft walls, it was noticed that the mounting holes were interfering with the mounting holes of the solar panels. So, aluminum blocks with two offset holes were used as an adapter. This allowed for the standoffs and the solar panels to mount to the spacecraft walls. Figure 4.8 shows the interior of the daughter cube, containing the PCBs, storage box, standoffs and the adapters.

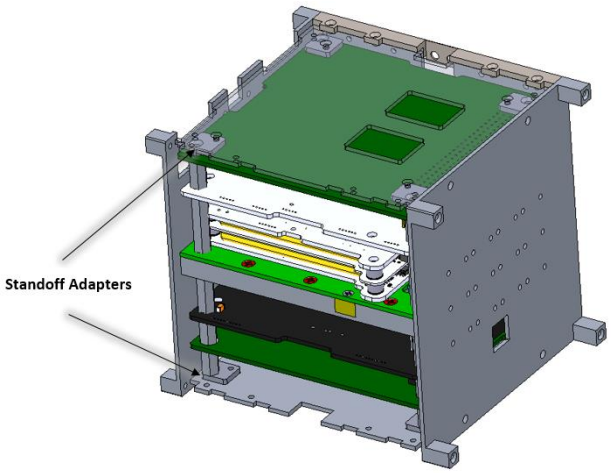

Figure 4. 8: Standoffs, adapters and internal components of daughter CubeSat

Next, the exterior payloads and bus components can be mounted to the CubeSat chassis. These components include, external PCBs, the spindt array, UHF antenna and the solar panels. Figure 4.9 shows the daughter CubeSat with the external components mounted.

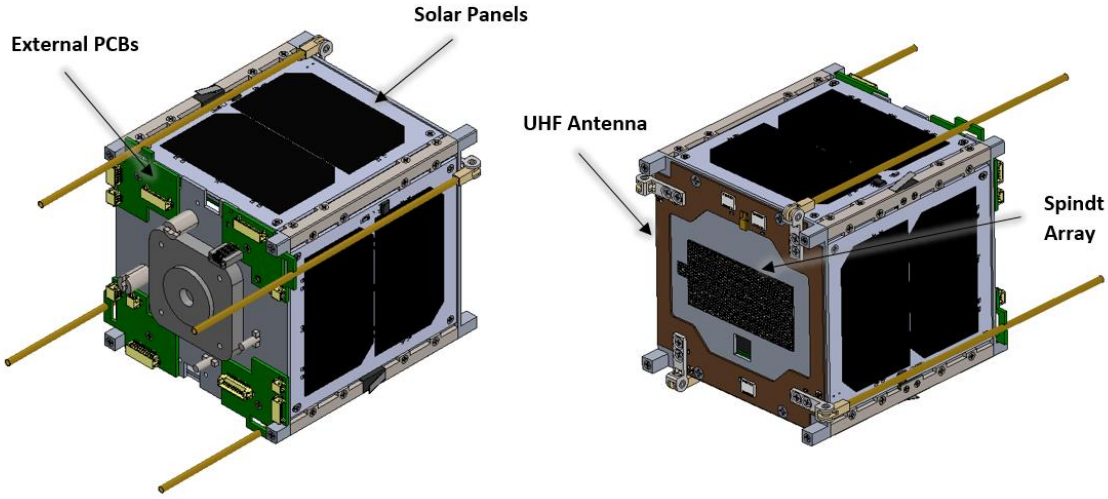

Figure 4. 9: Daughter satellite after mounting exterior components

4.4 Detailed Structural Component Designs for Mother Satellite

The details regarding the mother satellite's structural design will be covered in this chapter. Similar to section 4.3, this will include the individual structural components and the completion of the mother satellite's solid model.

4.4.1 Mother Satellite's Rails

The structure of the mother satellite is very similar to the daughter satellite. The posts/rails of the mother CubeSat is also designed to be out of stainless steel 316. Figure 4.10 shows the mother satellite's post.

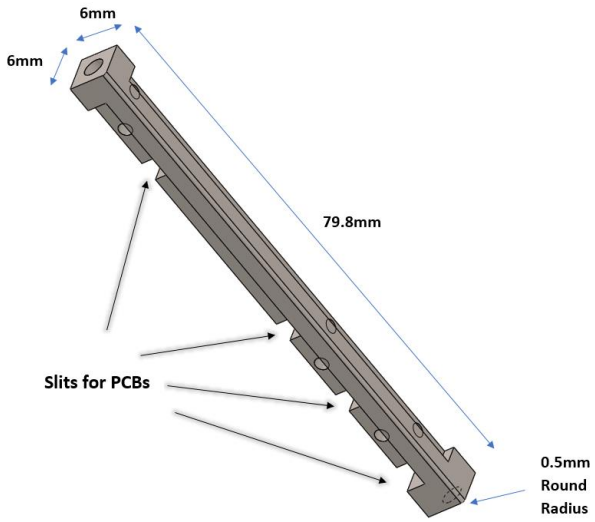

Figure 4. 10: Mother CubeSat's post

The mother CubeSat's posts meet all of NanoRacks requirements from dimensions to surface hardness. There are two major differences between the mother satellite's posts and the daughter satellite's posts. The first are the four slits found along the length of the posts. The slits exist to avoid interference between the internal PCB boards and the corner posts of the CubeSat. The reason why the daughter satellite's posts don't require similar slits are because of the directions the PCBs are stacked within the cube. For the mother satellite the PCBs are stacked parallel to the top and bottom plates. A PC104 board has dimensions of 95.89 x 90.17 mm and had to fit in a space of 96.4 x 96.4 mm. Therefore, in order to have sufficient clearance slits were made along the posts at locations where the PC104 boards would be. On the other hand, in the daughter satellite the boards are stacked perpendicular to the top and bottom plates. This allows for a space of 110.3 x 96.4 mm, which means there is sufficient clearance for the boards. Therefore, no slits are required for the daughter satellite posts. The second difference between the daughter and mother satellite posts are that in the daughter satellite the posts fasten to the walls. The opposite case holds for the mother satellite; The walls fasten to the posts. Similar to the daughter satellite, the mother satellite is also required by NanoRacks to contain three deployment switches. These switches are placed

on 3 out of the 4 mother CubeSat posts in an identical manner as the daughter satellite. This is shown in figure 4.11.

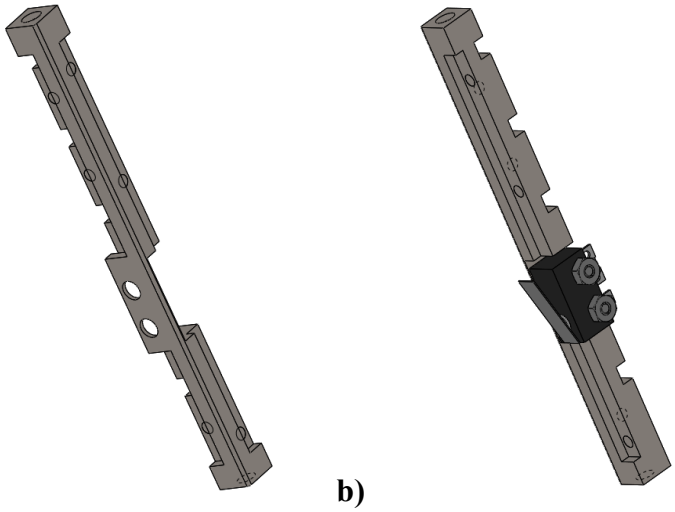

a) **b)**

Figure 4. 11: a) Mother post with switch housing b) Mother post with switch

4.4.2 Mother Satellite's Walls

The walls of the mother satellite are very similar to the daughter satellite. They are also designed to be manufactured using aluminum 6061-T6 and have identical cut-outs for the solar panel connectors. Figure 4.12 shows the mother satellite wall.

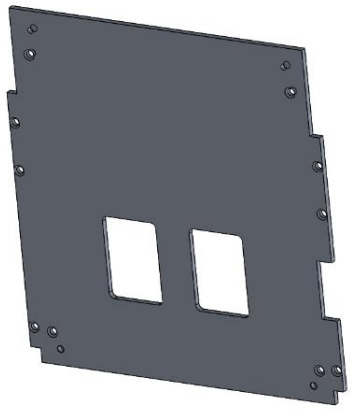

Figure 4. 12: Mother satellite wall

Identical to the daughter satellite's walls, the mother satellite walls also have cut-outs to accommodate the deployment switches.

4.4.3 Mother Satellite's Plates

The next structural components for the mother satellite are the top and bottom plates. Just like the daughter satellite, the top and bottom plates are manufactured using aluminum 6061-T6, in order to save weight. The plates are shown in Figure 4.13.

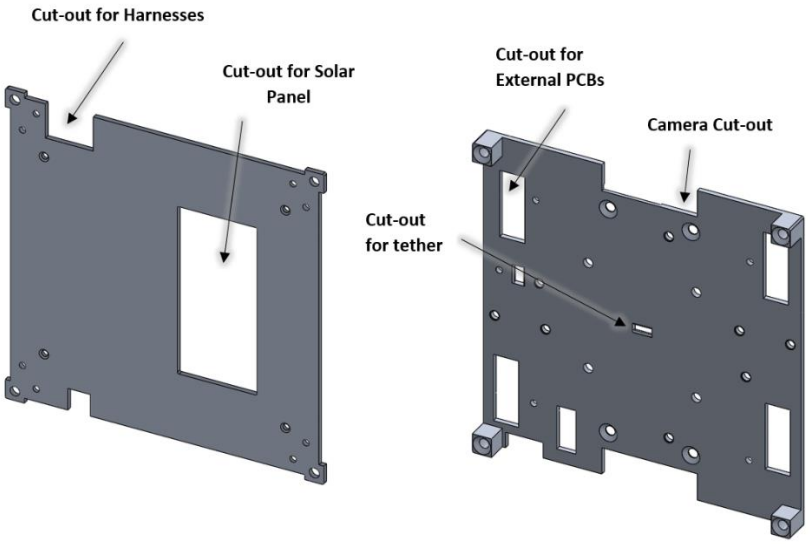

Figure 4. 13: Top (left) and bottom (right) mother CubeSat plates

The top plates contain two type of cut-outs. The first is for the wire harnesses and are located on two opposite sides of the top plate. Near the center of the plate there is a large cut-out for the top solar panel's connectors. Unlike the daughter satellite, the mother satellite will have 5 body mounted solar panels (excluding the SCIENCE payload). The bottom plate contains two small cuts-out for the tether to pass through. The larger cut-outs are for the connectors of external PCBs and the CubeSat cameras.

Since the mother satellite will house the SCIENCE payload on the top face of the top plate, custom posts were designed. These posts connect to the CubeSat posts/rails through the top plate. The posts are referred to as the upper posts and they contain mounting holes for the SCIENCE payload. Figure 4.14 shows the upper posts on the top plate.

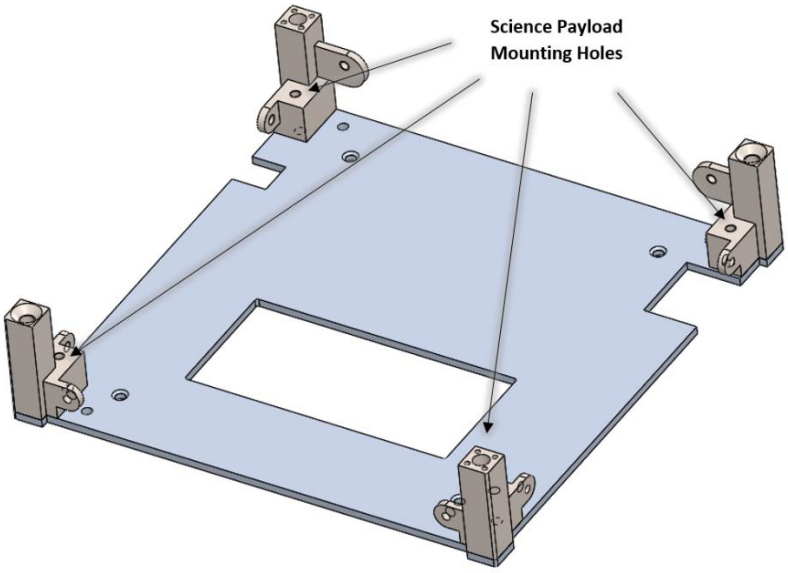

Figure 4. 14: Upper posts and top plate of mother CubeSat

Since the upper posts are a continuation of the CubeSat posts, stainless steel 316 was chosen as the manufacturing material.

The upper posts also serve an additional purpose. As stated in section 3.2, NanoRacks requires two separation springs to be placed on diagonal ends of the mother Satellites' -Z posts. The reason as to why this is only required for the mother satellite and not the daughter satellite is because when the DESCENT CubeSats are being deployed from the rack, the mother satellite will be the last of the two DESCENT spacecrafts to leave the rack. Therefore, the mother satellite must provide a smooth separation from the adjacent CubeSat that is left over in the rack. The separation springs are designed using a spring and plunger mechanism. A compression spring made from zinc plated steel is used with an aluminum 6061-T6 plunger. Figure 4.15 shows the spring plunger system.

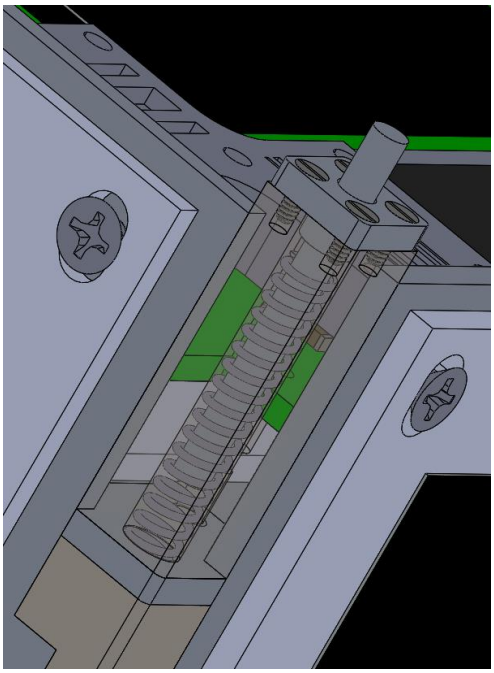

Figure 4. 15: Spring and plunger system on mother satellite's upper post

The spring force when the plunger descents fully is 6 N and therefore it meets NanoRacks requirement for the separation springs.

4.4.4 Mother Satellite's Miscellaneous Components

Finally, there are additional structural components needed for the mother satellite's structure. These components include camera support structures, tether anchor, tensioners, separation base with compression spring and the separation guiders. As mentioned in section 3.3, two Raspberry PI cameras will be used to capture images during the mission. These cameras require to be mounted to the spacecraft structure. So, a camera support structure was designed and is shown in Figure 4.16.

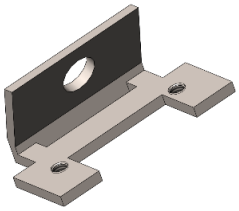

Figure 4. 16: Camera support structure

Since the cameras are an important device for the mission, it is required that the cameras are fixed in placed well throughout all phases of the mission. Therefore, stainless steel 316 was used as the manufacturing material. The tether will be contained within the tether storage box in the daughter satellite. One end of the tether will be anchored to the storage box and the other end will be anchored to the mother satellite. The tether anchor used for the mother satellite consists of an L-bracket and a face plate. Figure 4.17 shows the anchor.

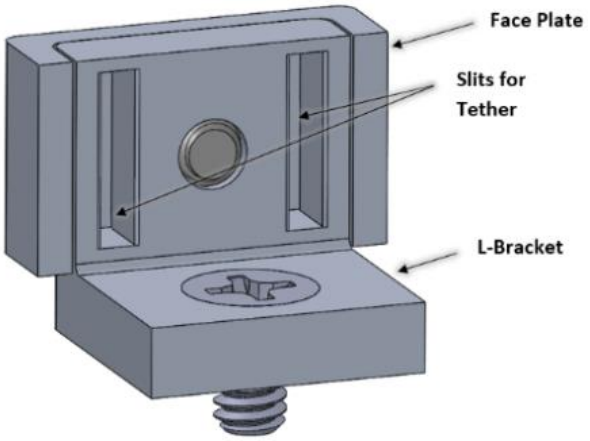

Figure 4. 17: Tether anchor

The tether will pass though the slits found on the L-bracket. Then the face plate will clamp the tether to the L-bracket. Finally, a screw will be used to fasten the face plate to the L-bracket. Since the tether is very light, aluminum 6061-T6 was chosen as the material for the tether anchor parts. Next, a tensioner is needed to tension the burn wire used to tie the two CubeSats together before separation. The tensioner consists of two L-brackets, a ratchet and a pawl. The ratchet and pawl ensure that the tensioning of the burn wire can only be done in one direction and therefore the burn wire cannot get loose after being tensioned. Figure 4.18 shows the tensioner and its components.

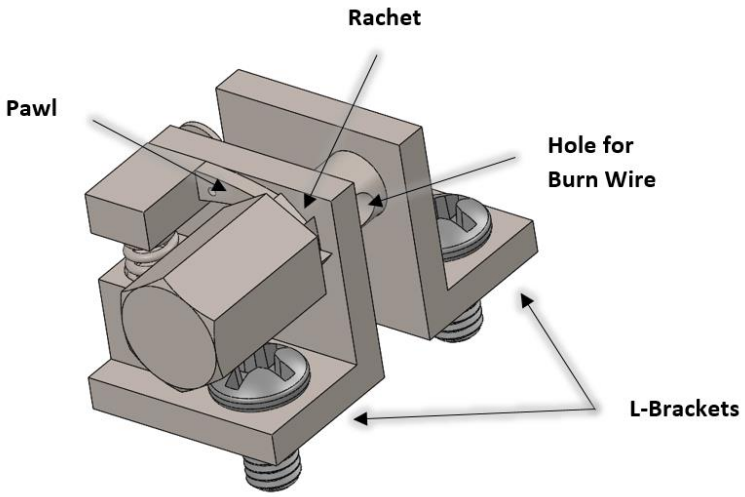

Figure 4. 18: Tensioner and its components

A high load capacity fishing wire made from Dyneema will be used as the burn wire. The burn wire will run between the interior of both satellites and through a tensioner. Initially, during assembly a large length of burn wire will be tied. After the assembly of both satellites are completed the tensioner will be used to tension the burn wire loop and bringing both satellites together. Figure 4.19 shows the burn wire loop.

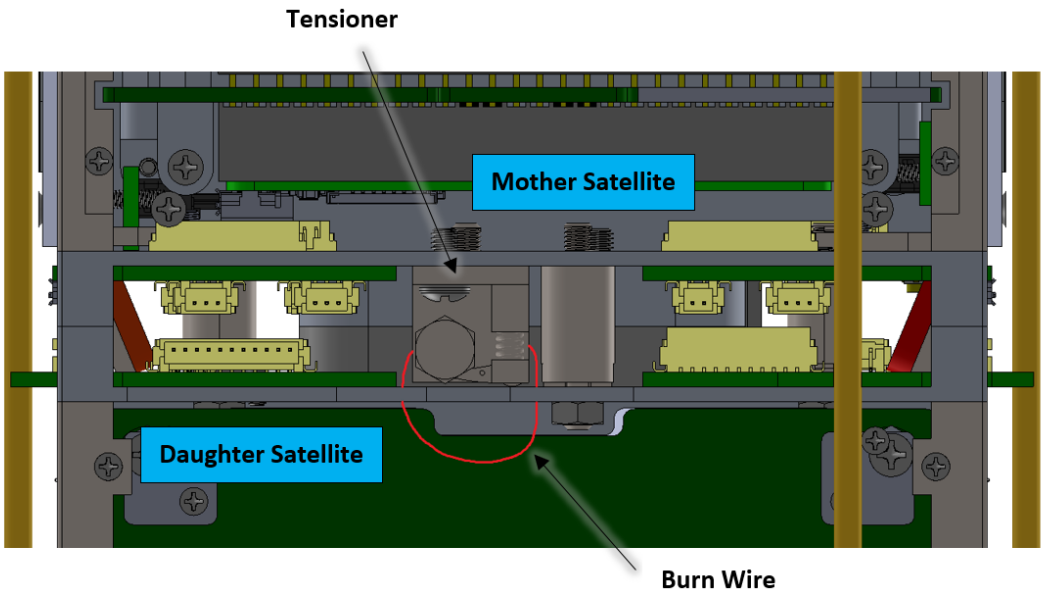

Figure 4. 19: Burn wire loop used to tension the two satellites

Since the tensioner holds both satellites together stainless steel 316 was used as the manufacturing material. Finally, there will be two tensioners in total. One will be mounted on opposite faces of the mother satellite. Similar to the daughter satellite, the mother CubeSat will also contain a separation base. However, the separation base on the mother satellite will contain the compression spring. Figure 4.20 shows the separation base.

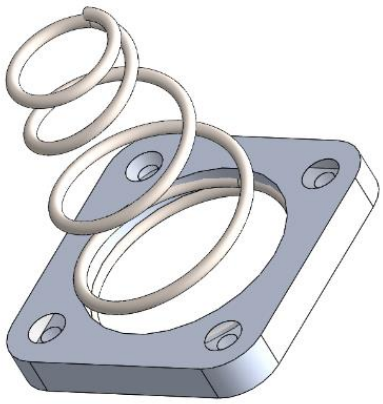

Figure 4. 20: Separation base with spring

The final structural components are the separation guiders. These guiders are identical to the ones used on the daughter satellite. There are two male guiders and two female guiders. The male guiders on the mother satellite connect to the female guiders on the daughter satellite. Likewise, the female guiders on the mother satellite connect to the male guiders on the daughter satellite.

4.4.5 Mother Satellite's Complete Solid Model

The next step is to create the assembly of the mother satellite's structure. It begins by fastening the walls to the posts. Then the top and bottom plates are mounted to the posts. Next, the upper posts are mounted to the top plate and posts. Finally, the camera support structures, tether anchor, tensioners, separation base and guiders are mounted to the bottom plate. The final structural CAD assembly is shown in Figure 4.21.

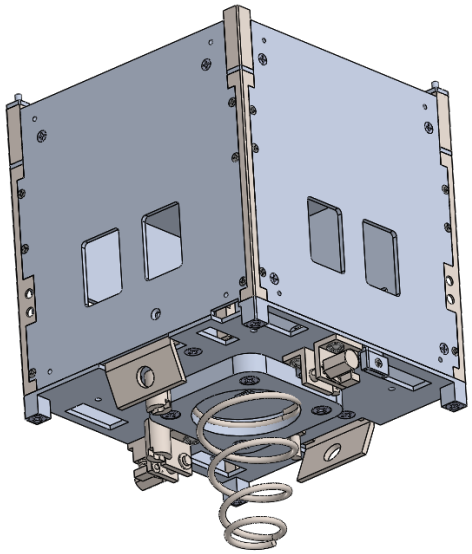

Figure 4. 21: Mother satellite's structural assembly

The CubeSat structure is now ready to have components mounted. The first components to mount to the chassis are the internal PCB boards. Therefore, similar to the daughter satellite a set of aluminum hex standoffs are needed to mount the boards to the chassis. Due to a misalignment between the standoff's holes and the holes of the top solar panel adapters were also needed for the mother satellite. These adapters are identical to the adapters used on the daughter satellite. However, since the bottom plate of the mother cube contains large cut-outs for the external PCBs, there was no way to mount the standoffs to the bottom plates. To resolve this issue a second set of adapters with an L-bracket like design was used to mount the standoffs to the walls of the satellite. Figure 4.22 shows the adapters and standoffs holding the internal components of the satellite to the structure.

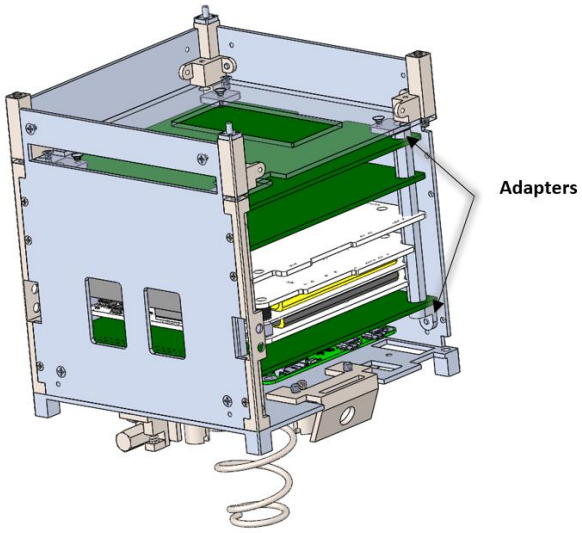

Figure 4. 22: Internals of the mother CubeSat

Next, the exterior payloads and bus components are mounted to the structure. The top plate contains a solar panel, the upper posts contain the SCIENCE Payload, the four walls include solar panels and the bottom plate contains the cameras. Figure 4.23 shows the exterior components mounted to the mother spacecraft's structure.

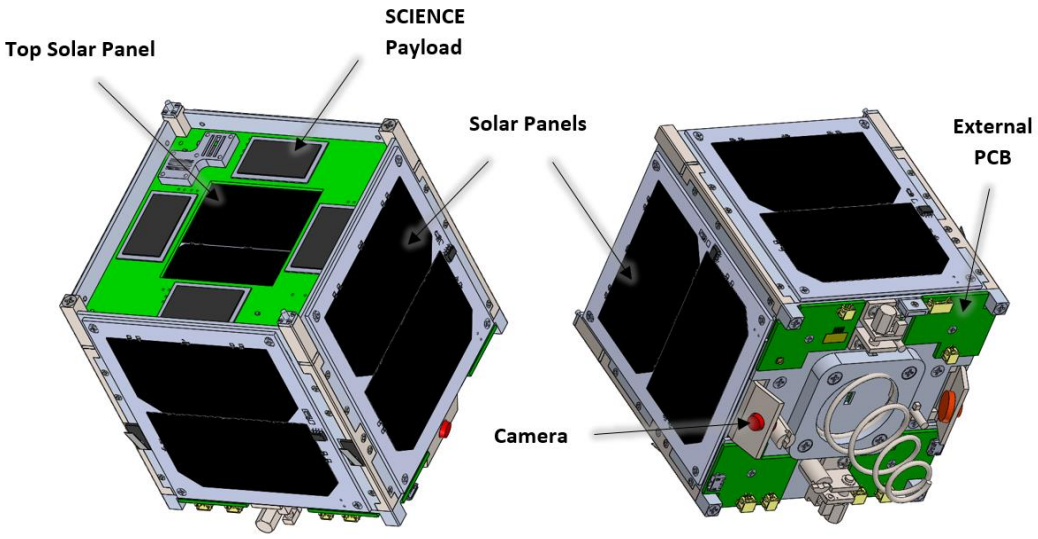

Figure 4. 23: External components mounted to mother structure

4.4.6 Complete Solid Model of DESCENT 2U CubeSat

Now that both CubeSat structures have been completed, it is time to assemble both spacecrafts together to produce the 2U configuration that will be stored in the NRCSD. Figure 4.24 shows both mother and daughter satellites together in a 2U configuration.

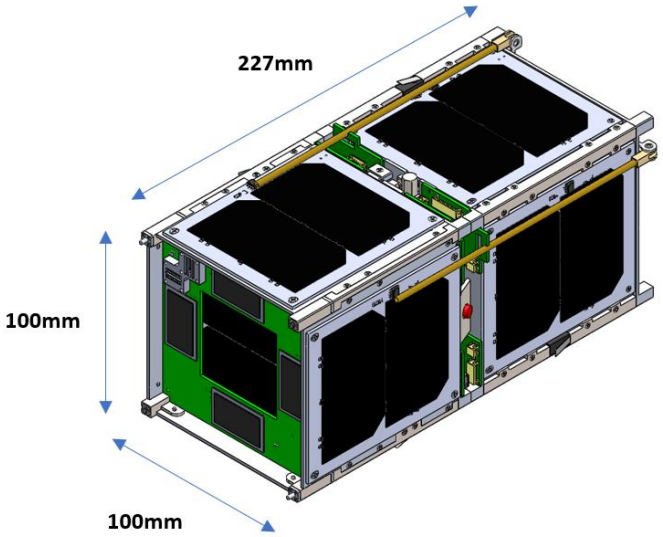

Figure 4. 24: Combined 2U DESCENT spacecrafts

By refereeing to section 3.5 of this paper, it can be seen that the outer dimensions of the combined CubeSats meet the requirements placed by NanoRacks. Finally, by refer to appendix A2 and A3 for the mass budget of the daughter and mother CubeSats, it can be seen that the satellites masses are within budget.

In conclusion, both CubeSats meet the requirements placed by the launch provider. The satellites are within the required mass and dimensions. Also, the structure of the spacecrafts are designed with acceptable materials. Now that the design for the structure is complete, it is necessary to see if the structure can survive two major operating environments. The method to evaluate the structural integrity of the spacecrafts will be covered in the next chapter.

Chapter 5 STRUCTURAL FINITE ELEMENT ANALYSIS

5.1 Introduction

As it was shown in the previous chapter the current structural design meets the material, dimensional and mass requirements. However, this is only a solid model which only gives limited information. To determine the response of the spacecraft to various environments requires the use of a Finite Element Analysis (FEA). One of the most critical environments that the CubeSat will experience is the launch environment. This is the time from when the satellite leaves the surface of the Earth and reaches the desired orbit. During this time, various vibrational loads will be subject to the spacecraft from the launch vehicle. According to W.T. Thomas in his book *Theory of Vibration with Applications*, a spacecraft can be viewed as a lump mass attached to the launch vehicle (base) via a spring and damper [27]. Figure 5.1 shows the mass, spring and damper system.

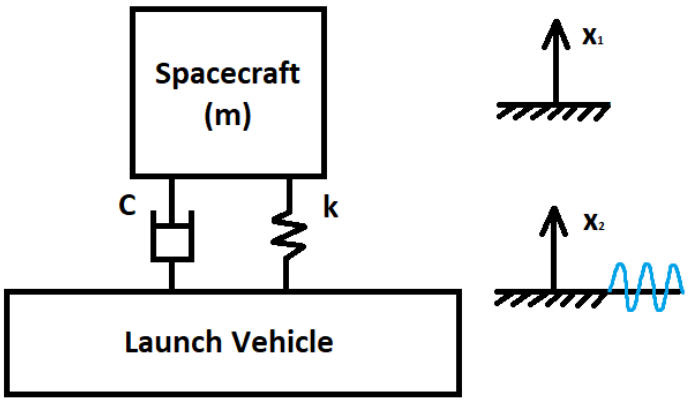

Figure 5. 1: Mass, spring and damper system

Newtons second law for the system gives,

$$\sum F = m\ddot{x} = -c(\dot{x}_1 - \dot{x}_2) - k(x_1 - x_2)$$

$$Let\ x_3 = x_1 - x_2$$

Plugging this in gives

$$m(\ddot{x}_3 + \ddot{x}_2) = -c\dot{x}_3 - kx_3$$

$$m\ddot{x}_3 + c\dot{x}_3 + kx_3 = -m\ddot{x}_2$$

$$m\ddot{x}_3 + c\dot{x}_3 + kx_3 = -m\omega^2 A \sin \omega t$$

Finally, the equation of motion describing the dynamics of the system is found to be,

$$\ddot{x}_3 + \frac{c}{m}\dot{x}_3 + \frac{k}{m}x_3 = \omega^2 A \sin \omega t$$

To determine whether the DESCENT spacecrafts will survive this environment, two FEA's must be completed. The first is a Normal Modes Analysis and the second is a Vibrational Analysis. By conducting these two analyses, the structural integrity of the spacecrafts during the launch phase can be quantified.

5.2 Limitations of the CAD Model & Purpose of a FEA

It was mentioned in the introduction of this chapter that the solid model (CAD model) provides limited information. To expand this statement, the solid model only provides information on dimensions, materials, mass, center of gravity and moments of inertia. These are all important data to the CubeSat developer. However, this information does not characterize the response of the satellite to different environments. During various phases of the mission, the DESCENT satellites will be subject to various vibrational and thermal loads. To determine the response of the satellites to these inputs, an FEA will be needed as a solid model will not be able to provide this information. Responses can include stress, strain, displacement, etc.

5.3 Finite Element Modeling Process

In order to obtain the results of the FEA, a series of steps must be taken from the current solid model stage. Since the solid model contains lots of detail for the interior and exterior of the satellites it will be very difficult to run a FEA on such a detailed model as computational resources are limited. Therefore, it is necessary to simplify the geometry of the satellites. When simplifying the geometry, it is important to only simplify what is necessary. As some aspects of the model are critical to the structure of the satellite. These parts shall either not be simplified or should only be slightly modified. On the other hand, there are aspects of the satellite that have a negligible affect on the structural integrity of the satellite. These components can be simplified greatly. This is an iterative process, if the FEA takes too long to run the geometry must be revisited and further simplified until a reasonable runtime is achieved. Once the geometry has been simplified it is time to create the Finite Element Model (FEM) of the satellite. Various nodes and elements will be used to create the optimized mesh. Similar to creating the idealized model, if the analysis run time is too long or if the solution of the FEA is not desired, the FEM must be modified until an optimized mesh have been achieved. Once the optimal idealized model and FEM have been created the FE simulation can be run and the desired results can be obtained. This process is shown in figure 5.2.

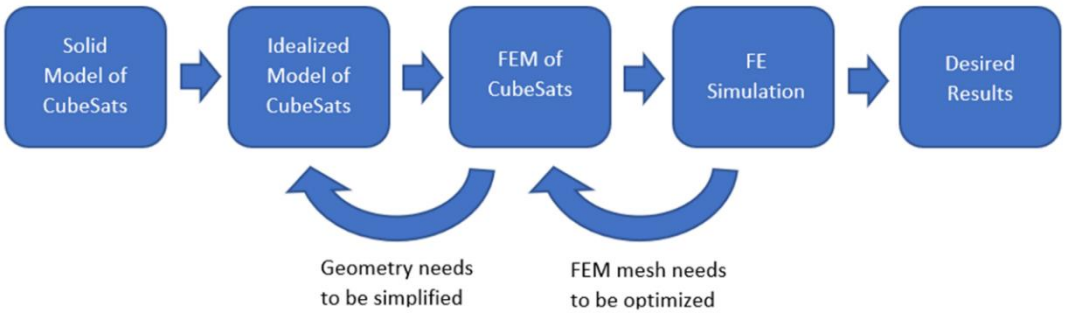

Figure 5. 2: The finite element design process

5.4 Normal Modes Analysis of Daughter CubeSat

The first analysis to be run is a Normal Modes Analysis. The purpose of this analysis is to determine the natural frequencies (normal modes) of the satellite. The natural frequencies are frequencies at which the spacecraft will get 'excited' and large displacements of the structure will occur when the satellite is subject to a vibration. The natural frequency can be obtained using the expression below, when viewed as the system shown in figure 5.1.

$$\omega_n = \sqrt{\frac{k}{m}}$$

where ω_n is the natural frequency, k is the stiffness of the spring and m is the mass.

These large displacements can cause large amounts of stress in the structure. By determining the natural frequencies, it can determine whether the spacecraft will avoid resonance with the launch vehicle. The frequency range of interest is from 20 Hz to 2000 Hz, as this is the range for most vibrational analysis tests. In the *NanoRacks Flight Acceptance Vibration Testing* document provides the vibration profile to simulate the vibrational loads across a frequency range of 20 to 2000 Hz [28]. The vibration profile is shown in Figure 5.3.

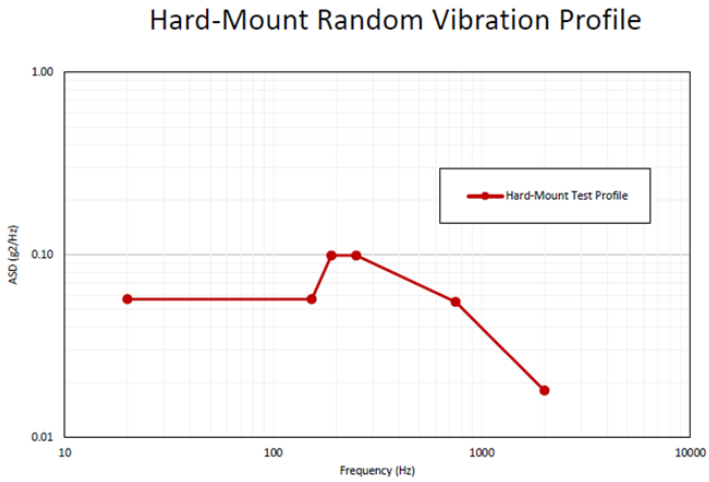

Hard-Mount Test Profile	
Frequency (Hz)	ASD (g^2/Hz)
20	5.700E-02
153	5.700E-02
190	9.900E-02
250	9.900E-02
750	5.500E-02
2000	1.800E-02
grms	**9.47**
Duration (sec)	**60**

Figure 5. 3: NanoRacks vibration profile [28]

There will be numerous normal modes in this frequency range, but only the first few modes are of interest. This is because, the first few modes have the largest displacements and therefore the largest stress. NanoRacks requires that the first normal mode of the satellite be greater than 100 Hz. To determine if the daughter satellite's first normal mode is greater than the desired value a normal modes simulation must be run.

Following the finite element modeling process established in section 5.3, it is first required to simplify the geometry of the solid model. Figure 5.4 shows the current solid model of the daughter satellite.

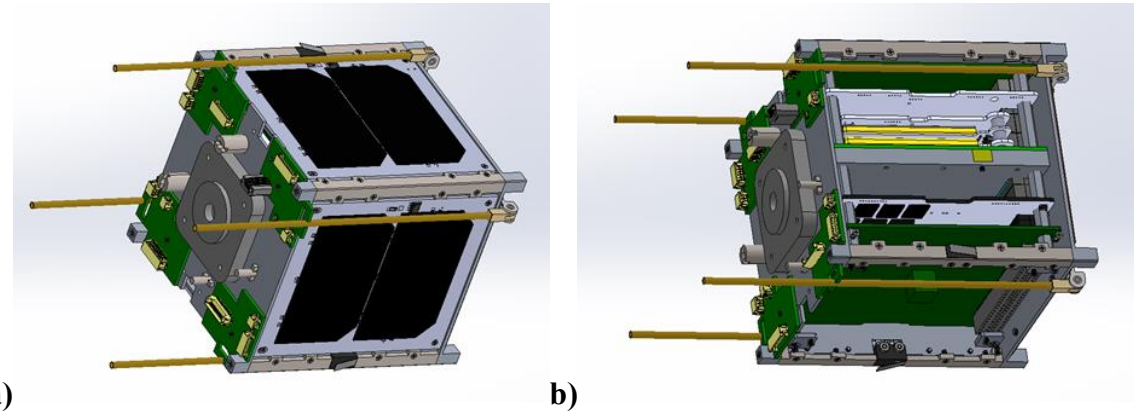

a) **b)**

Figure 5. 4: a) Exterior of daughter's solid model b) Interior of daughter's solid model

The solid model contains a lot of details in the geometry that is not necessary for the simulation. So, an idealized model of the daughter satellite was created and is shown in figure 5.5.

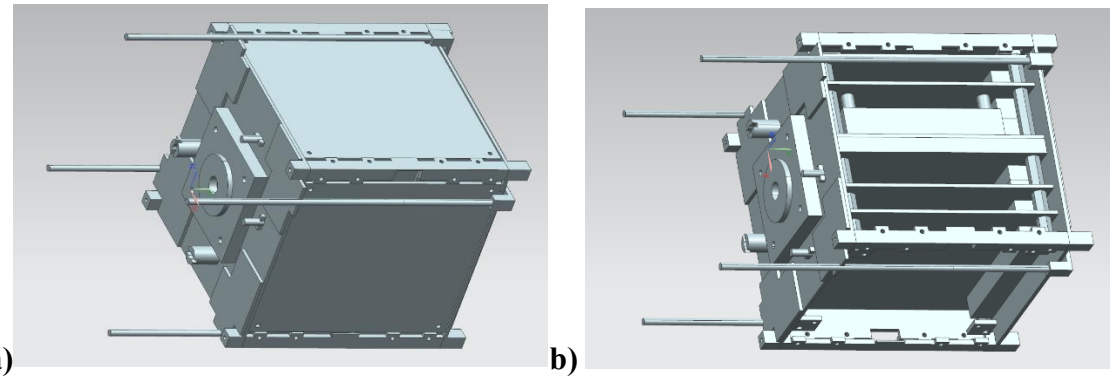

a) **b)**

Figure 5. 5: a) Idealized daughter model (exterior) b) Idealized daughter model (interior)

As it can be seen from figure 5.5, for every structural component the geometry of the parts were simplified. These simplifications are stated in Table 5.1.

Table 5. 1: Simplifications done to daughter CubeSat's structural components

Structural Component	Simplification (removal of geometry)
Posts	• Round radius along rail length • Deployment switch housing holes • Counter sinks for screws
Walls	• Center cut-outs for solar panel connectors
Top and Bottom Plates	• Cut-outs for connectors • Round radius also rail length • Counter sinks for screws
Separation Base	• Corner round radiuses
Standoff Adapters	• Counter sinks for screws • Corner round radiuses

In addition to the simplifications made to the structural components, simplifications were also done for payloads, bus components and internal electronics such as the PCBs. These simplifications are summarized in table 5.2.

Table 5. 2: Simplifications done to daughter CubeSat's payloads/electronic components

Payload / Electronic Component	Simplification (removal of geometry)
UHF Antenna	• Round radius on hinges
External PCBs	• External connectors • Cut-outs for cable harnesses
Spindt Array	• Removed full component
EPS	• Surface mounted components

	• Battery was replaced with a block of identical dimensions
Internal PCBs	• Round radiuses located on board corners • Cut-outs located along the sides of the board
Stacks	• Male pins and female connectors
Solar Cells	• Removed full component
Tether Storage Box	• Tether length measurement system • Breaking mechanism

After completing the idealized model, the next step in the FEM modeling process is to create the FEM. By using a variety of nodes and element types the FEM for the daughter satellite was created and is shown in Figure 5.6.

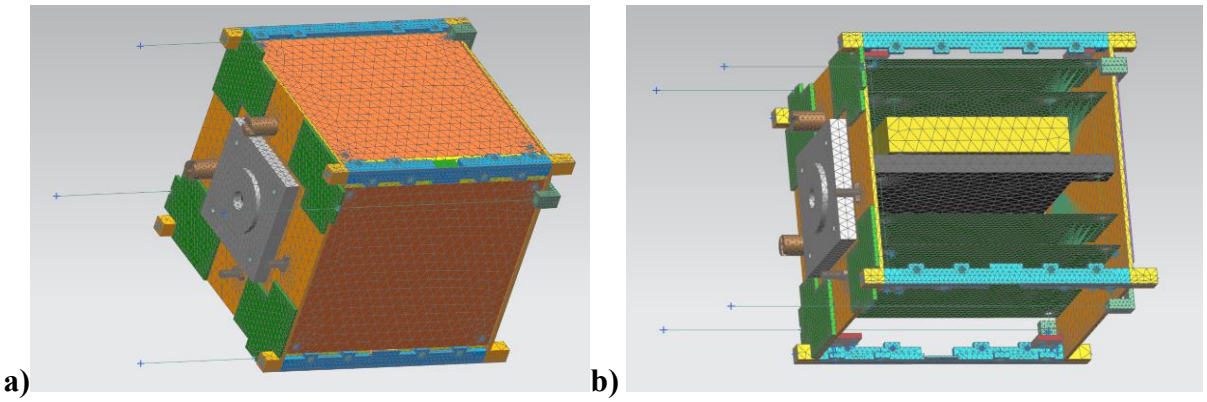

Figure 5. 6: a) Exterior of Daughter FEM b) Interior of Daughter FEM

In addition, Table 5.3 shows the various elements used to create the daughter satellite's FEM.

Table 5. 3: Element types used for daughter CubeSat's structural FEM

CubeSat Part	Mesh Type	Element Type	Material
Posts	**3D**	**CTETRA**	**Stainless Steel 316**
Top & bottom plates	**3D**	**CTETRA**	**Aluminum 6061-T6**
Guiders	**3D**	**CTETRA**	**Stainless Steel 316**
External PCBs	**3D**	**CTETRA**	**FR4**
Seperation base	**3D**	**CTETRA**	**Aluminum 6061-T6**
Antenna base/PCB	**3D**	**CTETRA**	**FR4**
Storage box	**3D**	**CTETRA**	**Aluminum 6061-T6**
EPS battery	**3D**	**CTETRA**	**Custom Material**
Adapters	**3D**	**CTETRA**	**Stainless Steel 316**
Walls	**2D**	**CTRIAR**	**Aluminum 6061-T6**
Solar panels	**2D**	**CTRIAR**	**FR4**
Storage box cover	**2D**	**CTRIAR**	**Aluminum 6061-T6**
Internal PCBs	**2D**	**CTRIAR**	**FR4**
Antenna Rods	**1D**	**PBEAML**	**Aluminum 6061-T6**
Standoffs	**1D**	**PBEAML**	**Aluminum 6061-T6**
Spacers	**1D**	**PBEAML**	**Aluminum 6061-T6**
Bolts	**1D**	**PBEAML**	**Stainless Steel 316**

The final step is to set up the simuation. The normal modes simulation requires boundary conditions to be placed on the satellite. Since the CubeSat will be placed inside the NRCSD the rails of the CubeSat will be in complete contact with the the rails of the NRCSD. This means that the CubeSat is only free to have translational motion along the z-axis. Therefore, in the simulation

the CubeSat has all 3 rotational degrees of freedom and the x and y translational degrees of freedom as fixed constratints. Leaving the z-axis transilational degree of freedom free. Table 5.4 states the boundary conditions and Figure 5.7 shows the boundary conditions on the model.

Table 5. 4: Boundary conditions for daughter CubeSat's normal modes analysis

Degree of Freedom	Z-Axis Excitation
DOF1	Fixed
DOF2	Fixed
DOF3	Free
DOF4	Fixed
DOF5	Fixed
DOF6	Fixed

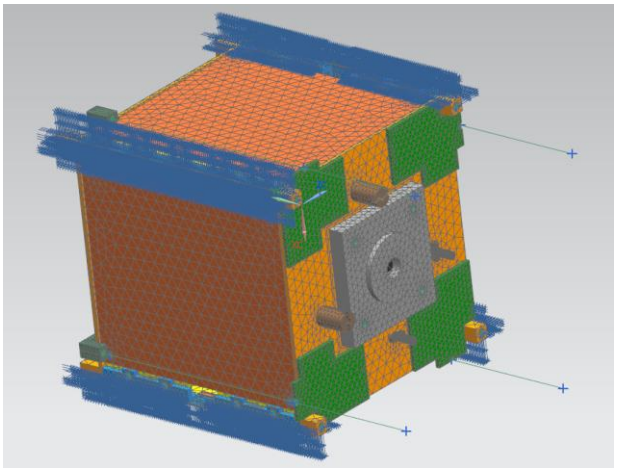

Figure 5. 7: Boundary conditions placed on CubeSat rails

Now that the boundary conditions are placed, it is time to conduct the simulation to determine the normal modes of the satellite.

After conducting the normal mode analysis for the daughter CubeSat, it was found that the first natural frequency occurs at 398.72 Hz. Furthermore, Table 5.5 shows the first 10 normal modes for the daughter satellite.

Table 5. 5: First ten normal modes of the daughter CubeSat

Normal Mode	Frequency (Hz)
1	398.72
2	398.75
3	401.73
4	409.75
5	452.44
6	463.27
7	463.63
8	490.96
9	513.91
10	599.60

At its first natural frequency one of the CubeSat walls move inwards into the cube. Figure 5.8 shows this motion.

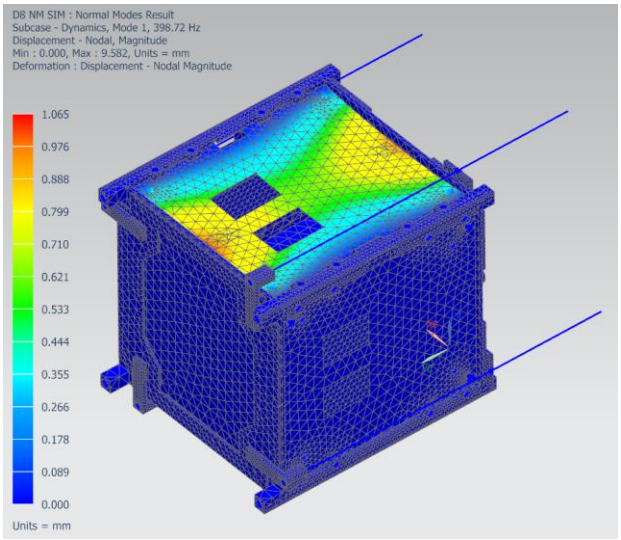

Figure 5. 8: First normal mode of daughter satellite

The maximum displacement occurs at the top and bottom ends of the wall and has a displacement of 1.065 mm.

At the third natural frequency (401.73 Hz) two solar panels begin to move. One panel moves outwards, and the opposite side panel moves inwards. This can be seen in figure 5.9 a). Since those two panels are connected to the walls which are in turn connected to interior standoffs via the adapters, the interior of the CubeSat also experiences motion. This interior motion can be seen in figure 5.9 b).

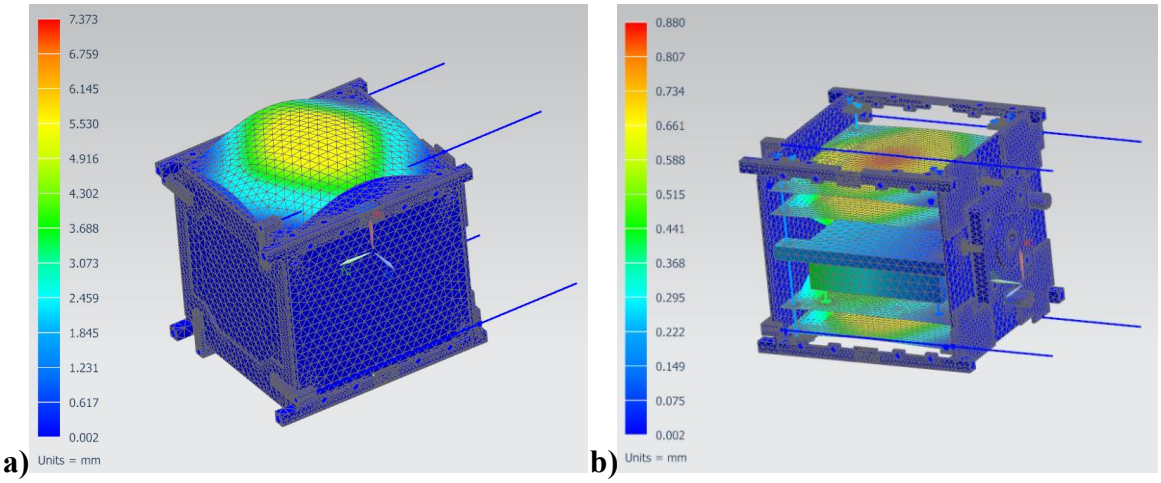

Figure 5. 9: a) Third normal mode (exterior) b) Third normal mode (interior)

At the tenth natural frequency (599.60 Hz) both the top and the bottom plates of the daughter satellite begins to move. This motion is captured in figure 5.10.

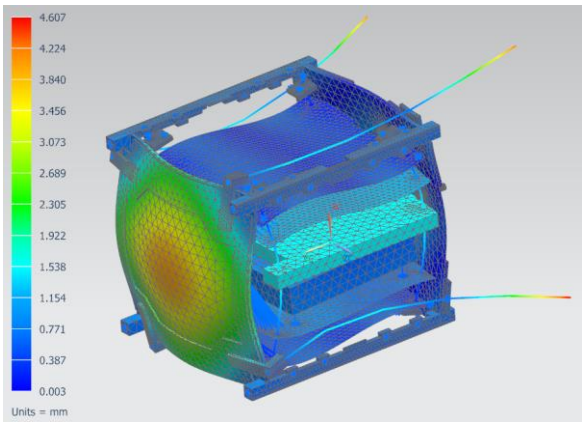

Figure 5. 10: Tenth natural frequency of the daughter CubeSat

The motion of the plates causes the UHF antenna and the interior components of the CubeSat to deform.

After conducting the normal modes analysis for the daughter CubeSat, it was found that the first natural frequency occurs at 398.72 Hz, which is greater than 100 Hz required by the launch provider. This means that the daughter satellite will avoid resonance with the launch vehicle. For comparison table 5.6 shows the first natural frequency of other CubeSats.

Table 5. 6: First Normal Mode of Various CubeSats

Spacecraft	1st Normal Mode (Hz)
TRIO CINEMA (3U)	339
ITU-pSAT II (3U)	216
EAC CubeSat (1U) [34]	202
ECOSat-III (3U)	248
KUFASAT (1U)	654

5.5 Normal Modes Analysis of Mother CubeSat

Similar to the daughter satellite, the current solid model of the mother satellite contains large amounts of detail as it can be seen from figure 5.11.

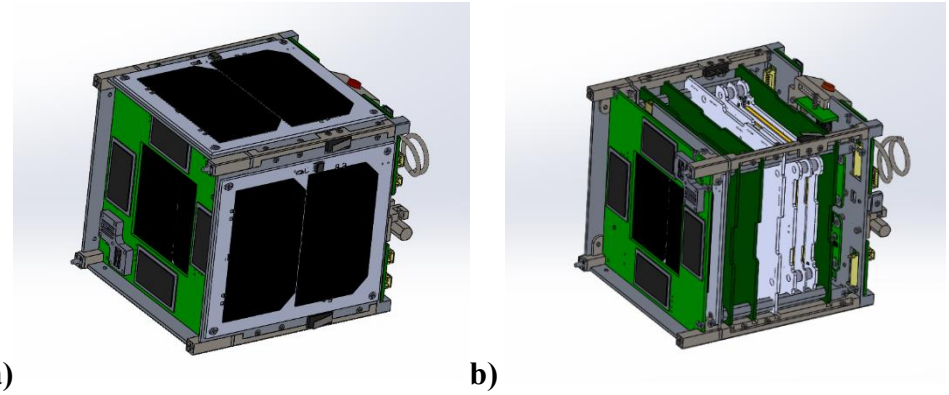

a) **b)**

Figure 5. 11: a) Mother satellite exterior b) Mother satellite interior

Having this much detail will affect the runtime of the simulation and more computational resources will be needed. So, in order to minimize the computational load an idealized model is generated with simplified geometry. This idealized model in shown in Figure 5.12.

a) 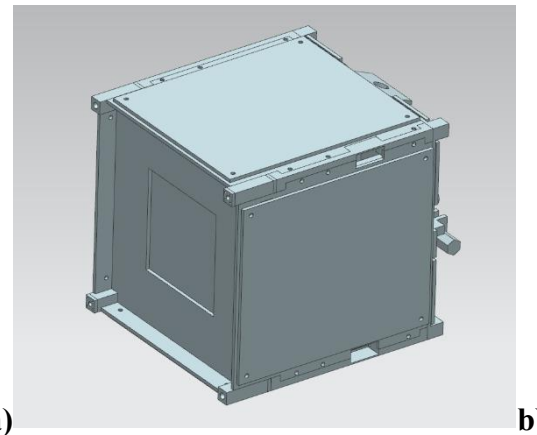 b) 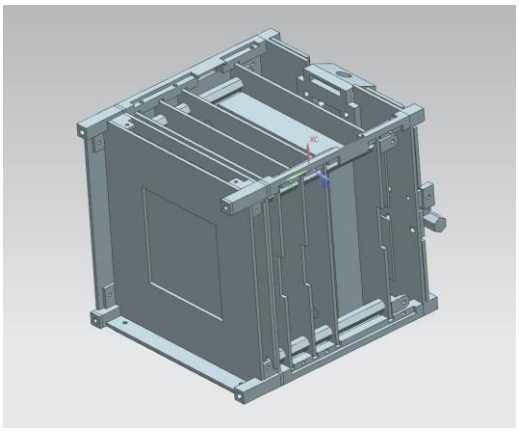

Figure 5. 12: a) Idealized mother exterior b) Idealized mother interior

Various geometry was simplified to get the idealized model. Starting with the structural components, the simplification of the geometry is shown in table 5.7.

Table 5. 7: Simplifications done to mother CubeSat's structural components

Structural Component	Simplification (removal of geometry)
Posts	• Round radius along rail length • Deployment switch housing holes • Counter sinks for screws
Upper Posts	• Round radius for lugs
Walls	• Center cut-outs for solar panel connectors
Top and Bottom Plates	• Cut-outs for connectors and top solar panel • Round radius also rail length • Counter sinks for screws
Separation Base	• Corner round radiuses

Standoff Adapters	• Counter sinks for screws • Corner round radiuses
Separation Spring	• Removed full component
Tensioner	• Spring and rachet system
Tether Anchor	• Slits for tether pass through • Counter sink for screw

Similar to the simplifications made to the structural components, simplifications were also done for payloads, bus components and other electronic components. These modifications are summarized in table 5.8.

Table 5. 8: Simplifications done to mother CubeSat's payloads/electronic components

Payload / Electronic Component	Simplification (removal of geometry)
External PCBs	• External connectors • Cut-outs for cable harnesses
SCIENCE Payload	• Solar cells and surface mounted components
EPS	• Surface mounted components • Battery was replaced with a block of identical dimensions
Internal PCBs	• Round radiuses located on board corners • Cut-outs located along the sides of the board
Stacks	• Male pins and female connectors
Solar Cells	• Removed full component

After completing the idealized model, it is time to create the FEM. A wide array of nodes and element types were used to create the mesh and is shown in table 5.9.

Table 5. 9: Element types used for mother CubeSat's structural FEM

CubeSat Part	Mesh Type	Element Type	Material
Posts	3D	CTETRA	Stainless Steel 316
Upper Posts	3D	CTETRA	Stainless Steel 316
Top & bottom plates	3D	CTETRA	Aluminum 6061-T6
Guiders	3D	CTETRA	Stainless Steel 316
External PCBs	3D	CTETRA	FR4
Seperation base	3D	CTETRA	Aluminum 6061-T6
Camera support structure	3D	CTETRA	Stainless Steel 316
Tether anchor	3D	CTETRA	Aluminum 6061-T6
Tensioner	3D	CTETRA	Stainless Steel 316
EPS battery	3D	CTETRA	Custom Material
Adapters	3D	CTETRA	Stainless Steel 316
Walls	2D	CTRIAR	Aluminum 6061-T6
Solar panels	2D	CTRIAR	FR4
SCIENCE payload	2D	CTRIAR	FR4
Internal PCBs	2D	CTRIAR	FR4
Standoffs	1D	PBEAML	Aluminum 6061-T6
Spacers	1D	PBEAML	Aluminum 6061-T6
Bolts	1D	PBEAML	Stainless Steel 316

Next, Figure 5.13 shows the exterior and interior images of the mother satellite's FEM.

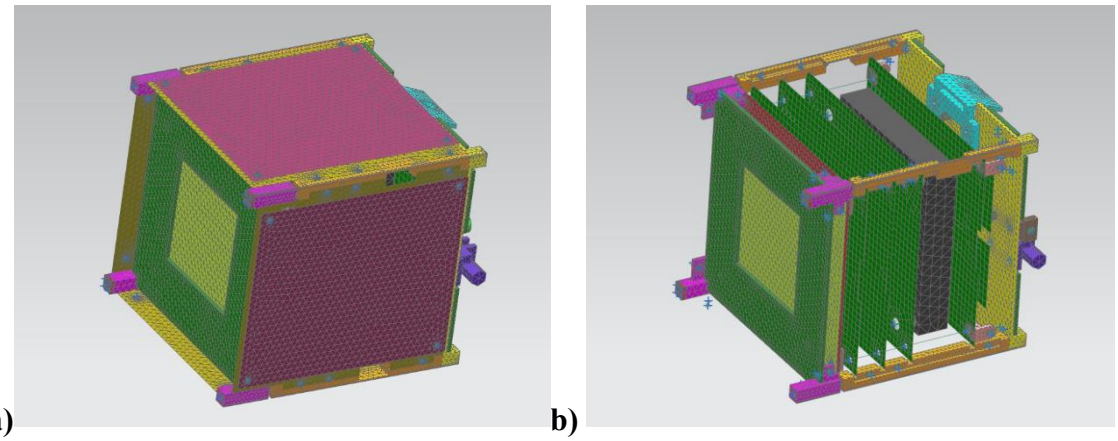

Figure 5. 13: a) Exterior of mother FEM b) Interior of mother FEM

After completing the FEM, the next step is to create the simulation and set the boundary conditions. The same boundary conditions were also used for the mother satellite. Which includes fixing all three rotational degrees of freedom and the x and y-axis translational degrees of freedom. Therefore, only the z-axis translational degree of freedom is set free. The constraints are applied to the CubeSat rails, since this is the location where the CubeSat contacts the NRCSD rails. Table 5.10 states the boundary conditions and figure 5.14 shows the boundary conditions on the model.

Table 5. 10: Boundary conditions for mother CubeSat's normal modes analysis

Degree of Freedom	Z-Axis Excitation
DOF1	Fixed
DOF2	Fixed
DOF3	Free
DOF4	Fixed
DOF5	Fixed
DOF6	Fixed

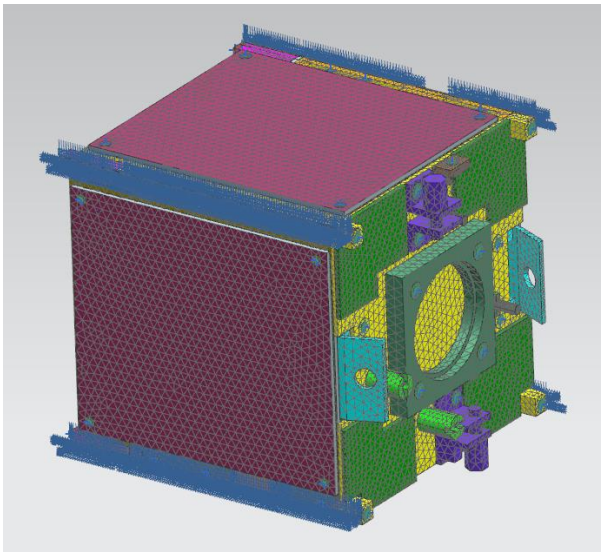

Figure 5. 14: Boundary conditions placed on mother CubeSat's rails

The simulation was run to determine the normal modes of the mother satellite. The first normal mode was found to be at 393.34 Hz. Figure 5.15 shows the displacement that occurs at this natural frequency.

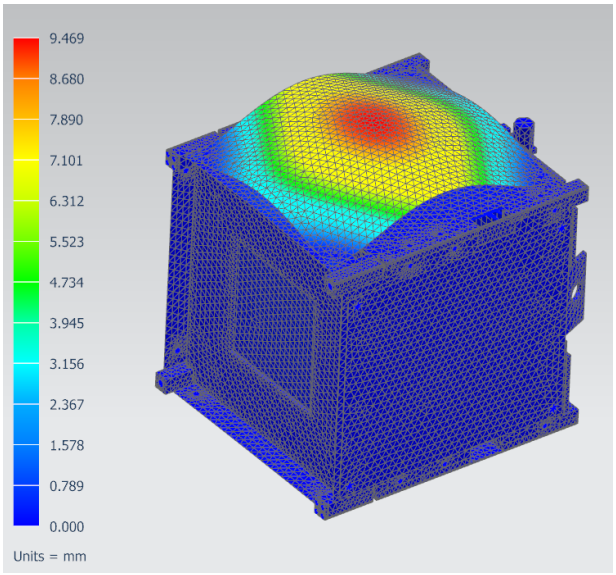

Figure 5. 15: First natural frequency of the mother satellite

The first normal mode excites one of the solar panels. The maximum displacement occurs at the center of the panel. Table 5.11 shows the first 10 normal modes of the mother CubeSat.

Table 5. 11: First ten normal modes of the mother CubeSat

Normal Mode	Frequency (Hz)
1	393.34
2	401.59
3	401.73
4	403.58
5	408.72
6	435.69
7	445.31
8	449.09
9	449.99
10	468.396

Figure 5.16 shows what happens to the mother spacecraft at its fourth natural frequency which occurs at 403.58 Hz.

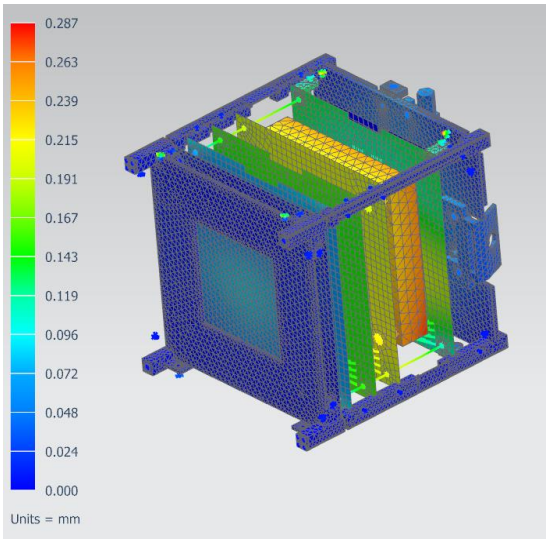

Figure 5. 16: Fourth natural frequency of the mother satellite

During this normal mode, one of the solar panels move inwards. This particular solar panel is connected to a wall that is connected to the internal standoffs via the standoff adapters. Therefore, the interior of the spacecraft will experience a displacement and can clearly be seen in Figure 5.16. At the spacecrafts sixth natural frequency which occurs at 435.69 Hz the internal battery gets excited. The motion of the battery causes displacements for other internal components of the satellite. This can be seen in Figure 5.17.

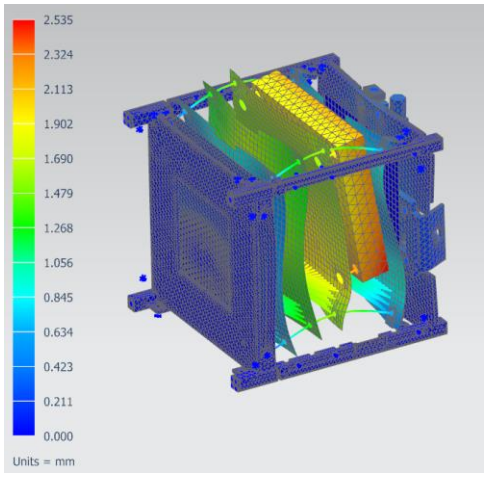

Figure 5. 17: Sixth natural frequency of the mother satellite

It can be seen from the normal mode's analysis that the first natural frequency of the mother spacecraft occurs at 393.34 Hz, which is greater than the 100 Hz required by NanoRacks. This means that the mother spacecraft will also avoid resonance with the launch vehicle.

5.6 Normal Modes Analysis of 2U DESCENT Spacecraft

Finally, the normal modes analysis was conduced for the combined 2U DESCENT spacecraft. Once again, the FEA design process was followed for the analysis. Since the satellite will be connect together in a 2U configuration when inside the NRCSD, it is important to conduct the simulation with the satellites in this configuration. Figure 5.18 shows the solid model of the DESCENT satellites in the 2U configuration.

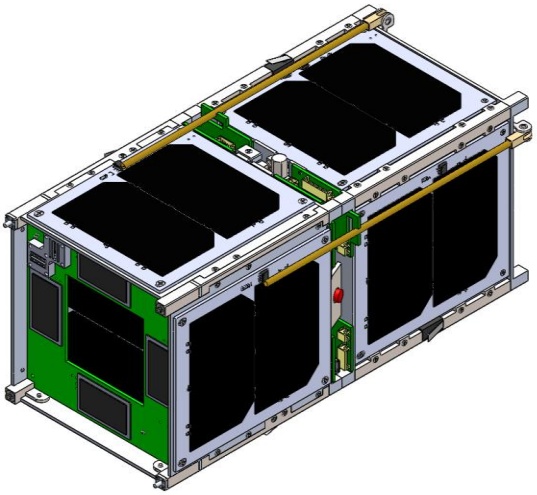

Figure 5. 18: Solid model of DESCENT CubeSats in the 2U configuration

The solid model of the CubeSat is too detailed in its current state, so it cannot be used for the analysis. Therefore, an idealized model was created from the solid model and is shown in figure 5.19.

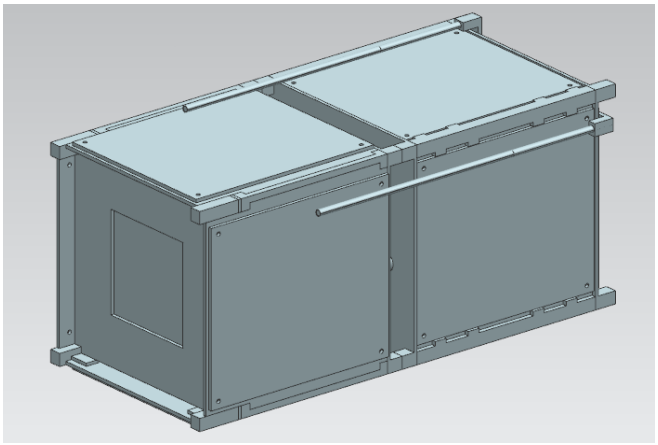

Figure 5. 19: Idealized model of the 2U DESCENT CubeSat

Similar to the previous idealized models, only geometry that provides significance for the structural analysis was kept, while all other geometry was either removed or simplified.

Next, the FEM of the 2U DESCENT satellite was created. The mesh was made from a wide variety of nodes and element types. An image of the FEM is shown in Figure 5.20.

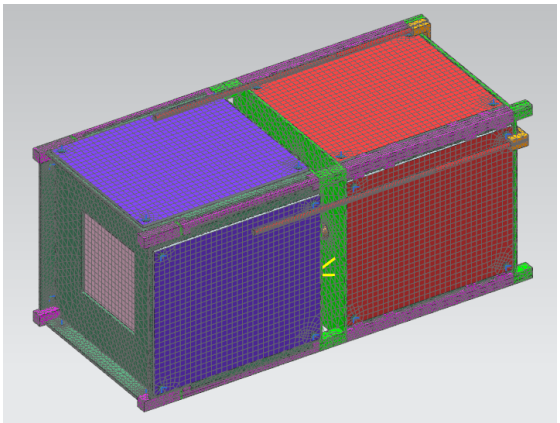

Figure 5. 20: FEM of the 2U DESCENT CubeSat

When creating the FEM, the burn wire loops used to hold the two satellites together were modeled using a rigid 1D connection with material properties of the Dyneema wire. Figure 5.21 shows a close-up image of one of the modeled burn wire loops.

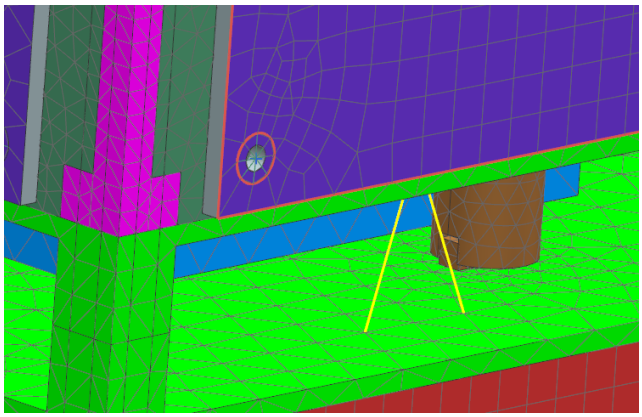

Figure 5. 21: Close up image of the burn wire loop

Before running the analysis, the simulation must be set up. The first step is to apply any loads to the model. The only load is the forced exerted by the separation spring. This force is equal to 85 N and is applied to the separation base found on the daughter satellite. Figure 5.22 shows the location of the applied spring force on the FEM.

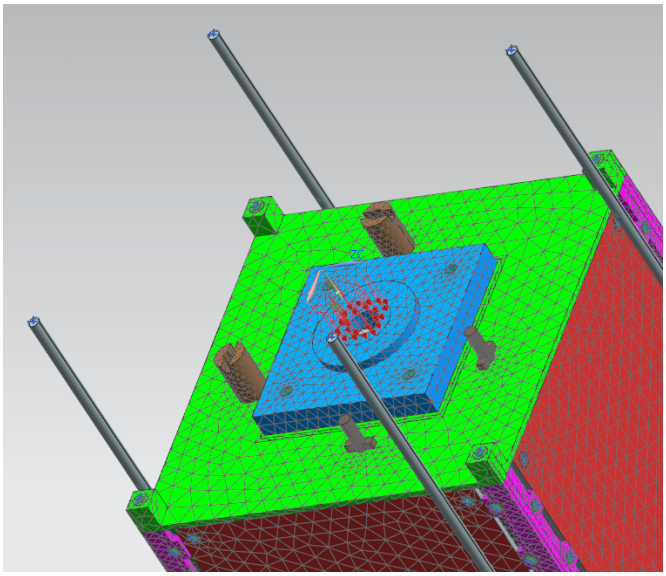

Figure 5. 22: Location of applied spring force

The second step is to place the boundary conditions. Since the CubeSat is placed in the NRCSD, only the CubeSats rails come in direct contact with NRCSD rails. Therefore, the boundary conditions were placed on the rails of the CubeSat and is shown in table 5.12.

Table 5. 12: Boundary conditions for the 2U CubeSat's normal modes analysis

Degree of Freedom	Z-Axis Excitation
DOF1	Fixed
DOF2	Fixed
DOF3	Free
DOF4	Fixed
DOF5	Fixed
DOF6	Fixed

After the boundary conditions had been placed, the normal modes analysis was conducted. The first normal mode was found to be at 404.016 Hz. At this frequency one of the solar panels

gets excited and begins to deflect outwards. This can be seen in figure 5.23.

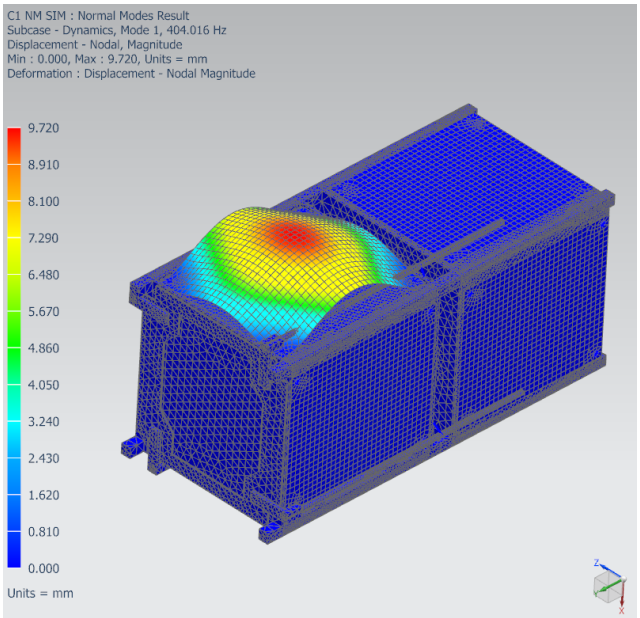

Figure 5. 23: First normal mode of the 2U CubeSat

This frequency is well above the 100 Hz requirement that was placed by NanoRacks. This implies that the 2U satellite will avoid resonance with the launch vehicle. Furthermore, table 5.13 shows the first ten normal modes for the 2U satellite.

Table 5. 13: First 10 modes of the 2U CubeSat

Normal Mode	Frequency (Hz)
1	404.016
2	405.342
3	405.9
4	405.926
5	406.063
6	406.233
7	406.287

8	406.393
9	408.724
10	474.989

5.7 Vibrational Analysis of DESCENT CubeSats

During the launch phase of the mission, the CubeSat deployer will induce vibrations onto the CubeSats. In the previous section, it was confirmed that the CubeSat structures are rigid and have normal modes higher than what is required by NanoRacks. However, during the launch phase various vibrational loads will cause stress in the CubeSat chassis. So, it is important to simulate the full launch phase and see if the stress induced onto the structure is less than the yield strength of the chassis materials. If the stress is less than the yield strength, then it can be confirmed that the structure will survive launch.

The vibration test of the satellite will be conducted on a vibration table using the vibration profile shown in figure 5.3. The spacecraft will be placed in an NRCSD, which will then be hard mounted to a vibration table. The vibration test setup can be seen in Figure 5.24.

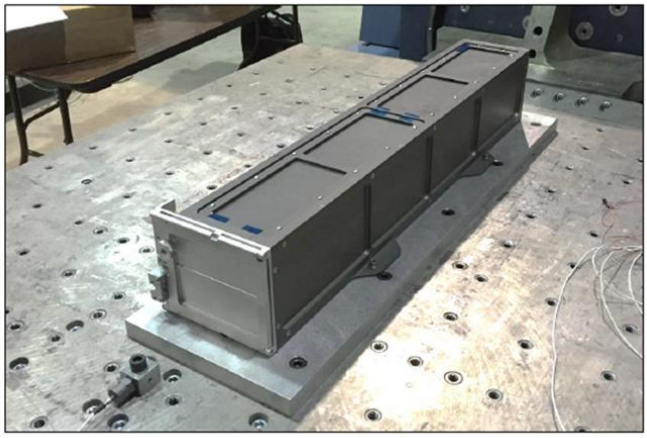

Figure 5. 24: Vibration test setup [28]

After mounting the NRCSD to the vibration table a vibration test will be conducted on all three axis of the satellite using the vibration profile shown in figure 5.3. However, before conducting the vibration test, a vibration simulation can be run using a FEA. The benefit of running an FEA before conducting the vibration test is that it allows the CubeSat developers to see if the current structural design is adequate. If the structure cannot withstand the stress, then the model can be modified before having the structure machined. This saves both cost and time for the project.

The same model used for the normal modes analysis was used for the vibrational analysis. However, since the vibrational simulation has to be run on all three axis, the boundary conditions vary. The boundary conditions will be placed on all four CubeSat rails (see figure 5.25) and table 5.14 shows the different boundary conditions based on the different axis of motion.

Table 5. 14: Boundary conditions used for launch simulations

Degree of Freedom	X-Axis Excitation	Y-Axis Excitation	Z-Axis Excitation
DOF1	Free	Fixed	Fixed
DOF2	Fixed	Free	Fixed
DOF3	Fixed	Fixed	Free
DOF4	Fixed	Fixed	Fixed
DOF5	Fixed	Fixed	Fixed
DOF6	Fixed	Fixed	Fixed

The next step is to enforce a motion to simulate the vibrations from the vibration test. The eight corner posts were selected as the positions to enforce the motion. These locations were chosen because the rails had already contained the boundary conditions, so the enforced motion

was not able to be placed on these locations, so the next best locations were the corner posts. Figure 5.25 shows the boundary conditions and enforced motion locations.

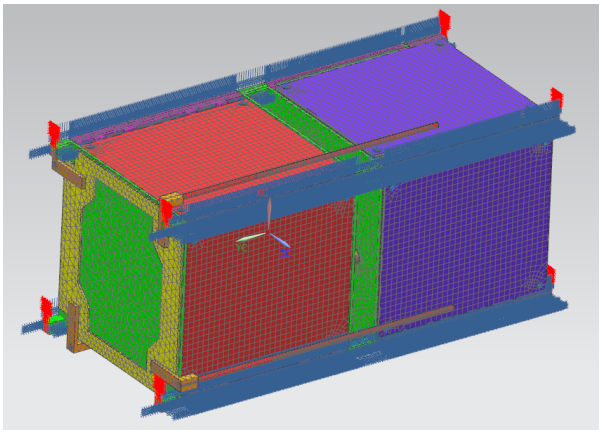

Figure 5. 25: Boundary conditions and enforced motion locations

In Figure 5.25, the boundary conditions are shown in blue and the enforced motion locations are shown in red.

Next, the vibrational profile shown in figure 5.3 was added to the simulation as a function for the enforced motion. Figure 5.26 shows a non-log plot of the function used in the simulation.

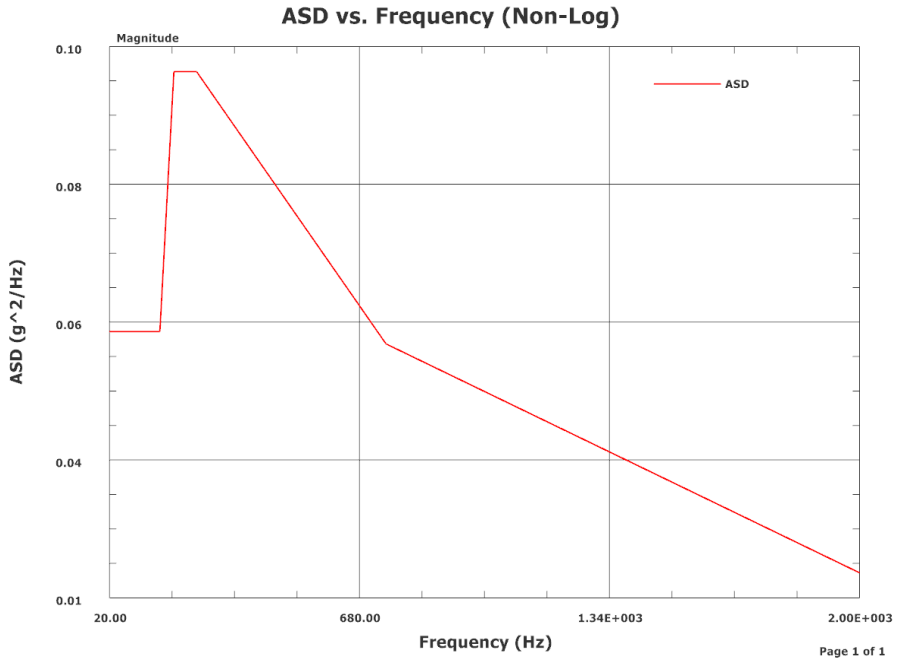

Figure 5. 26: Vibration profile used for the simulation

After setting up the simulation, the analysis was run, and the results were obtained. Any node in the FEM can be selected and various data such as velocity, displacement, acceleration, stress etc. can be obtained for that node for the full vibration test across the frequency range. For instance, a node on the solar panel was selected (see figure 5.27).

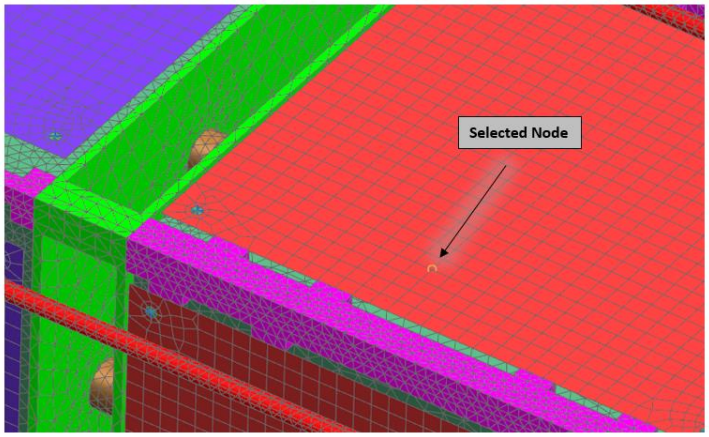

Figure 5. 27: Image showing the selected node

Now various data for that node can be plotted. The acceleration data is chosen to show as a sample plot. This plot can be seen in figure 5.28.

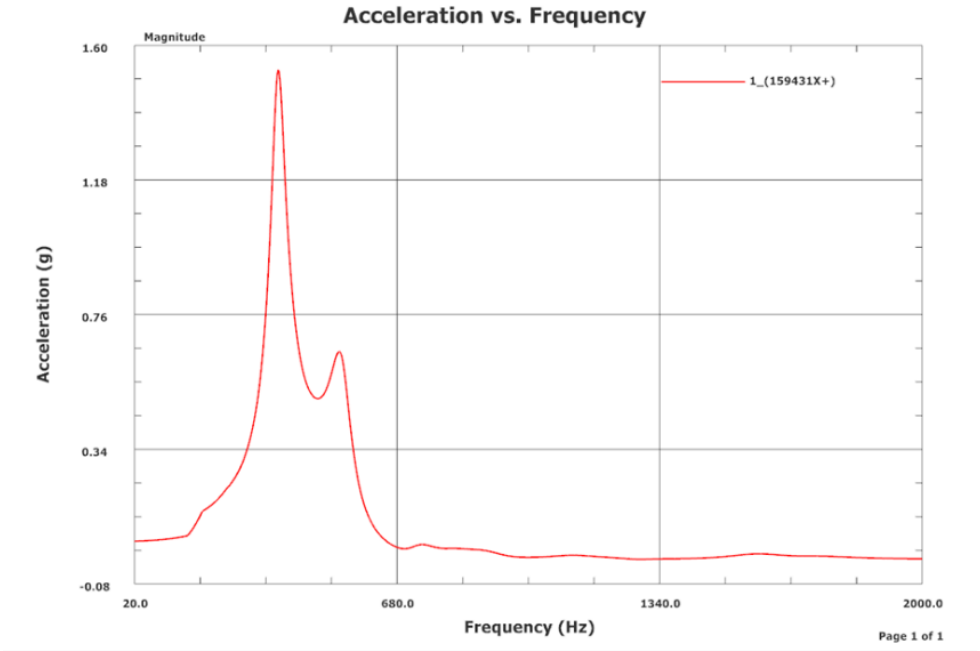

Figure 5. 28: Acceleration plot for the selected node

It can be seen from figure 5.28 that the peak acceleration of 1.57g's for the selected node occurs at 381 Hz. The FEM at this frequency can be viewed to see how the model is behaving at that particular frequency (Figure 5.29).

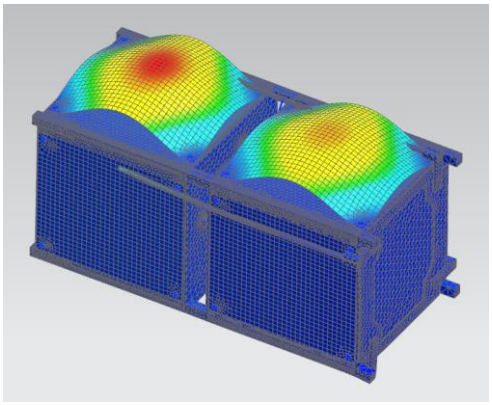

Figure 5. 29: Displacement of FEM at 381 Hz

At 381 Hz a solar panel from both satellites become excited. The selected node is a node that is on one of the solar panels. Thus, explaining the spike in the acceleration graph of that node at that frequency.

By sweeping through the frequency range from 20 to 2000 Hz, the von Mises stress of the 2U satellite can be observed. For instance, at 403 Hz the maximum stress on the CubeSat structure is found to be 228 MPa. This can be seen in figure 5.30.

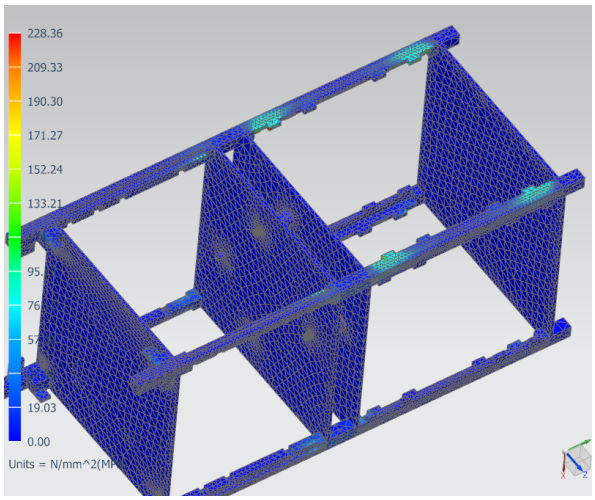

Figure 5. 30: Stress on CubeSat chassis at 403 Hz

The spacecraft structure is constructed using stainless steel 316 and aluminum 6061-T6. The yield strength for the materials are 310 MPa and 276 MPa respectively. The maximum stress at that frequency was found to be 228 MPa, which is below the yield strength of both stainless steel 316 and aluminum 6061-T6. Therefore, the structure will survive at that frequency since it will not yield and not experience any plastic deformation. At a frequency of 483 Hz the structure experiences a maximum Von-Mises stress of 194 MPa (Figure 5.31).

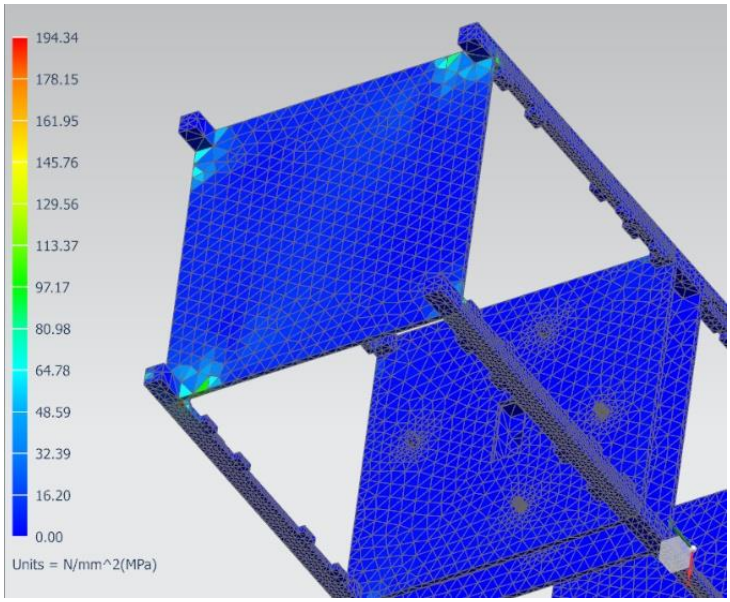

Figure 5. 31: Stress on structure at 483 Hz

Once again, the yield strength of both stainless steel 316 and aluminum 6061-T6 is greater than the stress induced on the spacecraft chassis. Therefore, the structure will not experience plastic deformation. After sweeping through the entire frequency range the highest stress was found to be 331 MPa and it occurs at a frequency of 485 Hz. Figure 5.32 shows the location of the stress on the structure at this frequency.

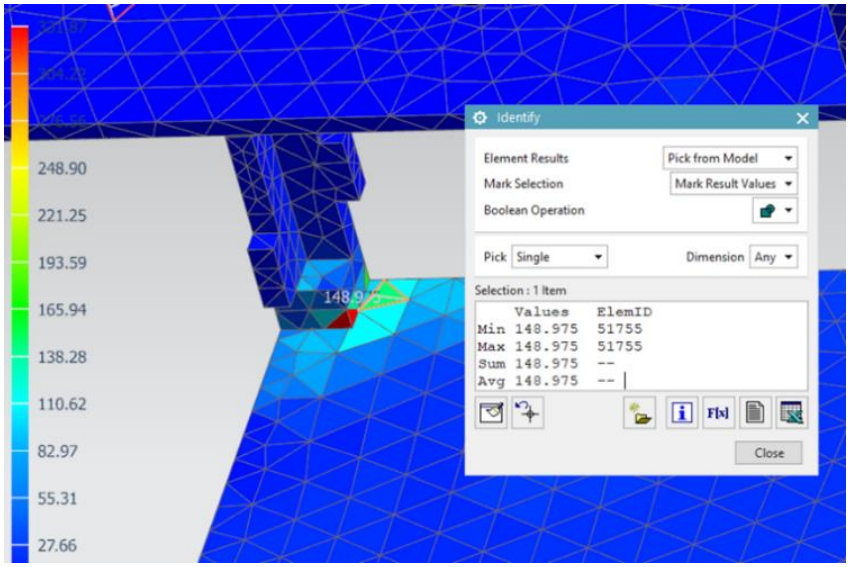

Figure 5. 32: Stress on structure at 485 Hz

The peak stress is greater than both the yield strength of stainless steel 316 and aluminum 6061-T6. However, the maximum stress occurs at a tapped hole where the plate is fastened to the post. This high stress value is due to the lack of geometry in the mesh, which results in all the stress from the bolt being concentrated onto a single element. If a finer mesh was used the stress would be distributed. Therefore, the high stress value shown is not a realistic representation of the actual stress in that location and the stress value can be ignored.

Across the full frequency range, the average stress found for the structure was less than 200 MPa. Table 5.15 shows the average stress for all 3 axis.

Table 5. 15: Average stress found for launch simulations

Axis of vibration	Average Stress (MPa)
X-Axis	175.343
Y-Axis	181.732
Z-Axis	185.231

These stress values are below the yield strength of both stainless steel 316 (310 MPa) and aluminum 6061-T6 (276 MPa). Therefore, since the stress induced on the structure during launch is less than the yield strength of the materials used to construct the structure, the spacecraft will survive the launch environment.

The structural integrity of the chassis can be further verified by preforming a Margin of Safety calculation. The following formula was used to compute the margins of safety,

$$Margin\ of\ Safety = \frac{Yield\ Strength}{\sigma\ \times Factor\ of\ Safety} - 1 > 0$$

where σ is the expected stress and the Factor of Safety is a value typically given by the launch provider. However, NanoRacks does not provide a factor of safety value so the industry standard of 1.1 was used. The calculated margins of safety for each axis of vibration is shown in Table 5.16.

Table 5. 16: Margins of Safety for 3 Axis Vibration Test

Axis of vibration	Margin of Safety
X-Axis	0.431
Y-Axis	0.381
Z-Axis	0.355

It can be seen from table 5.16 that that margins of safety for all three axis are greater than 0. Therefore, the CubeSat structure will withstand the vibrational loads during launch.

Chapter 6 THERMAL FINITE ELEMENT ANALYSIS

6.1 Introduction

Once the spacecraft survives the launch environment, it will be placed in its desired orbit around the Earth. During its time in orbit the spacecraft will experience large temperature changes. For instance, when the satellite is in sunlight, it will experience high overall temperatures. Then, when the satellite is in the eclipse, it will experience very low overall temperatures. The temperature changes of the spacecraft occurs due to the various sources of radiation that are present in the space environment. There are four radiation sources in the low Earth orbit space environment. Table 6.1 shows the radiation flux values for the three major sources.

Table 6. 1: Average Radiative flux values of three major sources in LEO

Radiation Source	Radiation Flux Value (W/m^2)
Solar	1362
Earth IR	237
Albedo	420

The solar flux is the radiation received directly from the sun. The Earth IR is the infrared radiation received from the Earth and albedo is the solar radiation reflecting of the Earth and incident on the satellite. Figure 6.1 shows an image of the 4 radiation sources.

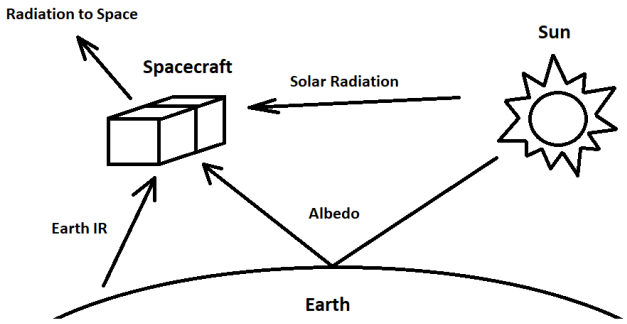

Figure 6. 1: Radiation sources in low Earth orbit

To find the value of the fourth radiation source, which is the radiation emitted by the spacecraft; Stefan–Boltzmann law is used,

$$\dot{Q} = A\dot{q}$$

where $\dot{Q}$ is the heat transfer rate, A is the surface area of the body and $\dot{q}$ is the energy radiated per unit surface area, per unit time (radiation flux),

$$\dot{q} = \sigma\varepsilon T^4$$

T is the temperature of the body, σ is the Stefan–Boltzmann constant and ε is the emissivity of the body. The heat transfer rate from the spacecraft can then be expressed as,

$$\dot{Q}_{Spacecraft} = A\sigma\varepsilon T^4$$

Finally, the total heat transfer rate for the full system is expressed as,

$$\dot{Q}_{Total} = \dot{Q}_{Spacecraft} + AF_{Sun}\alpha\dot{q}_{Sun} + AF_{Albedo}\alpha\dot{q}_{Albedo} + AF_{IR}\varepsilon\dot{q}_{IR}$$

where α is the solar absorptivity, ε is the infrared emissivity and F is the view factor.

Since the CubeSats are in a similar orbit to the International Space Station (ISS), they complete one full orbit in about 90 minutes. Therefore, the satellites experience thermal cycling at a rapid rate. This thermal cycling will cause the structures to expand and contract, thus creating internal stress within the structures. A FEA analysis must be conducted to confirm that the current

CubeSat structures are capable of withstanding the internal stress produced from the thermal cycles.

6.2 Thermal Analysis of Daughter Satellite

To begin, the exact same finite element analysis design process shown in section 5.3 was used for the thermal analysis of the DESCENT spacecrafts. A thermal analysis is more complicated than a structural analysis, this means more computational resources and longer run times are needed to conduct the analysis. So, to shorten the run time of the analysis a more simplified model is needed compared to the structural model. The idealized model for the thermal analysis for the daughter spacecraft is shown in figure 6.2.

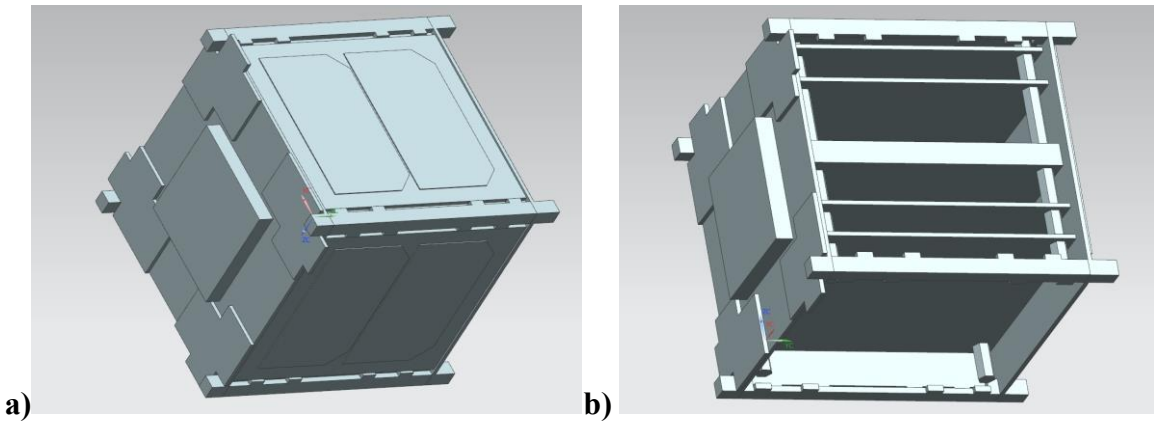

Figure 6. 2: Daughter cube's thermal idealized model a) Exterior b) Interior

For the exterior of the satellite the antenna rods and guiders were removed. For the interior the adapters and the battery structure was removed. However, compared to the structural idealized model solar cells were added to the model as they play a significant role in heat transfer of the exterior faces of the satellite. The next step was to create the mesh for the FEM. Unlike the structural model which used a verity of mesh types from 1D to 3D elements, the thermal model needed an even greater simplified mesh. The mesh details are shown in Tables 6.2 and 6.3.

Table 6. 2: Element types used for daughter CubeSat's thermal FEM

CubeSat Part	Mesh Type	Element Type	Material
Posts	2D Shell	TRI3 Thin Shell	Stainless Steel 316
Walls	2D Shell	QUAD4 Thin Shell	Aluminum 6061-T6
Top & bottom plates	2D Shell	QUAD4 Thin Shell	Aluminum 6061-T6
External PCBs	2D Shell	QUAD4 Thin Shell	FR4
Separation base	2D Shell	QUAD4 Thin Shell	Aluminum 6061-T6
Antenna Base/PCB	2D Shell	QUAD4 Thin Shell	FR4
Storage Box	2D Shell	QUAD4 Thin Shell	Aluminum 6061-T6
Internal PCBs	2D Shell	QUAD4 Thin Shell	FR4
Standoffs	2D Shell	TRI3 Thin Shell	Aluminum 6061-T6
Solar Panels	2D Shell	QUAD4 Thin Shell	FR4
Solar Cells	2D Shell	QUAD4 Thin Shell	UTJ

Table 6. 3: Thermo-Optical Properties of CubeSat materials

CubeSat Material	Thermo-Optical Properties
Stainless Steel 316	ε: 0.14 α: 0.47
Aluminum 6061-T6	ε: 0.24 α: 0.12
UTJ	ε: 0.85 α: 0.92
FR4	ε: 0.8 α: 0.8

As it can be seen, only 2D shell meshes were used for the thermal FEM. Figure 6.3 shows the FEM.

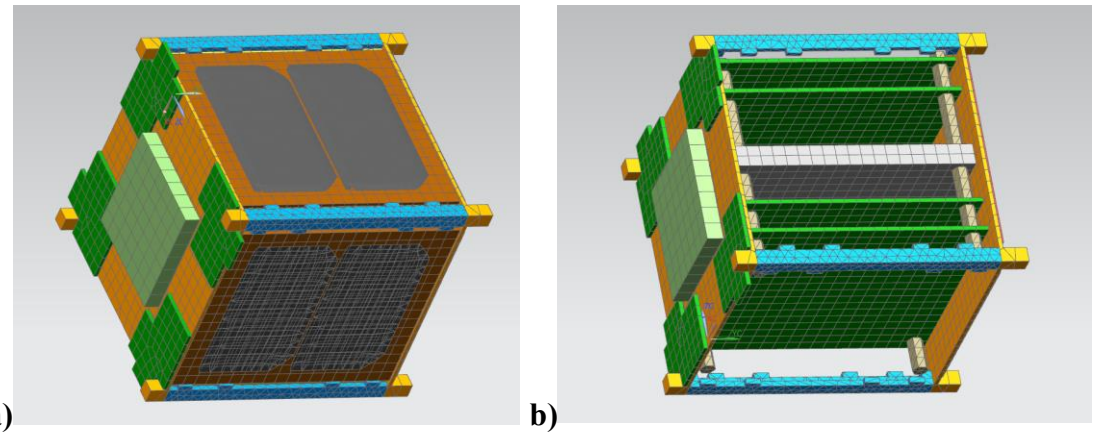

Figure 6. 3: a) Daughter cube's FEM exterior b) Daughter cube's FEM interior

Next, the simulation parameters must be set before running the analysis. It is important to note that two simulations will be conducted. One is referred to the Cold Case and that is if the CubeSats are launched into orbit during the eclipse. The second case is called the Hot Case, and that covers the scenario if the CubeSats are launched into orbit during the sun light. The first parameter is to create view factor calculation requests. This parameter will define how thermal energy is exchanged between model surfaces [29]. The second parameter is the orbit of the spacecraft. The orbit information is shown in table 6.4.

Table 6. 4: Orbital parameters used for thermal simulation

Orbital Parameters	Cold Case	Hot Case
Orbit Period (sec)	5463.10106423241	5463.10106423241
Minimum Altitude (km)	330	330
Eccentricity	0.0004808	0.0004808
Orbit Inclination (deg)	51.6399	51.6399
Argument of Periapsis (deg)	156.2823	156.2823
Right Ascension of Ascending Node (deg)	180	0

Figure 6.4 shows the image of the orbit that will be used for the thermal analysis simulation.

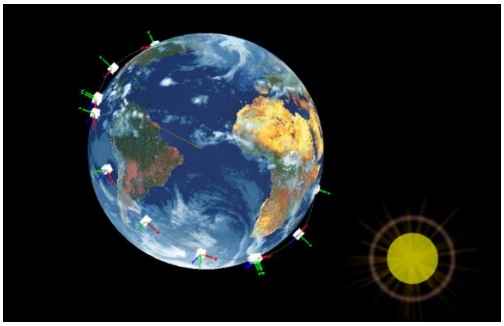

Figure 6. 4: Orbit used for the thermal analysis

The third parameter is the thermal paths defined within the spacecraft. The thermal paths are defined by the thermal conductance between two parts. Table 6.5 shows the two parts that are coupled and the thermal conductance between them. These values are obtained from the book, *Spacecraft thermal control handbook. Volume I, Fundamental technologies* [30].

Table 6. 5: Thermal paths and conductance values for daughter satellite

Thermal Path	Total Conductance (W/˚C)
Solar Panels to Walls	0.0133
Walls to Posts	0.21
Posts to Plates	0.21
Standoffs to Walls	0.21
Top Plate to Separation Base	0.21
Internal PCBs to Standoffs	0.155
Top Plate to External PCBs	0.0133
Bottom Plate to Antenna Base	0.0133
Solar Cells to Solar Panels	0.0133

The total of all the thermal couples create the complete thermal paths within the spacecraft.

The final parameters needed for the simulation are the thermal loads. Various components on the spacecraft such as the internal PCBs, the solar panels, external PCBs etc. generate heat when they are active. These thermal loads apply heat to the satellite and increase its over all temperature. Table 6.6 shows the thermal loads of all the components on the daughter satellite that produce heat. These values were obtained from the DESCENT power budget for the daughter satellite (refer to appendix A5 for power budget).

Table 6. 6: Thermal loads on daughter satellite

Thermal Load Location	Heat Load Magnitude (W)
COMMs Board	0.112
On Board Computer (OBC)	0.3
Electric Power System (EPS)	0.1
ADCS Board	0.075
Solar Panels	0.6

Figure 6.5 shows the locations of the thermal loads within the daughter CubeSat

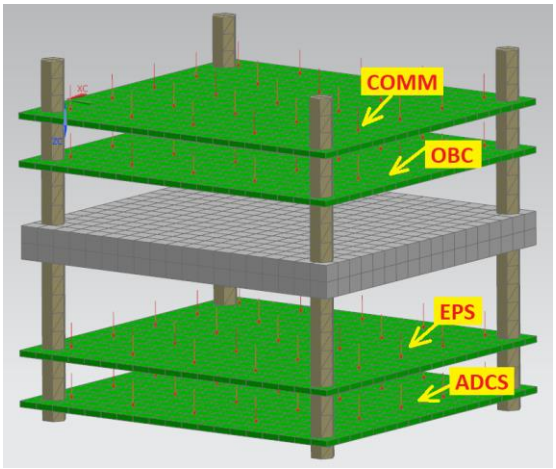

Figure 6. 5: Thermal loads locations in the daughter satellite

All the parameters are set, and the simulation for the cold case will be run first. After

running the simulation, temperature information at any node of the satellite can be obtained. Figure 6.6 shows a sample image of the daughter satellite's temperature profile.

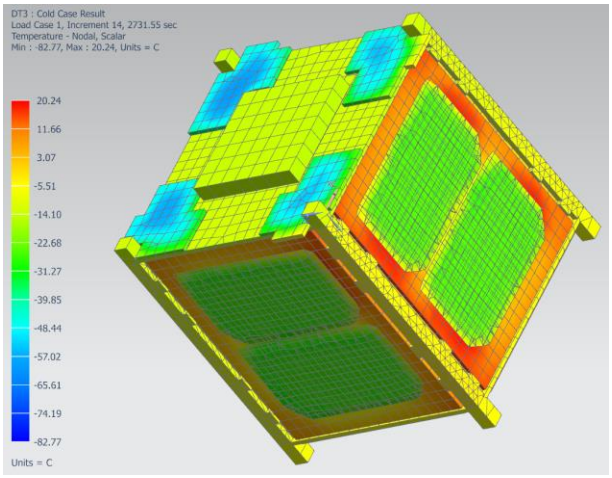

Figure 6. 6: Sample of the daughter satellite's temperature profile

Although the temperature profile can be viewed for the model at various times in the orbit, it is most effective to view the temperatures as a graph. This allows viewers to see the temperature of various locations of the satellite across the full orbit in one graph instead of looking at multiple models with different temperature profiles. Figure 6.7 shows the temperatures of all six satellite's exterior faces during one complete orbit.

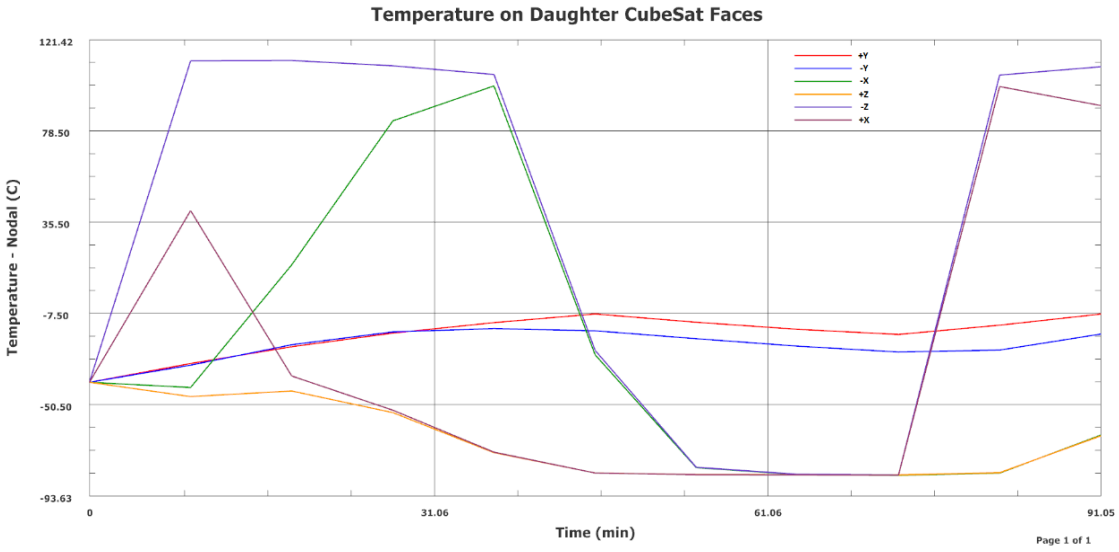

Figure 6. 7: Exterior face temperatures of daughter satellite

As it can be seen from Figure 6.7, the temperatures of the exterior faces range from -83˚C to 115˚C. This is an expected temperature range for the daughter CubeSat since satellites in LEO generally have a temperature range of -170 ˚C to 123 ˚C [31]. The interior of the spacecraft contains all the major PCBs, which can be seen from table 6.6 that produce the most amount of heat. Therefore, the temperatures of the interior of the satellite will be different than the exterior. The interior temperatures of most interest are the temperatures of the PCBs boards, as they contain mission critical components that need to be within a certain temperature range. Figure 6.8 shows a sample image of the interior of the daughter satellite.

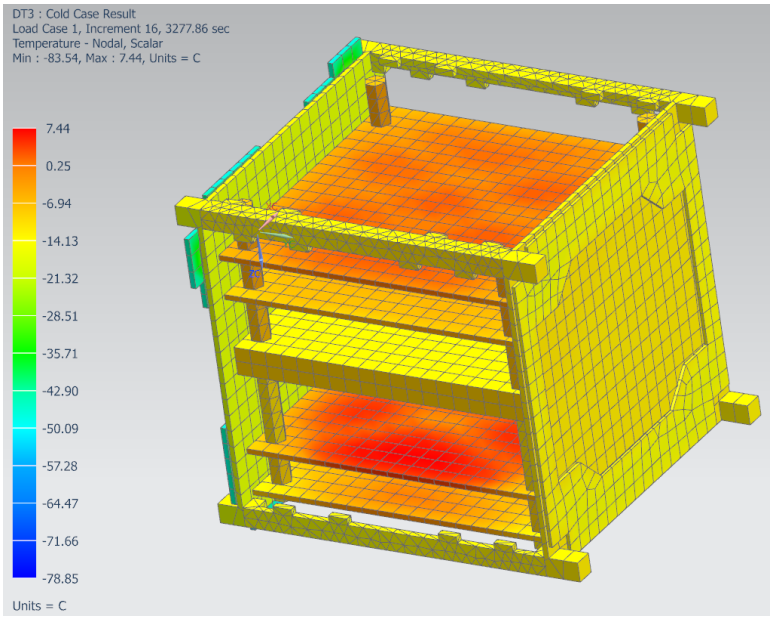

Figure 6. 8: Sample of the interior temperature profile of the daughter cube

Similar to viewing the exterior temperatures, using the models to get the temperature profile of the satellite's interior boards is inefficient. Therefore, it is more efficient to generate a plot of the satellite's interior PCB temperatures across ten orbits. This plot is shown in figure 6.9.

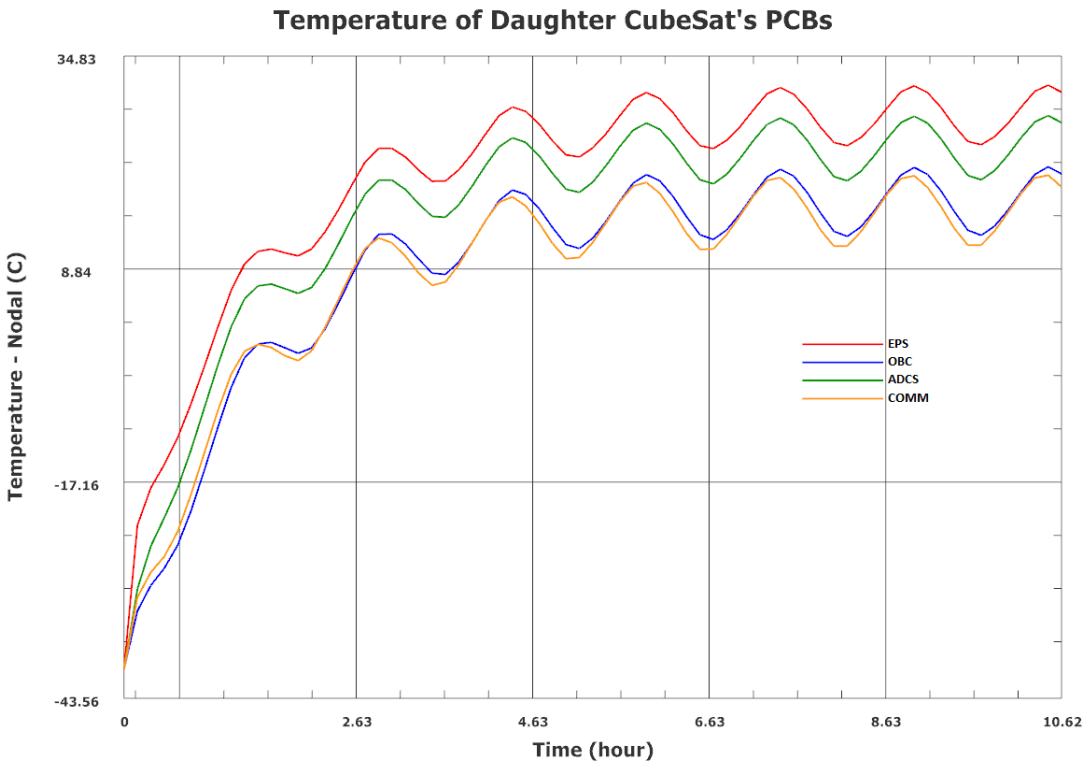

Figure 6. 9: Temperatures of internal daughter PCBs

By seeing the trend from figure 6.9, the temperatures of the boards are increasing and have started to stabilize to a stead value. Once stabilized the temperatures of the PCBs range from 12 ˚C to 31 ˚C.

Now that the temperature profile was obtained for the daughter CubeSat, it is time to take this temperature profile and map it to a structural model. By mapping the temperature profile to a structural model, a structural analysis can be run to determine the thermal stress induced onto the structure. There are two cases where the thermal stress will be the highest. The first is when the spacecraft is the warmest and the second is when the spacecraft is the coldest. Beginning with the warmest case first, Figure 6.10 shows the stress of the structure at the warmest temperature.

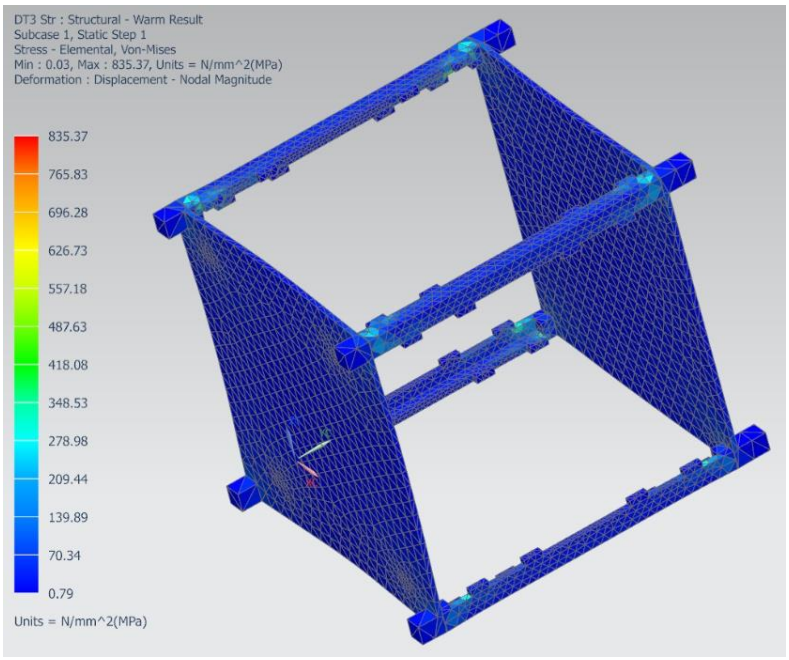

Figure 6. 10: Stress on daughter cube's structure at the warmest temperature

It can be seen from figure 6.10 that the highest stress occurs on the CubeSat's posts near the top and bottom plates. figure 6.11 shows a close-up image of the stress contained at the CubeSat's posts.

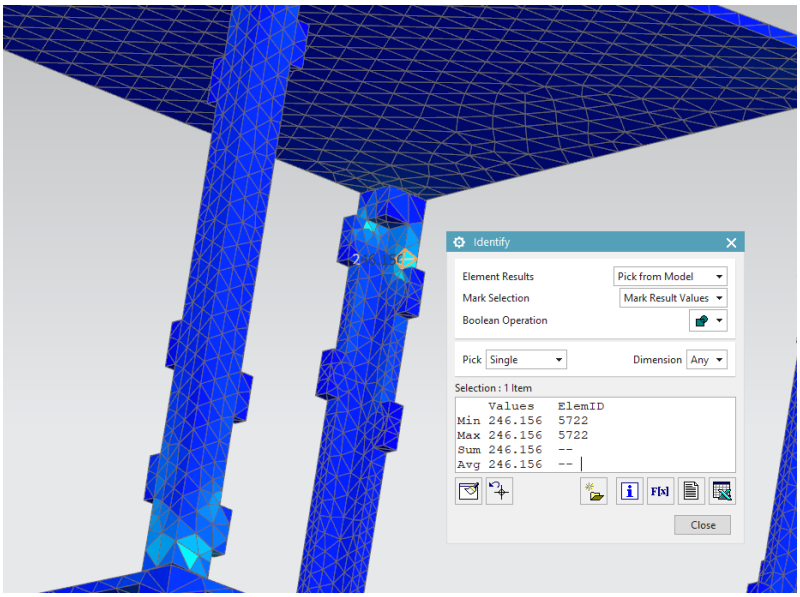

Figure 6. 11: Close-up of stress found on daughter satellite's posts

From the analysis, the average stress is found to be 136.328 MPa. However, the yield

strength of stainless steel 316 at 100 ˚C is 280 MPa and the yield strength of aluminum 6061-T6 at 100 ˚C is 262 MPa. Since the yield strength of both structural components are greater than the stress induced at the warmest temperature, the daughter CubeSat's structure can endure the thermal stress. The highest stress that was found had a value of 835 MPa. Figure 6.12 shows the location of this stress value.

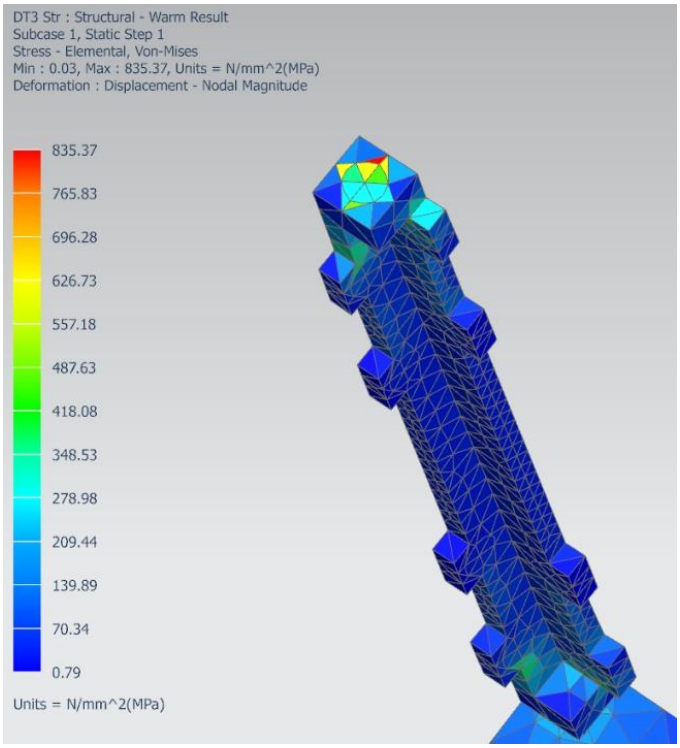

Figure 6. 12: Location of maximum stress value

The stress was found to be well above the yield strength of the structure, it occurs at the tapped hole at the interface between the post and the plate. Once again, the stress at the bolt hole was due to the low geometry of the mesh. Therefore, this stress value is not realistic and can be neglected.

Next, it is time to evaluate the structure at the coldest temperature. Figure 6.13 shows an image of the structure's stress at its coldest temperature.

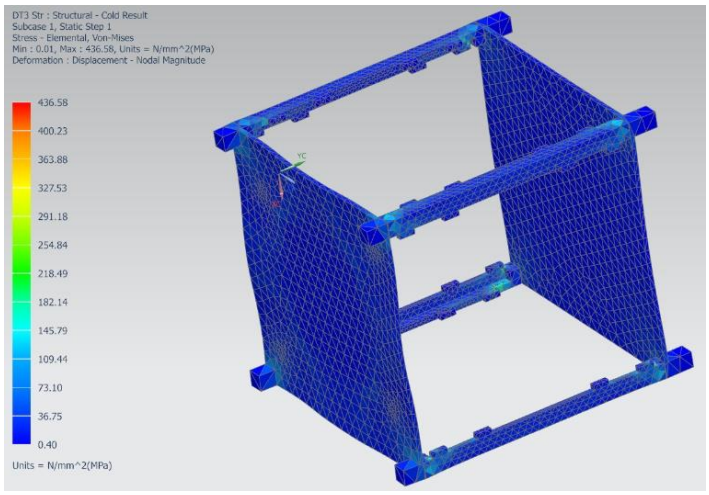

Figure 6. 13: Thermal stress on daughter satellite at the coldest temperature

Similar to the warm case, the stress occurs on the posts near the top and bottom plates. From the analysis the average stress was found to be 199.021 MPa. A major advantage is that at colder temperatures the yield strength of materials increases. The yield strength of stainless steel 316 at -100 ˚C is 416 MPa and aluminum 6061-T6 is 295 MPa. Both these values are above the induced thermal stress found in the structure. Therefore, the structure will survive even in the coldest part of the orbit. The largest stress found has a value of 426 MPa and its location is shown in Figure 6.14.

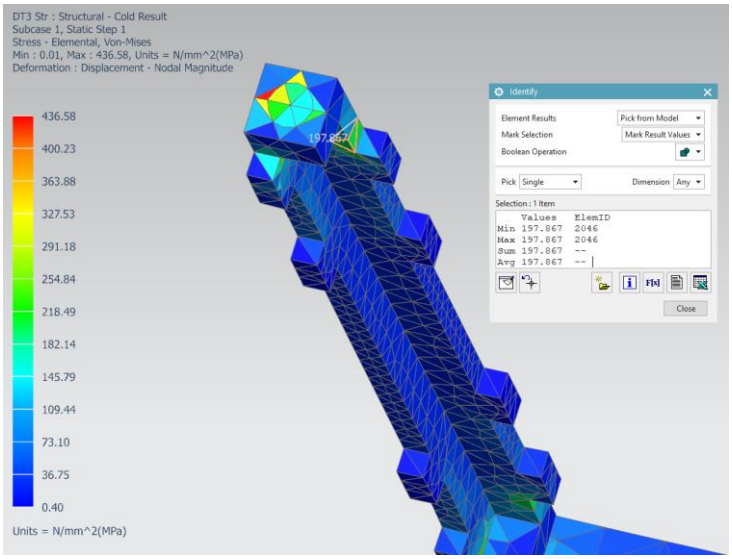

Figure 6. 14: Location of maximum stress on daughter cube at the coldest temperature

Once again, the location of the maximum stress is at a tapped hole found at the interface of the post and the plate. Since this is due to a lack of geometry in the mesh, it can be ignored. All in all, after completing the thermal analysis it was shown that based on these FEMs the daughter satellite can survive the thermal environment for the cold case.

6.3 Thermal Analysis of Mother Satellite

The same procedure followed in section 6.2 will now be applied to the mother satellite. Similar to the daughter satellite the model used for the structural analysis is still too complicated for the thermal analysis. So, a new idealized model was created for the mother satellite. In this model the guiders were removed on the exterior of the satellite and for the interior of the satellite the adapters and the battery components were removed. The new idealized model of the mother satellite is shown in figure 6.15.

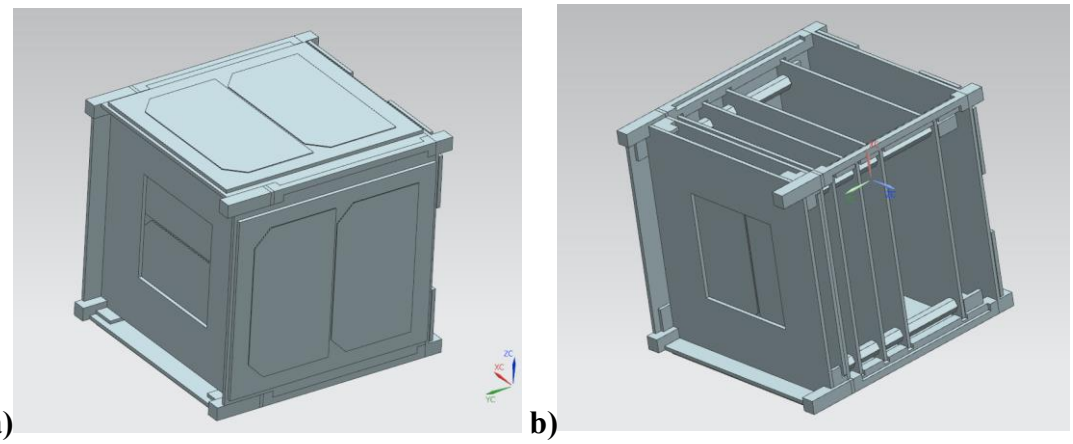

a) **b)**

Figure 6. 15: Mother cube's thermal idealized model a) Exterior b) Interior

Likewise, the mesh used in the structural analysis is too complicated for the thermal analysis as a verity of 1D to 3D elements were used. To simplify the FEM, only 2D shell meshes were used to create the new FEM (Table 6.7). Figure 6.16 shows the updated FEM.

Table 6. 7: Element types used for mother CubeSat's thermal FEM

CubeSat Part	Mesh Type	Element Type	Material
Posts	2D Shell	TRI3 Thin Shell	Stainless Steel 316
Upper Posts	2D Shell	TRI3 Thin Shell	Stainless Steel 316
Top & bottom plates	2D Shell	QUAD4 Thin Shell	Aluminum 6061-T6
Walls	2D Shell	QUAD4 Thin Shell	Aluminum 6061-T6
Solar Panels	2D Shell	QUAD4 Thin Shell	FR4
Solar Cells	2D Shell	QUAD4 Thin Shell	UTJ
SCIENCE PCB	2D Shell	QUAD4 Thin Shell	FR4
External PCBs	2D Shell	QUAD4 Thin Shell	FR4
Separation Base	2D Shell	QUAD4 Thin Shell	Aluminum 6061-T6
Internal PCBs	2D Shell	QUAD4 Thin Shell	FR4
Standoffs	2D Shell	TRI3 Thin Shell	Aluminum 6061-T6
Adapters	2D Shell	QUAD4 Thin Shell	Stainless Steel 316

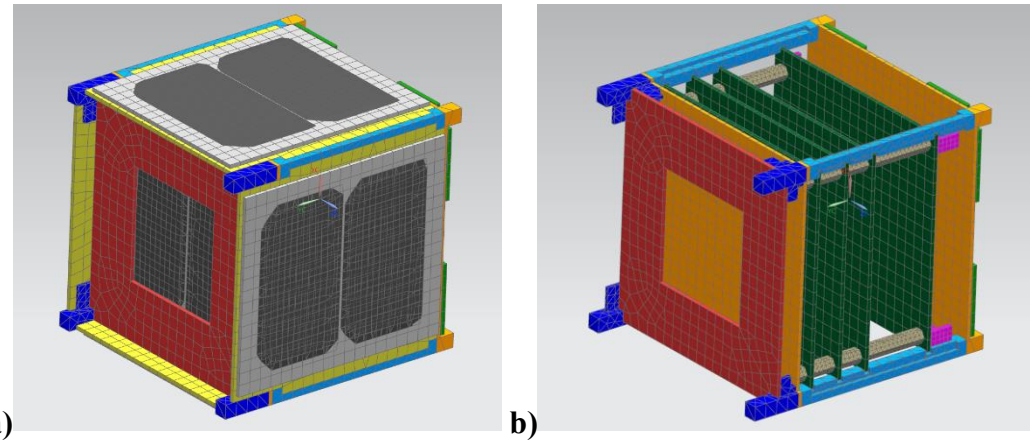

a) **b)**

Figure 6. 16: a) Mother cube's FEM exterior b) Mother cube's FEM interior

Now that the FEM has been created the next step is to setup the simulation for the cold

case thermal analysis. The same items were used to set up the thermal analysis for the mother satellite. The first parameter is to create the view factor calculation requests, this was done identical to the daughter satellite, as the enclosed radiation remains the same. Likewise, the orbit parameters were also identical to the daughter satellite, since the mother satellite orbits is very similar. Finally, the thermal paths and the loads (refer to Appendix A5 for the power budget) are summarized in Table 6.8 and 6.9.

Table 6. 8: Thermals paths and conductance values for mother satellite

Thermal Path	Total Conductance (W/˚C)
Top Plate to Upper Posts	0.21
Bottom Plate to External PCBs	0.0133
Upper Posts to SCIENCE PCB	0.0133
Solar Cells to Solar Panels	0.0133
Top Plate to Top Solar Panel	0.0133
Internal PCBs to Standoffs	0.155
Standoffs to Adapters	0.21
Solar Panels to Walls	0.0133
Walls to Posts	0.21
Bottom Plate to Separation Base	0.21
Top Solar Cells to Top Solar Panel	0.0133
Posts to Plates	0.21
Adapters to Walls/Plate	0.21

Table 6. 9: Thermal loads on mother satellite

Thermal Load Location	Heat Load Magnitude (W)
PI Boards PCB	0.35
Electric Power System (EPS)	0.1
SUGAR Payload PCB	0.0015
ADCS Board	0.125
Solar Panels	0.6

Figure 6.17 shows the locations of these thermal loads in the interior of the mother CubeSat

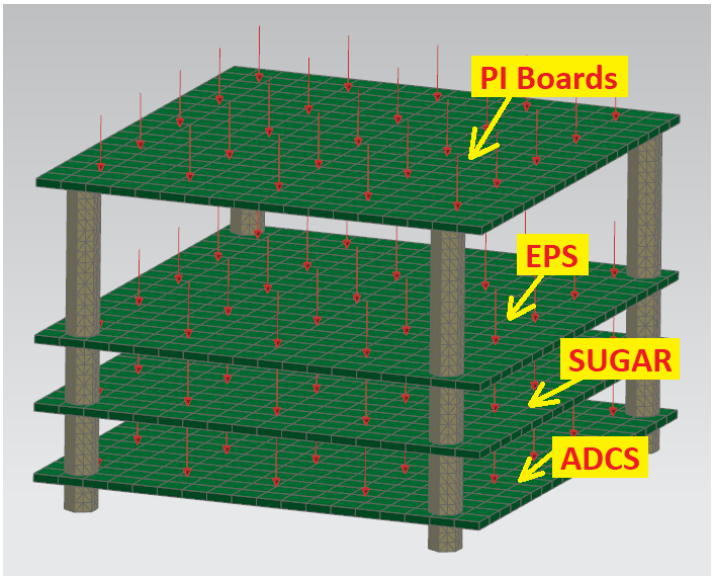

Figure 6. 17: Thermal loads locations in the mother satellite

After the parameters have been inputted into the simulation, it was time to run the analysis. The analysis outputted the full temperature profile of the satellite for one complete orbit. Figure 6.18 shows a sample temperature profile of the mother satellite.

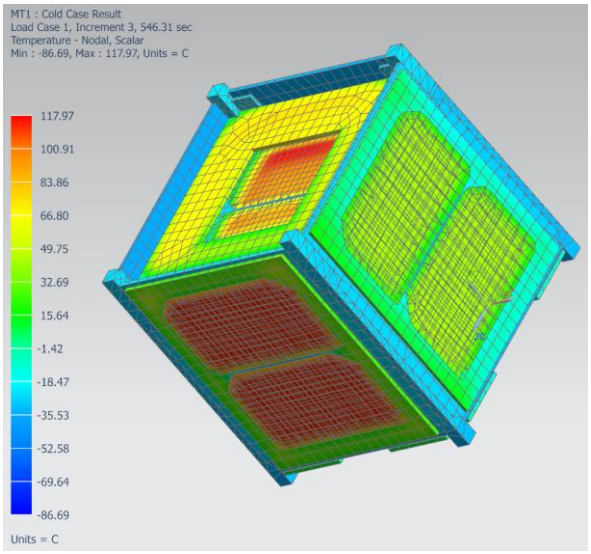

Figure 6. 18: Sample of Mother satellite's exterior temperature profile

Once again, it is ineffective to use the models and their temperature profiles to determine the exterior temperature of the satellite throughout the full orbit. Instead it is better to plot the exterior temperature profile. Figure 6.19 shows the temperature plot of all six exterior faces of the mother satellite.

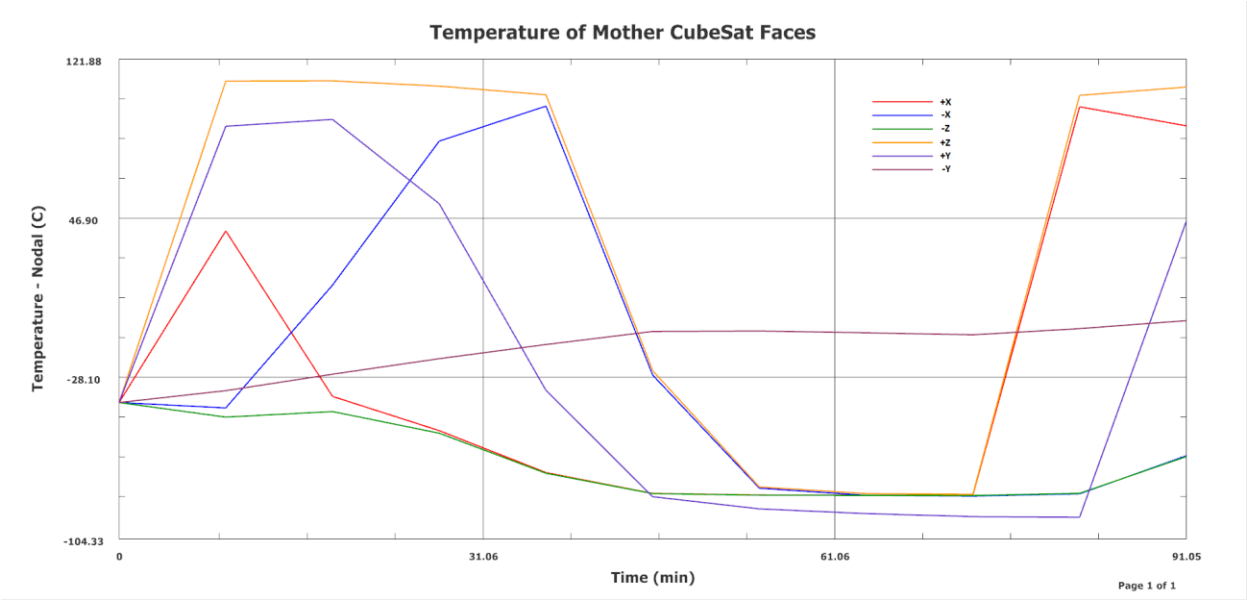

Figure 6. 19: Exterior face temperatures of mother satellite

From the plot it can be determined that the exterior faces temperature ranges from -91 ˚C

to 117 ˚C. By comparing these temperature ranges to the daughter satellite, it can be seen that the temperatures are very similar, which is to be expected since the satellites are mostly composted of the same materials and the orbits are identical. Next, the interior of the satellite must be inspected. Figure 6.20 shows a sample image of the mother satellite's interior temperature profile.

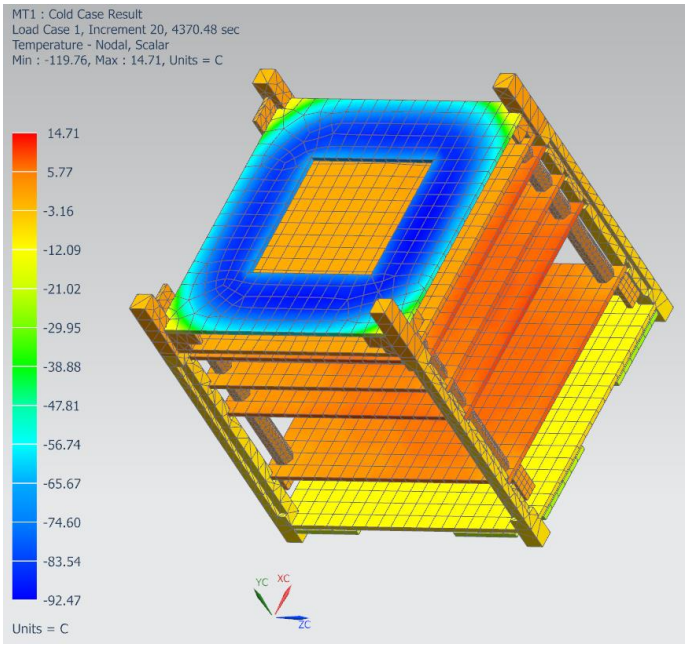

Figure 6. 20: Sample of Mother satellite's interior temperature profile

The interior information that is most valuable is the temperature of the PCBs that are contained inside the mother CubeSat. Their temperatures are important as they determine whether the components will be within their operating range. Figure 6.21 shows the plot of the interior PCB temperatures across ten orbits.

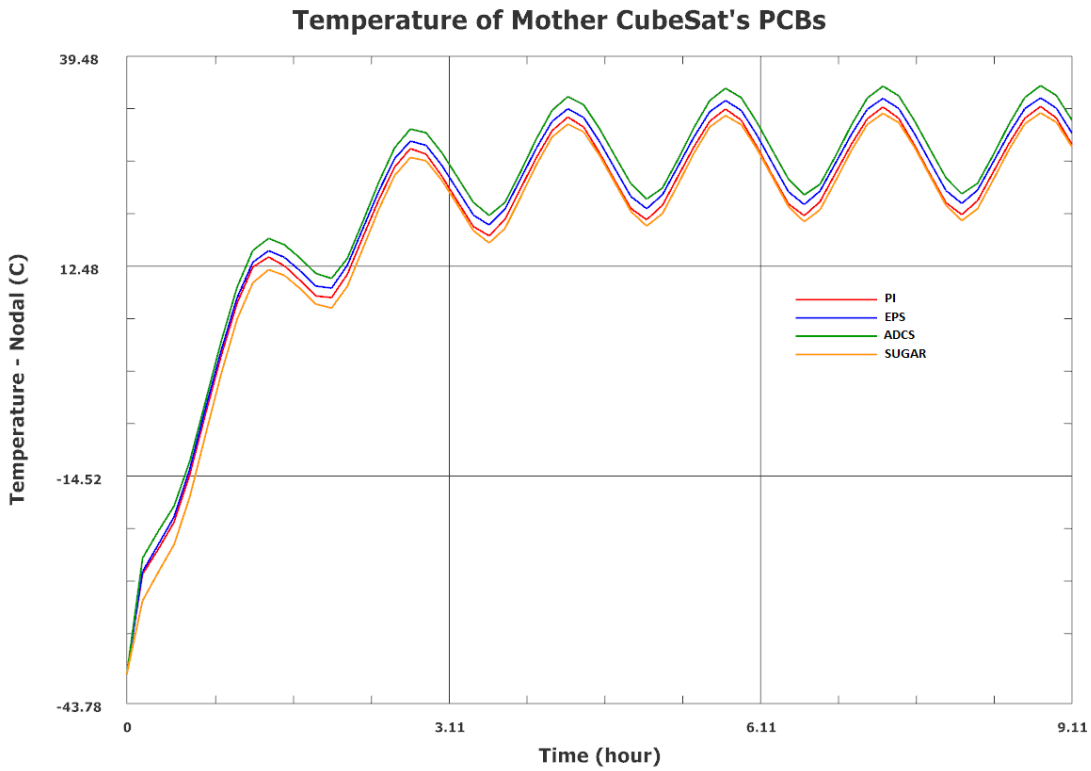

Figure 6. 21: Temperatures of internal mother PCBs

Similar to the daughter satellite the temperature of the internal PCBs start to rise and then begin to stabilize over time. Once stabilized, the temperatures of the PCBs range from 18 ˚C to 33 ˚C.

Now that the temperature profiles have been obtained, it is now time to determine the thermal stress induced onto the structure. Once again, the thermal stress will be analyzed when the satellite is at its warmest and coldest temperatures. In order to do this the temperature profile must be mapped onto a structural FEM. Then a structural analysis must be completed to receive the thermal stress results. Starting with the warmest temperature, figure 6.22 shows an image of the mother satellite after the structural analysis.

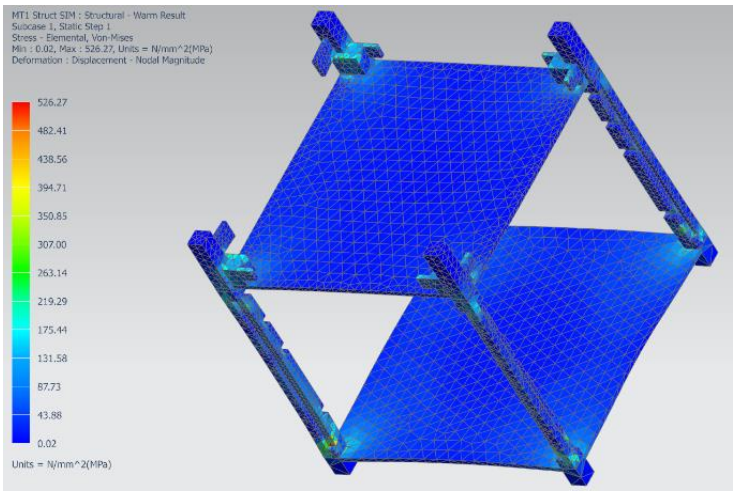

Figure 6. 22: Stress induced on mother cube's structure at the warmest temperature

From Figure 6.22 it can be seen that the stress in the warmest temperature occurs at the posts between the plates and the upper posts above the top plate. From this model the average stress was found to be 141.765 MPa. At 100 ˚C the yield strength of stainless steel 316 is found to be 280 MPa and the yield strength of aluminum 6061-T6 is found to be 262 MPa. Both structural materials yield strengths are above the stress induced. Therefore, the CubeSat will survive the warmest condition. The largest stress value found is 526 MPa and its location is shown in Figure 6.23.

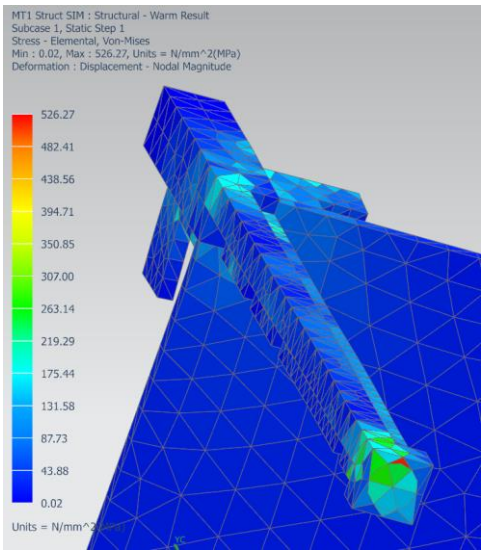

Figure 6. 23: Location of max stress on mother satellite for warm case

Similar to the daughter spacecraft, the location of maximum stress occurs at the tapped hole where the post and plate meet. This is due the low geometry in the mesh. So, it results in an unrealistic stress value, that can be ignored. Next, the coldest case is taken into consideration. Figure 6.24 shows the mother satellite's structure at its coldest temperature.

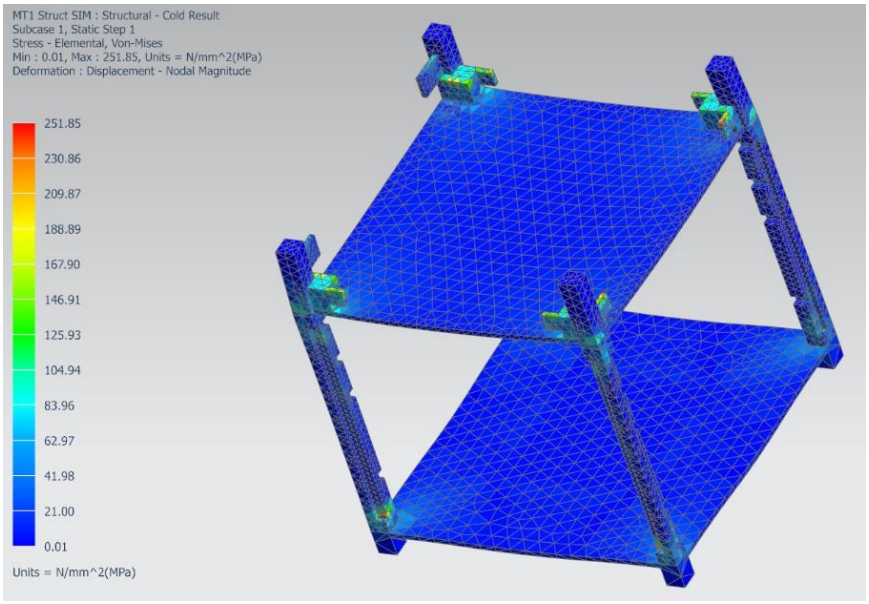

Figure 6. 24: Thermal stress on mother satellite at the coldest temperature

The maximum stress found in this case is 251 MPa. The yield strength of both stainless steel 316 and aluminum 6061-T6 at cold temperatures are increased. At -100 ˚C the yield strength of stainless steel 316 is found to be 416 MPa and the yield strength of aluminum 6061-T6 is found to be 295 MPa. Therefore, even with a maximum stress value of 251 MPa, it is still well under the yield strength of both materials and thus, the structure can survive the cold case at the coldest temperature.

To conclude, table 6.10 shows the summary of the average stress found in all orbital cases.

Table 6. 10: Average stress found for each satellite for different thermal cases

Satellite	Simulation Case	Average Temperature (˚C)	Average Stress (MPa)
Daughter	Cold Case – Coldest	-43.6297	199.021
	Cold Case – Warmest	5.80103	136.328
	Hot Case – Coldest	-3.74608	122.963
	Hot Case – Warmest	50.4912	210.526
Mother	Cold Case – Coldest	-42.7775	170.099
	Cold Case – Warmest	16.7993	141.765
	Hot Case – Coldest	-1.69156	126.551
	Hot Case – Warmest	52.6708	188.79

Thus, based on these models of the CubeSats the structures will survive the thermal environment. Since the yield strength of the structures materials are greater than the stress induced on the structures during its time in orbit. Finally, margins of safety for the structures of both satellites for all orbital case are summarized in table 6.11.

Table 6. 11: Margins of safety for thermal analysis

Satellite	Simulation Case	Margin of Safety
Daughter	Cold Case – Coldest	0.348
	Cold Case – Warmest	0.747
	Hot Case – Coldest	1.181
	Hot Case – Warmest	0.131
Mother	Cold Case – Coldest	0.577
	Cold Case – Warmest	0.680
	Hot Case – Coldest	1.119
	Hot Case – Warmest	0.262

Table 6.11 further validates that the structures will survive its time in orbit, since the margins of safety have a value greater than zero.

Chapter 7 TECHNICAL DRAWINGS AND DRY ASSEMBLY

7.1 Introduction

In this section of the thesis the technical drawings for structural components and the dry assembly procedure will be discussed. At this phase the design of the CubeSat structures have been completed and validated. The next step is to create technical drawings of the parts and have them machined. Once the parts have been machined it is time to complete a dry assembly of the structure. The dry assembly will confirm that the various structural components fit together correctly in the assembly. Once this is complete, the structure is ready for full integration with the other CubeSat components and payloads.

7.2 CubeSat Technical Drawings

Technical drawings are needed to specify the exact dimensions of parts and their tolerances. They provide various details about the part such as the material and surface finishes. Depending on the part, the drawings were specified differently. However, all parts used the same drawing template. The template contains a wide variety of information. The details are specified below:

- Part name
- Drawing scale
- Material
- Tolerances

The next figure shows a sample drawing that was completed for the daughter satellite's post.

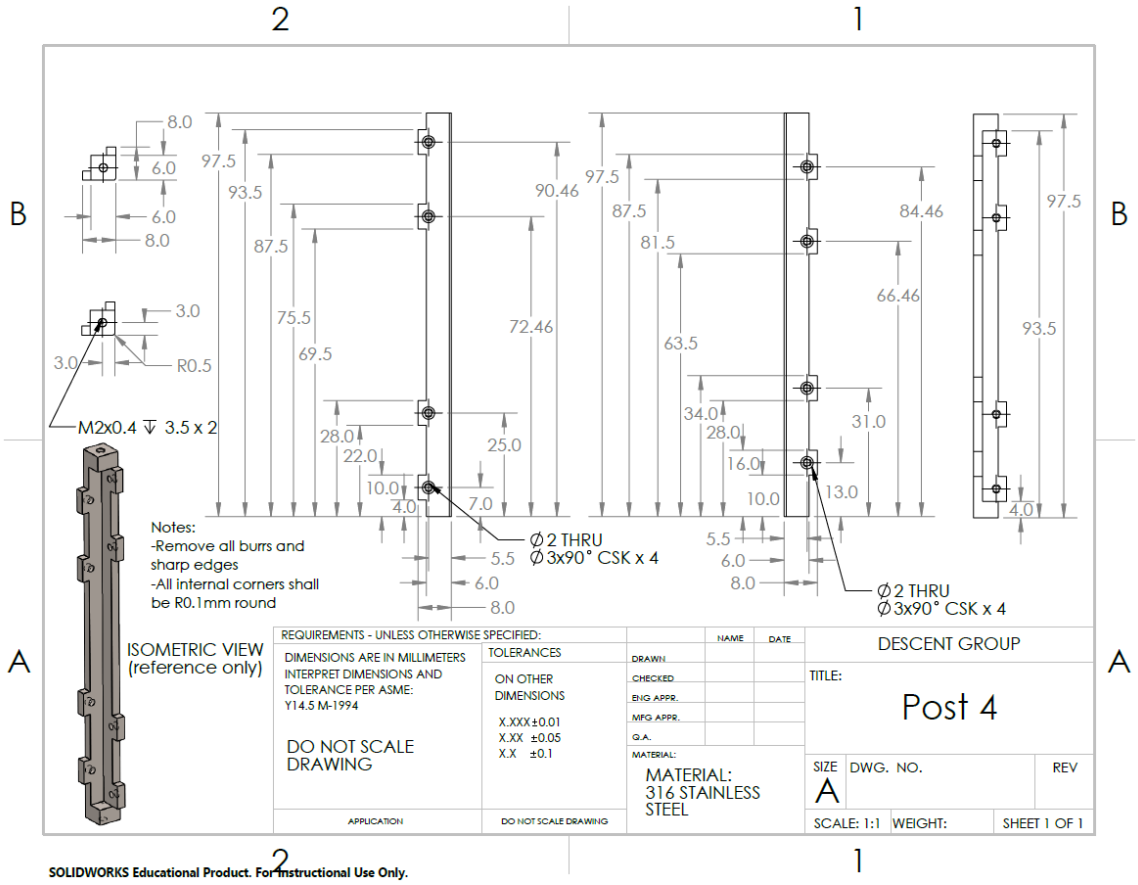

Figure 7. 1: Technical drawing of daughter satellite's post

In addition to the general template there are other details contained in the drawings. It can be seen in figure 7.1 that multiple views of the part are shown. The views help the technician to understand the complete geometry of the parts and its details. Dimensions are specified using a common reference. In figure 7.1 it can be seen that all the dimensions are made relative to the same reference even when the dimensions are shown in a different view. Next, metric hole specifications containing the diameter and pitch are used to define tapped and clearance holes. Counter sinks are also specified at areas where screw heads need to be flush with the surrounding surface. Finally, notes were created to specify surface finishes. Once all drawings were created for all the parts for each satellite, the drawings were then submitted to a local machine shop for

manufacturing.

The parts were manufactured as per the drawing's specifications. Figure 7.2 shows the manufactured daughter post.

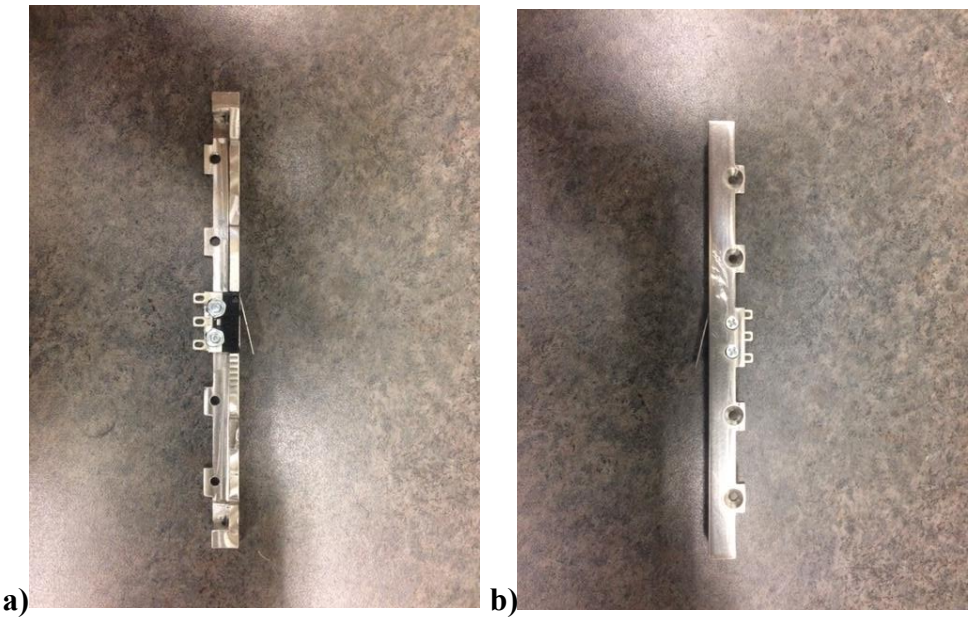

a) b)

Figure 7. 2: a) First view of daughter post b) Second view of daughter post

The posts were precisely machined and matched the technical drawings. Likewise, all the other parts of the CubeSat were also machined to the desired specifications.

7.3 Dry Assembly and Fit Check

Now that all the structural components have been manufactured. The next step is to see whether the parts fit with each other correctly in a complete assembly of both satellites. To check their fit a dry assembly must be competed for each structure. The dry assembly for the daughter satellite was completed first. Before the assembly began, an assembly sequence was first determined. This sequence is as follows:

1. Mount top plate to corner posts
2. Fasten the walls to the posts

3. Mount the bottom plate to the posts
4. Attach the miscellaneous structural components (ex. guiders)

By following this assembly sequence, the dry assembly of the daughter satellite was completed and is shown in figure 7.3.

Figure 7. 3: Dry assembly of daughter spacecraft structure

It can be seen from figure 7.3 that the dry assembly for the daughter satellite was completed successfully. The individual structural components fit together correctly as it did in the CAD model.

Next, a dry assembly was completed for the mother satellite. The following assembly sequence was used:

- Corner posts fastened to bottom plate
- Top plate placed over the corner posts
- Upper posts fastened into the corner posts
- Walls mounted to the corner posts

- Attach the miscellaneous structural components (ex. guiders)

After completing the procedure outlined above, the dry assembly was completed. Figure 7.4 shows the result after the completion of the mother satellite's structure assembly.

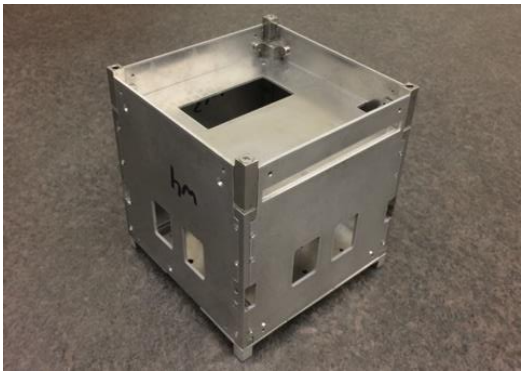

Figure 7. 4: Dry assembly of mother spacecraft structure

Once again, the assembly was completed successfully. The mother satellite's structure matched the structure designed using the CAD tool.

Now that the dry assembly has been successfully completed for both DESCENT spacecrafts, the next task is to confirm that the outer dimensions meet the requirements placed by NanoRacks. One such method to confirm that the outer dimensions are correct is to place the CubeSats into a Fit Check Gauge. A fit check gauge is a dummy rack made to have identical dimensions as the NRCSD. Figure 7.5 shows the dimensions of the fit check gauge as specified in the *NanoRacks CubeSat Interface Control Document*.

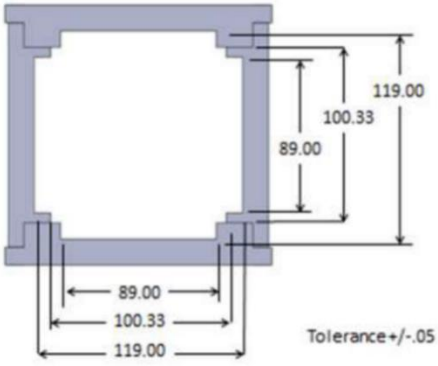

Figure 7. 5: Fit check gauge dimensions [21]

Using these dimensions, a fit check gauge was designed using aluminum 6061-T6 and a CAD model is shown in Figure 7.6.

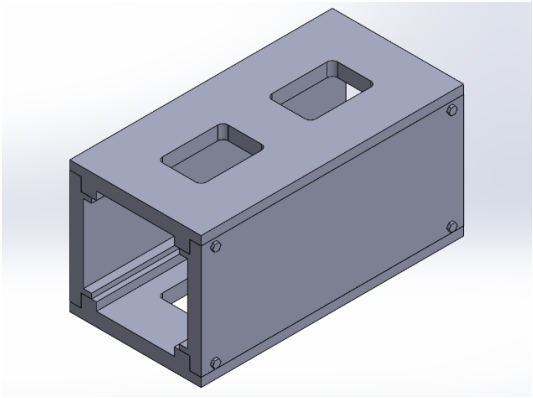

Figure 7. 6: Fit check gauge model

After getting the fit check gauge manufactured, the next step was to place both spacecrafts into the dummy rack. Unfortunately, on the first attempt, both CubeSats had failed to enter the rack successfully. This was due to the excess tolerance of the outer dimensions. So, using a hand file, the extra tolerance was removed on both spacecrafts. Both satellites where then placed into the rack again to check the fit. This time both spacecrafts had successfully entered the rack. Figure 7.7 shows the satellites in the dummy rack.

a) 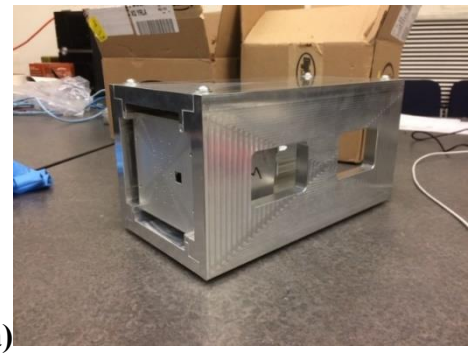 **b)** 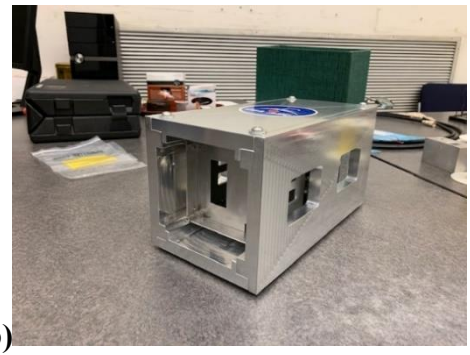

Figure 7. 7: a) Daughter cube in the dummy rack b) Mother cube in the dummy rack

The final fit check was assembling the miscellaneous structural components, such as the guilders, separation bases and tensioners. There components were placed on both spacecrafts and are shown in Figure 7.8.

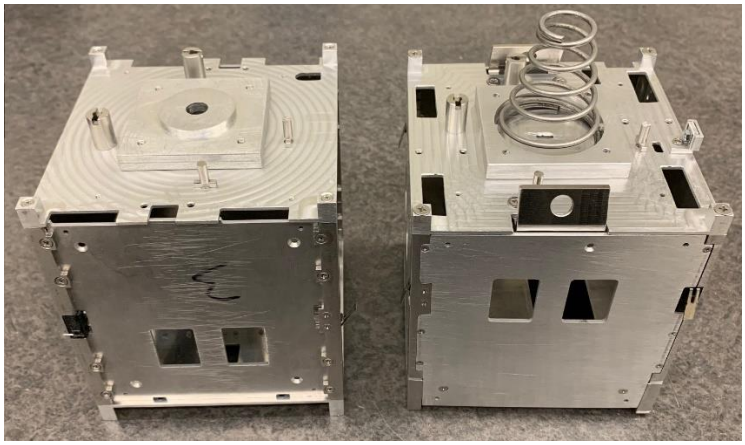

Figure 7. 8: Full structural assembly of both CubeSats

Finally, after completing the full dry assembly of all structural components for the mother and daughter spacecrafts, the final step was to place the combined 2U spacecraft into the fit check gauge. Figure 7.9 shows the results of the fit check.

Figure 7. 9: Fit check of combined 2U DESCENT spacecraft

It can be seen from figure 7.9 that the combined 2U satellite had successfully entered the dummy rack. All in all, the dry assembly and fit check of the structural components of both satellites was successful.

7.4 Final Assembly

The next step of the assembly process was to conduct the final assembly of the DESCENT spacecrafts. The final assembly includes, all the internal components and external components mounted to the CubeSat structure as well as epoxies, Loctite and conformal coating. All members of the DESCENT team had worked together to complete the final assemblies. Figure 7.10 shows the final assembly of the daughter and mother spacecrafts.

a)  b) 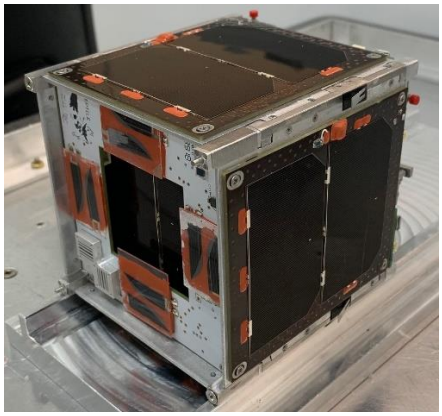

Figure 7. 10: Final assembly of a) Daughter satellite b) Mother satellite

After the completion of the individual satellite assemblies, the complete 2U satellite was integrated together. Image 7.11 shows the DESCENT satellite in its 2U configuration.

Figure 7. 11: Final assembly of 2U DESCENT satellite

Chapter 8 CONCLUSIONS AND FUTURE WORK

8.1 Introduction

This is the final chapter of the thesis. It will provide general conclusions about the design and development of the DESCENT CubeSat structures and the accomplishments made in conducting this research. Then, the challenges encountered during the design of the structures will be highlighted and contributions of this thesis work will be discussed. Finally, the future work plan will be highlighted and the way forward for the DESCENT project will be covered.

8.2 General Conclusions and Thesis Accomplishments

This thesis aimed to discuss the development of a new CubeSat structure for the DESCENT mission. At the time this paper was written, there were multiple COTS CubeSat structures that can be purchased from third party suppliers. However, these structures have a general form so that they can be integrated into numerous CubeSat projects. DESCENT has multiple payloads and bus components that require a custom-made chassis to interface with. So, it was decided by the DESCENT team that a custom CubeSat structure would be developed.

8.2.1 Development of CubeSat Structures

Two separate CubeSat structures had to be developed; one for the daughter satellite and the other for the mother satellite. The structures were designed using a CAD tool and were designed to meet the requirements placed by the launch provider and other onboard subsystems. The

NanoRacks CubeSat Interface Control Document was used to see the requirements needed for the CubeSats to interface with the NRCSD. Requirements included, dimensions, materials, mass, placement of deployment switches and separation springs. In addition to the requirements placed by NanoRacks, the payloads and other bus components placed their own requirements on the structure. The SCIENCE Payload needed mounting holes on the top face of the mother satellite, the daughter satellite needed to fit the tether storage box in its interior, and there had to be cut-outs and slits made on both satellite structures for connectors and harnessing cables. The design for both structures was successfully able to meet all the requirements placed by the launch provider and the other sub systems.

8.2.2 Finite Element Analysis of CubeSat Structures

The next step was to validate the design of the CubeSat structures. This was done by ensuring that both satellites can survive the launch and thermal environments. The launch environment places various vibrational loads onto the CubeSats. It is important that the structure of the satellite can withstand these loads. To determine whether the satellites can survive the launch environment, two simulations needed to be conducted. The first is a normal modes analysis, used to determine the natural frequencies of the satellites. The launch provider requires that the first normal mode must be greater than 100 Hz. After conducting the normal modes analysis, it was determined that the first normal mode for the daughter satellite was 398.72 Hz, the first normal mode for the mother satellite was 393.34 Hz and the first normal mode for the 2U satellite was 404.016 Hz. These first normal modes are well above the 100 Hz requirement placed by the launch provider. The second structural simulation consists of simulating the launch environment. A random vibration profile was obtained from the launch provider and was used to enforce a motion onto the CubeSat to mimic the launch phase of the mission. After conducting the simulation, it was

found that the average stress induced onto the chassis for all three axis was below 200 MPa. This value is less than the yield strength of both structural materials, stainless steel 316 (310 MPa) and aluminum 6061-T6 (276 MPa). Therefore, the spacecraft will survive the launch environment.

The second environment is the thermal environment, which occurs once the spacecrafts are in orbit. During its time in orbit the DESCENT spacecrafts will experience rapid changes between hot and cold temperatures as they move in and out the eclipse. This thermal cycling will induce stress in the CubeSat structures. A separate FEA was conducted to determine the temperature profile of both spacecrafts. This temperature profile was then mapped onto a structural simulation to determine the thermal stress inducted on the structures. Two orbital cases were considered for both satellites. The first is the cold case and the second is the hot case. The greatest thermal stress in the chassis occurs when the spacecrafts overall temperature is the warmest and coldest for either case. For the cold case during the warmest temperature, the daughter satellite had an average stress of 136.328 MPa and the mother satellite had an average stress of 141.765 MPa. At 100 ˚C the yield strength of stainless steel 316 is 280 MPa and for aluminum 6061-T6 is 262 MPa. The stress in both satellites are less than the yield strength of both materials. For the cold case at the coldest temperature the daughter satellite had an average stress value of 199.021 MPa and the mother satellite had a maximum stress value of 251 MPa. At -100 ˚C the yield strength of stainless steel 316 is 416 MPa and for aluminum 6061-T6 it is 295 MPa. Once again, the stress is less than the yield strength of both materials. After completing the simulations for each case at the coldest and warmest temperatures for both satellites it was concluded that both structures will survive the thermal environment.

8.2.3 Technical drawings and Dry Assembly

After the CubeSat structures had been designed and validated, technical drawings for

structural components had to be completed so that the parts can be manufactured. The drawings contained details such as, dimensions, tolerances, materials and surface finishes. Depending on the part, the drawings specifications had varied. After the drawings were submitted to a local machine shop, the parts were manufactured. A dry assembly was conducted to confirm that the parts fit correctly into the assembly. The dry assembly was successful for both mother and daughter satellites. The next step was to confirm that the outer dimensions of the structure were to the standards posed by the launch provider. To evaluate this, a fit check gauge was used as a dummy rack. Initially both CubeSat structures did not fit into the fit check gauge. So, a hand file was used to remove the extra tolerance on both satellites. After this both satellites were able to fit successfully into the dummy rack. Finally, the complete assembly of the final satellites were done.

8.3 Major Differences Between the Models and the Real Satellites

After completing the final assembly of both DESCENT spacecrafts, a comparison was conducted to highlight the major differences between the models and the real spacecrafts. Beginning with the mass. The models suggested that the daughter spacecraft will have a mass of 1.38 kg and the mother spacecraft will have a mass of 1.33 kg. However, in reality when the spacecrafts were weighed the daughter spacecraft had a mass of 1.27 kg and the mother spacecraft had a mass of 1.15 kg (refer to Appendix A2 & A3 for the CubeSat mass budgets). It is clear that the models had an overestimate of the spacecraft's masses. This is due to the mass margins placed on various components.

Next, according to the model the Centre of Gravity (CG) for the 2U satellite was found to be at (x, y, z) = (49.5 mm, 49.6 mm, 113.4 mm) using the coordinate system shown in figure 8.1.

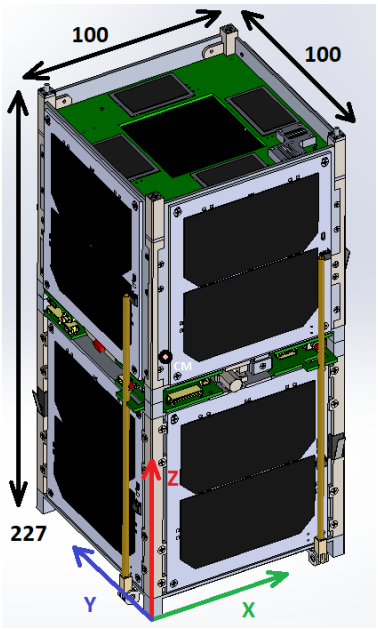

Figure 8. 1 : Reference frame used for the CG location

But, in reality the measured CG of the real satellite was found to be at (51.8 mm, 53.4 mm, 110.6 mm). The shift in CG is due the placement of components in and on the actual satellite that was not represented in the model.

The outer dimension are the next major difference found on the satellite. Since the models are represented perfectly the outer dimensions for the daughter satellite is (100 mm x 100 mm x 116. 45mm) and for the mother satellite it is (100 mm x 100 mm x 110.55 mm). When measured with a digital caliper the real daughter satellite had outer dimensions of (100.05 mm, 99.98 mm, 116.37 mm) and the real mother satellite had dimensions of (100.1 mm, 100.08 mm, 110.43 mm). This difference exists because the dimensions of the model are perfect and have zero tolerance. On the other hand, the actual satellites have a tolerance associated with their outer dimensions.

Finally, some additional differences include the use of epoxies, Loctite, conformal coatings and Kapton tape which exist on the actual satellites but do not exist in the models. Also, certain components on PCBs, do not exist in the models as well as connectors and wires. These differences contribute to the uncertainties of the FEA.

8.4 Uncertainties in the Finite Element Analysis

The previous section highlighted the major differences between the models and the real CubeSats. These differences have had an impact on the uncertainties of the FEA. Beginning with the difference in mass and CG, these discrepancies will have an impact on the normal modes analysis. Since the real satellites have masses located in different positions this can affect the modes of the satellites. Furthermore, it can affect the amount of displacements that can occur at the normal modes. Due to the lack of modeling epoxies and Loctite, surface to surface interactions will vary. The epoxies and Loctite are used to bond components together, this will increase the rigidness of the structure. This can impact both the normal modes and vibrational analysis. Finally, the connectors and harnesses (wires) were not modeled. The harnesses in particular connect one component to an another (ex. PCB to solar panel). These connections cause the components to become coupled and this is not represented in the models. Thus, leading to uncertainties in values such as stress, stain and displacement.

For the thermal analysis, the conformal coating used on the internal PCBs was not represented in the model. The conformal coating will affect the optical and thermal properties of the PCBs. This leads to uncertainties in temperature results of the PCBs as well as thermal stress in the PCB structures. Likewise, due to the lack of modeling harnesses, the thermal paths between components through the harnesses is not represented. This can cause uncertainties in the temperature distribution of the components. Finally, the thermal loads used in chapter 6 are the maximum values for the loads. In reality these loads change based on duty cycles and positions in the orbit. So, the thermal analysis only represents the worst case. The uncertainties arise, since not all possible cases are considered.

8.5 Design Challenges, Solutions and Lessons Learned

During the design of the CubeSat structures, a number of challenges were encountered. The purpose of this section of the thesis is to highlight these challenges and to state the solution / potential solutions to the challenges. The challenges encountered will be stated in the following order: daughter satellite challenges, mother satellite challenges, challenges with the 2U configuration and finally all additional challenges.

8.5.1 Daughter Satellite's Challenges

The design of the daughter satellite had two major challenges. Beginning with the placement of the stack within the CubeSat structure. When the original internal stack of PCBs and storage box was created the stack did not fit inside the CubeSat structure and the storage box was not in the center of the interior of the CubeSat. This issue existed as the purchased standoffs were not the correct length. The solution for this was filing longer standoffs until the desired lengths were obtained, allowing the entire stack to fit inside the structure and the storage box to fall right in the center of the interior of the CubeSat. The lesson learned here is to purchase standoff lengths that are the correct size and to confirm the lengths with the CAD model before purchasing.

The second challenge was insulating the spindt array from the CubeSat structure. Initially when the spindt array was placed onto the structure, it was not insulated from the structure. This was determined by conducting a continuity test using a multimeter. When the spindt array was assembled there existed three layers. The first layer contains the needles, the second layer is a plastic insulation and the third layer was the aluminum mesh. After investigating the problem, it was found that the plastic insulation was not thick enough. So, the solution was to place two layers of plastic insulation instead of one. This had resolved the issue and a continuity test was conduced to confirm that the spindt array was electrically insulated. The lesson learned is to either have a

single layer of think plastic insolation or have multiple layers of thin insulation.

8.5.2 Mother Satellite's Challenges

The satellite structure had three major challenges. Beginning with the first challenge, the heads of the screws that were needed to mount the CubeSat walls to the CubeSat posts were extruding out. When conducting the fit check with the dummy rack, the extruding heads prevented the CubeSat from entering the dummy rack. The solution was to file the head of the screws until they were flush with the walls. The lesson learned is to specify a larger counter sink for the holes where the screw heads were extruding. Larger counter sinks will allow the heads to sit flush.

The second challenge was locking the separation spring to the structure of the satellite. Initially once the separation spring was attached to the separation base, the spring was free to rotate along its long axis. This was due to the lack of a locking mechanism. The solution was to use an epoxy to bond the spring to the separation base, thus preventing the spring from rotating. The lesson learned is to design a locking mechanism to mechanically lock the spring in place without rotating. Having a mechanical lock is more reliable than using an epoxy.

The third challenge was resolving an interference issue with components on a PCB and the bottom plate. The PCB had two Raspberry PI boards and one of the boards was contacting one of the camera support structures when trying to close the CubeSat structure. The solution to the interference problem was cutting of the part of the camera support structure that was in contact with the PI. The lesson learned was that the camera support structure was larger in dimensions than it needed to be. If the dimensions were reduced in the original design the interference would not exist.

8.5.3 2U Satellite's Challenges

The assembly of the 2U satellite had two major challenges. The first was with the separation guiders. One of the earlier iterations of the CubeSat structure design was to only use two separation guiders per satellite. When conducting separation tests of the satellites, it was noticed that the separation was guided only during some instances. The separation was not consistent as two guiders were inefficient in guiding the separation of the CubeSats. The solution to the issue was to add two more guiders on each satellite. Having a total of four guiders had ensured that the separation of the CubeSats was consistent each time. The lesson learned was to place four guiders in the original design.

The second major challenge was tensioning the two CubeSats when forming the 2U configuration. Each time the tensioners were used to compress the separation spring and to bring the satellites closer together, the burn wire used to tension the two satellites would cut. After conducting a root cause analysis, it was found that the burn wire would cut when it was at 90 degrees between one of the holes the wire passes through. This was due to the sharp circular edge of the holes. The solution to the issue was to place a heat shrink at the holes where the wire passes so that the soft material of the heat shrink would make the edges blunt, thus preventing the burn wire from getting cut on the circular edges. The lesson learned was to specify a round radius in the drawings for the holes where the burn wire passes. This round radius would keep the circular edges smooth and prevent the need to use a heat shrink.

8.5.4 Additional Challenges

Finally, there were additional challenges encountered. The first challenge was specifying the direction of the tolerances in the technical drawings of structural components. After the parts were manufactured and the dry assembly was conducted, the walls and posts did not initially fit

together. This was due to the way the tolerances on the parts were specified. The technical drawings had a tolerance of +/- 0.1mm for the edges of the parts. This was an issue because the tolerance was specified in the + and – directions. So, during assembly it was noticed that some parts had conflicting tolerances. The solution was to file one of the parts until the two parts fit together. The lesson learned was to specify the tolerance only in one direction in one part and the opposite on the other interfacing part.

The second challenge encountered was the outer dimensions of the CubeSat structure. As mentioned earlier in section 7.3, the initial CubeSat dry assembly did not fit the dummy rack. This was due to not adding the tolerances correctly for the assembly. So, a hand file was used to remove the additional tolerance. The lesson learned is to confirm that the outer tolerances add to create the correct outer dimensions of the satellite once the assembly is completed.

8.6 Contributions of the Thesis Work

By conducting this research, it led to the development of two new CubeSat structures. This section of the thesis will highlight all the unique features of the new structural designs. Then the usefulness of the structure to the broader CubeSat developer community will be specified.

8.6.1 Tether Storage

The CubeSat design accommodates a tether. For the DESCENT mission, the EDT is one of the main payloads and the tether is stored in a tether storage box. In addition to its ability to store a tether, the storage box provided a great load path for thermal loads. Since the box is made from aluminum, it has a higher thermal conductivity than the FR4 material used for the PCB's, thus it servers as a heat sink when heat travels from the outer faces of the satellite through the standoffs. Also, since the storage box is located at the center of the CubeSat it helps to keep the

center of gravity close to the geometric center.

8.6.2 Separation System

A unique separation system consisting of a separation spring, base, guiders and burn wires was developed. This system is needed to deploy the EDT and separate the two CubeSats. The use of a coil spring is a reliable form of storage of potential energy needed to separate the satellites. The separation bases ensure that the spring is held in place and restricts its motion when faced with vibrational loads. The separation guiders provide a smooth release of the satellites in a guided path. Finally, the burn wires are used along with a thermal knife as a release mechanism.

8.6.3 Tensioning of CubeSats

Two tensioners are used to tension the burn wire needed for the release mechanism. By tensioning the wires, the two CubeSats are brought closer together and the separation spring is compressed. The novelty of the tensioners is that it uses a ratchet and pawl system to restrict motion in one direction when tensioning the burn wires.

8.6.4 Internal Stack Arrangement

The DESCENT CubeSats have a unique internal stack arrangement. A traditional CubeSat would have all the components in the stack arranged in one direction. The DESCENT CubeSats have the internals of the stack placed in one direction for one satellite and the other direction for the other satellite. As it can be seen in figure 8.2.

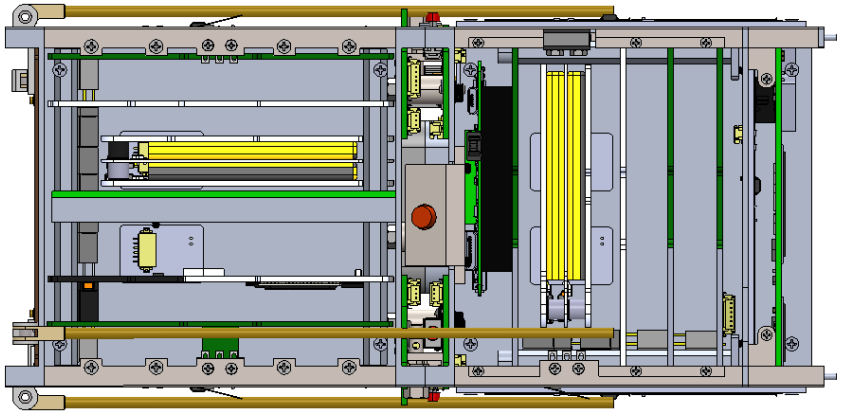

Figure 8. 2: Image showing internal stack arrangements

8.6.5 Usefulness to the CubeSat Developer Community

The unique structural design used for the DESCENT mission is a useful contribution to the greater CubeSat developer community. The tether storage and separation features can be utilized for future CubeSat missions that require the use of a tether. Furthermore, the FEA has validated that the structure is capable of surviving the launch and thermal environments. Therefore, future CubeSat developers can use the same structural design for their satellites without conducting a FEA of their own. Also, the CubeSat structures meet all of NanoRack's interface requirements, therefore this structure can be used by CubeSat developer who are planning on using the NRCSD as the launch system. Finally, the lessons learned section of this thesis had outlined the challenges that were encountered in the development of the structures. Future CubeSat developers can learn from these mistakes and can take the preventive measures when developing their CubeSat structures.

8.7 Future Work

The future work consists of further validation of the structure. At its current stage the structure has been validated through simulations and a vibration table test. The purpose of the

vibration test is to induce the same vibrational loads to the CubeSat as the original launch vehicle. The loads will be applied to all three axes of the satellite. If the satellite can survive the loads imposed by the vibration table, then it can survive the loads imposed by the launch vehicle. Figure 8.3 shows an image of a vibration table. Experimental tests on the physical CubeSat structures must be done to further validate the design.

Figure 8. 3: Vibration table used for CubeSat Testing [32]

A vibration test was conducted for the complete assembly of the DESCENT CubeSats. Figure 8.4 shows an image of the vibration test conducted on the DESCENT spacecrafts.

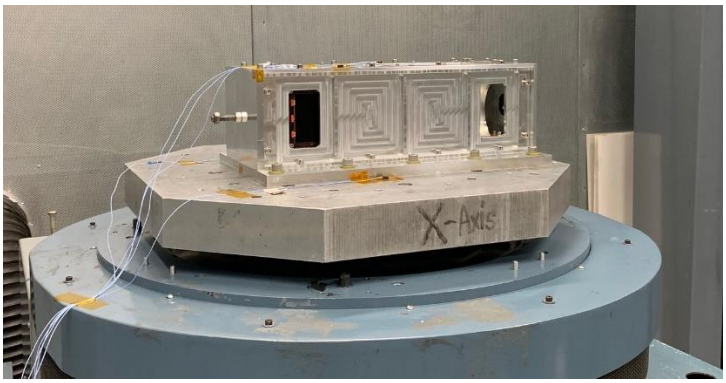

Figure 8. 4: Vibration test of DESCENT satellites

After conducting the vibration test, the structure had survived. However, the satellite as a whole did not survive the test since one of the wires connecting a deployment switch was cut. So, a second vibration test must be conducted and this time both the structure and the entire CubeSat

needs to survive the test.

The second test would consist of using a thermal vacuum chamber, which can be seen in figure 8.5.

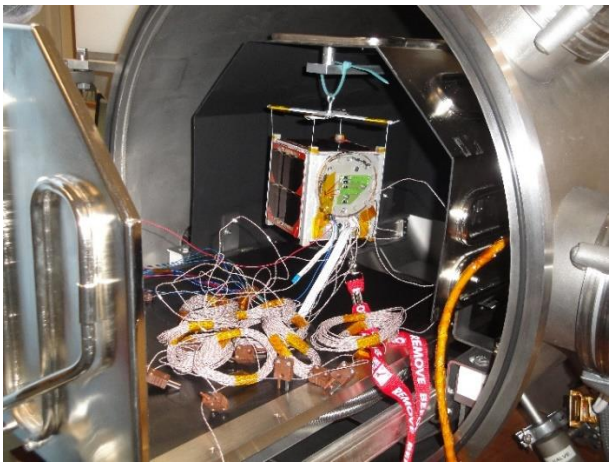

Figure 8. 5: Thermal vacuum chamber used for CubeSats [33]

The thermal vacuum chamber will extract all the air from inside the chamber and then heat loads will be applied to mimic thermal cycling. This test will validate whether materials outgas and if the structure can survive the thermal loads. By completing these two tests the structures can be fully validated. The additional methods are used to deem the structure as space qualified. Once the spacecrafts have been launched and placed into orbit, the operation of the spacecraft will be monitored. If the satellite structures have been in tacked throughout all phases of the mission then, the chassis can be deemed to have a space heritage. Therefore, the structures can be used for future missions with less testing required.

The other part of the future work plan is to update the FEA and run them on a more powerful computer. Appendix A4 shows the specs of the machine used to conduct the FEA. When conducting the FEA, the CPU resources were used the most. So, a more advanced CPU such as an Intel Core i9, with its greater processing power and speed can be used to achieve faster run times and more accurate results for the simulations. Having the more powerful CPU can allow the mesh

used in the FEM to be finer, as different element types and smaller sizes can be used to optimize the results. A more accurate FEA can be used to better validate the structure in the launch and thermal environments. Next, a thermal analysis for the 2U satellite can be conduced with the access of a more powerful computer. Due to the size of the 2U model, more computational resources will be needed to run the analysis. The reason why a thermal analysis of the 2U satellite is useful is to analyze a scenario if the separation system fails and the satellite remains in its 2U configuration during the entire mission. Finally, the tolerances in the technical drawings will be adjusted if other copies of the structures are to be manufactured. This is being done because the original structure assemblies did not initially fit into the fit check gauge. Only after a hand file was used to trim the tolerances did the satellites fit into the dummy rack. Future copies of the structure must fit inside the rack without any filing. This can be achieved by adjusting the tolerances in the technical drawings.

References

[1] Garcia, Mark. “Space Debris and Human Spacecraft.” *NASA*, NASA, 14 Apr. 2015, www.nasa.gov/mission_pages/station/news/orbital_debris.html.

[2] Andrenucci, M., et al. “Active Removal of Space Debris Expanding Foam Application for Active Debris Removal.” *Final Report,* 21 Feb. 2011, www.esa.int/gsp/ACT/doc/ARI/ARI Study Report/ACT-RPT-MAD-ARI-10-6411-Pisa-Active_Removal_of_Space_Debris-Foam.pdf.

[3] *Space Surveillance*, www.au.af.mil/au/awc/awcgate/usspc-fs/space.htm.

[4] Esa. “European Conference on Space Debris Risks and Mitigation.” *European Space Agency*, www.esa.int/Our_Activities/Space_Safety/Space_Debris/European_conference_on_space_debris_risks_and_mitigation.

[5] Stansbery, Gene. “NASA’s Orbital Debris Program Office.” *Briefing to the NASA Advisory Council*, www.nasa.gov/sites/default/files/files/OrbitalDebrisProgramOffice.pdf.

[6] Pardini, Carmen, et al. "Are de-orbiting missions possible using electrodynamic tethers? Task review from the space debris perspective." Acta Astronautica 60.10-11 (2007): 916-929.

[7] Zhong, R., and Z. H. Zhu. "Dynamics of nanosatellite deorbit by bare electrodynamic tether in low earth orbit." Journal of Spacecraft and Rockets 50.3 (2013): 691-700.

[8] Pelaez, J., Lorenzini, E. C., Lopez-Rebollal, O., and Ruiz, M., "A New Kind of Dynamic Instability in Electrodynamic Tethers," Journal of Astronautical Sciences, 48.3(2000): 449–476.

[9] "CubeSat Electrodynamic Tether Deorbit Experiment (CETDE)." *Preliminary Design Review*, 14 Oct. 2016.

[10] "What Is a CubeSat." *Canada.ca*, 27 Nov. 2018, www.asc-csa.gc.ca/eng/satellites/cubesat/what-is-a-cubesat.asp.

[11] "CubeSat." *CubeSat*, www.cubesat.org/.

[12] "A Basic Guide to Nanosatellites." *Alén Space*, 26 June 2019, alen.space/basic-guide-nanosatellites/.

[13] "CubeSat101." *Basic Concepts and Processes for First-Time CubeSat Developers*, no. NASA CubeSat Launch Initiative, Oct. 2017, www.nasa.gov/sites/default/files/atoms/files/nasa_csli_cubesat_101_508.pdf.

[14] "Pumpkin, Inc." *Pumpkin, Inc.*, www.pumpkinspace.com/.

[15] Jaegun Yoo, Taeyeon Kim, Ho Jin, Jongho Seon, David Glaser, Dong-Hun Lee, Robert P. Lin. *A Thermal and Mechanical Analysis of TRIO CINEMA CubeSat Mission*. KHU/SSR.

[16] Aboobakar, Sofia de Fatima Caeiro. "Dynamic and Thermal Models for ECOSat-III." *Instituto Superior T´Ecnico, Universidade De Lisboa, Portugal*, Nov. 2016.

[17] Melahat Cıhan, et al. "Design and Analysis of an Innovative Modular Cubesat Structure for ITU-PSAT II." *Proceedings of 5th International Conference on Recent Advances in Space Technologies - RAST2011,* no. IEEE Xplore, 29 July 2011, doi:10.1109/RAST.2011.5966885.

[18] Firas T. Al-Maliky, and Mohamed J. AlBermani. "Structural Analysis of Kufasat Using

Ansys Program." *Artificial Satellites*, 53(1), Mar. 2018, pp. 29–35.

[19] Armen Toorian. "CubeSat Developers' Workshop." *1st Annual Cal Poly San Luis Obispo*, Apr. 2004.

[20] W. Lan, et al. "Poly Picosatellite Orbital Deployer Mk. III Rev. E User Guide." California Polytechnic State University, San Luis Obispo, CA 93407, 3 Apr. 2014.

[21] NanoRacks, LLC. "NanoRacks CubeSat Deployer (NRCSD) Interface Control Document." 10 Dec. 2013.

[22] "Images." *NanoRacks*, nanoracks.com/resources/images/.

[23] "Inspire 2 Payload." *The University of Sydney*, sydney.edu.au/science/our-research/research-areas/physics/inspire-2-cubesat/inspire-2-payload.html.

[24] "NanoCom ANT430." *Datasheet - 70 Cm Band Omnidirectional UHF CubeSat Antenna*, 2018, gomspace.com/UserFiles/Subsystems/datasheet/gs-ds-nanocom-ant430-34.pdf.

[25] "Omnidirectional Canted Turnstile UHF Antenna System." *GOMspace*, gomspace.com/shop/subsystems/communication-(1)/nanocom-ant430.aspx.

[26] "Raspberry Pi Camera." *The Pi Hut*, thepihut.com/collections/raspberry-pi-camera.

[27] W.T. Thomson, "Theory of Vibration with Applications", 2nd ed.

[28] NanoRacks, LLC. "NanoRacks Flight Acceptance Vibration Testing NRCSD, NRDD." 21 June 2018.

[29] [SIMENS. "Radiation." *NX Help*, NX 11.0.2 Help, docs.plm.automation.siemens.com/tdoc/nx/11.0.2/nx_help/#uid:id631986.

[30] Gilmore, David G. (2002). Spacecraft Thermal Control Handbook, Volume 1 - Fundamental Technologies (2nd Edition). American Institute of Aeronautics and Astronautics/Aerospace Press. Retrieved from

https://app.knovel.com/hotlink/toc/id:kpSTCHVFT2/spacecraft-thermal-control/spacecraft-thermal-control

[31] "How Do Satellites Survive Hot and Cold Orbit Environments?" *Astrome*, 21 July 2017, www.astrome.co/blogs/how-do-satellites-survive-hot-and-cold-orbit-environments/.

[32] Ryan Nugent, et al. *The CubeSat: The Picosatellite Standard for Research and Education.* Aerospace Engineering Department California Polytechnic State University.

[33] Esa. "Belgian Students Closer to Their 'Ticket to Orbit'." *European Space Agency*, www.esa.int/Education/CubeSats_-_Fly_Your_Satellite/Belgian_students_closer_to_their_Ticket_to_Orbit.

[34] Eiswy, Moustafa, et al. "Emirates Aviation College CubeSat Project: Tuning of Natural Modes, Static and Dynamic Analyses of the Strength Model." Proceedings of 5th International Conference on Recent Advances in Space Technologies - RAST2011, 2011, doi:10.1109/rast.2011.5966842.

Appendix

A1: Material Properties*

Material Property	Stainless Steel 316	Aluminum 6061-T6	FR4	Custom Material
Density (kg/m^3)	8000	2700	2145	2087
Yield Strength (MPa)	310 at 25˚C 280 at 100˚C 416 at -100˚C	276 at 25˚C 262 at 100˚C 295 at -100˚C		
Young's Modulus (GPa)	200	68.9	21.9	68
Poisson's Ratio	0.27	0.33	0.18	0.36
Thermal Expansion Coefficient (/dK)	0.0000165	0.0000252	0.000032	
Thermal Conductivity (W/m-dK)	16.3	167	0.23	
Specific Heat (J/kg-dK)	500	896	1200	

*Values obtained from MatWeb and Wikipedia

A2: Mass Budget for Daughter CubeSat

Daughter Cube		
Component	**Mass (kg)**	**Margin (%)**
Side wall 1	0.03484	5
Side wall 2	0.03477	5
Side wall 3	0.03287	5
Side wall 4	0.03195	5
Upper plate	0.04392	5
Lower plate	0.04558	5
Corner posts - 4 in total	0.02988	5
Solar panels - 4 in total	0.188	5
Antenna	0.03	5
Separation Base	0.01492	5
Anti sliding - 2 in total	0.00364	5
Bare PCB (external PCB) - 2 in total	0.0086	10
Bare PCB 2 (external PCB) - 2 in total	0.0084	10
DF 13A-2P (external connector) - 4 in total	0.000211	10
DF 13A-11P (external connector)	0.00014	10
FSI (external connector)	0	5
Total of all stand offs	0.08096	10
Tether storage box	0.116	5
Tether	0.035	50
Stacks	0.048	50
EPS	0.339	5
OBC	0.0619	5
Total of all screws	0.0104	100
Xbee	0.00392	5
Harness (wires + connectors)	0.00672	100
Torquers & power (wires + connectors)	0.00528	100
Xbee antenna wire	0.0008	50
Connectors on PCB	0.0035	100
RF cable	0.015	10
Xbee connectors	0.001	100
Magnetic torquer coil (copper only)	0.0074	5
Jig, screws, paint and wire for magtorque	0.028	100
Voltage boost module	0.01	50
Coin cell battery - 2 in total	0.0064	50

GOM space Transciever	0.03	5
Custom PCB's (PC104) - 2 in total	0.066	5
Total Structure Mass (walls+plates+posts)	**0.25381**	
Total Daughter Mass (without margin)	**1.383001**	
Total Final Daughter Mass (measured)	**1.27**	
Contingencies		
Epoxy		
Loctite		
Kapton tape		
Antenna burn wires		

A3: Mass Budget of Mother CubeSat

Mother Cube		
Component	**Mass (kg)**	**Margin (%)**
Side wall 1	0.03198	5
Side wall 2	0.03484	5
Side wall 3	0.03367	5
Side wall 4	0.03484	5
Upper plate	0.03352	5
Lower plate	0.04463	5
Corner posts - 4 in total	0.02988	5
Solar panels - 4 in total	0.188	5
Camera support structure - 2 in total	0.012	5
Camera - 2 in total	0.0022	5
Hold on/off support - 2 in total	0.01266	10
Mother upper structure	0.02117	5
Separation spring	0.011	5
Bare PCB 2 (external PCB)	0.0042	10
EPS	0.339	5
Adapters	0.112	5
Tether anchor support	0.037	10
Comms board	0.022	5
Tensioner - 2 in total	0.02516	5
FSI (external connector)	0	5
Custom PCB's (PC104) - 2 in total	0.066	5
Stacks	0.048	50

Total of all screws	0.0104	100
Raspberry pi - 2 in total	0.02352	5
Xbee	0.00392	5
Harness (wires + connectors)	0.00672	100
Torquers & power (wires + connectors)	0.00528	100
Xbee antenna wire	0.0008	50
Connectors on PCB	0.0035	100
RF cable	0.015	10
Magnetic torquer coil (copper only)	0.0074	5
Jig, screws, paint and wire for magtorque	0.028	100
Xbee connectors	0.001	100
Total of all stand offs	0.08096	10
Total Structure Mass (walls+plates+posts)		**0.24336**
Total Mother Mass (without margin)		**1.33025**
Total Final Mother Mass (measured)		**1.15**
Contingencies		
Epoxy		
Loctite		
Kapton tape		
Separation burn wires		

A4: Specifications of the Computer used for the FEA

Component	**Model / Specs**
CPU	Intel(R) Core (TM) i7-4790 CPU @ 3.60GHz
Memory	8.0 GB DDR3
Disk	TOSHIBA DT01ACA100
GPU	NVIDIA GeForce GT 720
OS	Windows 64bit

A5: Power Budget of the Daughter and Mother Satellites

Daughter Satellite				
Component	Power (W)	Margin (%)	Duty Cycle (%)	Max. Power (W)
ADCS & Xbee	0.0675	10	15	0.075
EPS	0.1	0	100	0.1
OBC	0.27	10	100	0.3
COMM	0.1	10	10	0.112

Mother Satellite				
Component	Power (W)	Margin (%)	Duty Cycle (%)	Max. Power (W)
ADCS & Xbee	0.1125	10	15	0.125
EPS	0.1	0	100	0.1
Pi Boards PCB	0.315	10	100	0.35
SUGAR	0.00135	10	5	0.0015